CHAPTER (6)
DISCUSSIONS

6.1 Introduction

This chapter presents a full analysis for the static tests and the experimental S-N curves obtained in chapter (5), accompanied by the effect of different fiber orientations $[0,90°]_{3s}$ and $[\pm45°]_{3s}$ and method of manufacturing M_1 and M_2, on the fatigue behavior of woven roving GFRE. Besides, it declares the effect of mean stress that coming from hoop stressσ_H and longitudinal stress σ_l with different pressure ratios, (P_r) on the fatigue behavior of the material. Validation of the SWT parameter and modified fatigue strength Ψ are then checked for studied cases. It ends with validating some failure criteria, for all fiber orientations, and selecting the best failure criterion applicable for the material.

6.2 Effect of Fiber Orientation and Method of Manufacturing

6.2.1 Static tests

Static tests were done on the specimens of both fiber orientations, $[0,90°]_{3s}$ and $[\pm45°]_{3s}$ with two methods of manufacturing M_1 and M_2 for each orientation, under bending, torsional and internal pressure with different specimens end conditions, in order to find out their ultimate global bending strength (S_u), ultimate global shear strengths (S_{us}) and the burst pressure (P_{max}) respectively. Figure 6.1 shows the comparison between experimental results of tests specimens under bending and torsional moment and Figure 6.2 shows the comparison between experimental results of tests specimens under internal pressure.

6.2.1.1 Effect of Fiber Orientation

It is important to note that the damage mechanisms responsible for static failure occur locally and are driven by the local stress fields. The same globally applied multiaxial loads will generally produce different local stress states depending on the fiber orientation. The comparison between both fiber orientation were done according to experimental results obtained in the present study, taking into account the local stresses given in Tables 3.1 to 3.4. On the other hand, the theoretically optimum value of fiber orientation corresponding to each type of loading was calculated by using four failure criteria. Plotting the right hand side of each criterion Table A3.85, equal the relative damage, R.D., then plotting the

relative damage, R.D., against the fiber orientation, Figures 6.3 to 6.5. The theoretically optimum value of fiber orientation for each loading type was found at the smallest value of relative damage, R.D.

(a)Bending tests

Under static bending tests the $[0,90°]_{3s}$ specimens have the higher bending strength than the fiber orientation $[\pm45°]_{3s}$ specimens with both methods of manufacturing M_1 and M_2. This may be explained by considering the local stresses and referring to Table 3.1, the fiber orientation $[0,90°]_{3s}$ has a minimum value of stress component σ_6 which is equal to zero. This conclusion was found in similar work **[83-88], [138]**.

Figure 6.3 present the theoretically optimum fiber orientation under bending, as shown in the figure the fiber orientation $[0,90°]_{3s}$ has the relative damage lower than fiber orientation $[\pm45°]_{3s}$ (i.e the relative damage of orientation $[0,90°]_{3s}$ is the nearest zero), this mean the fiber orientation $[0,90°]_{3s}$ is more safe than the fiber orientation $[\pm45°]_{3s}$ under bending load.

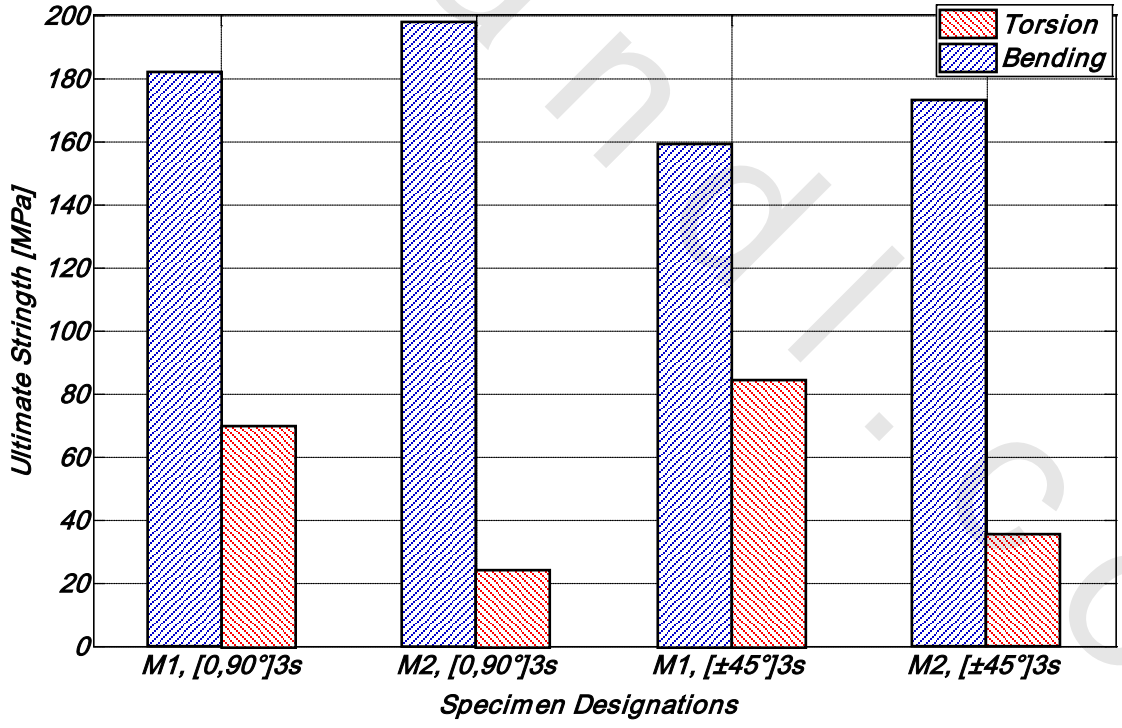

Figure 6.1 Ultimate strength for both fiber orientations with both methods of manufacturing

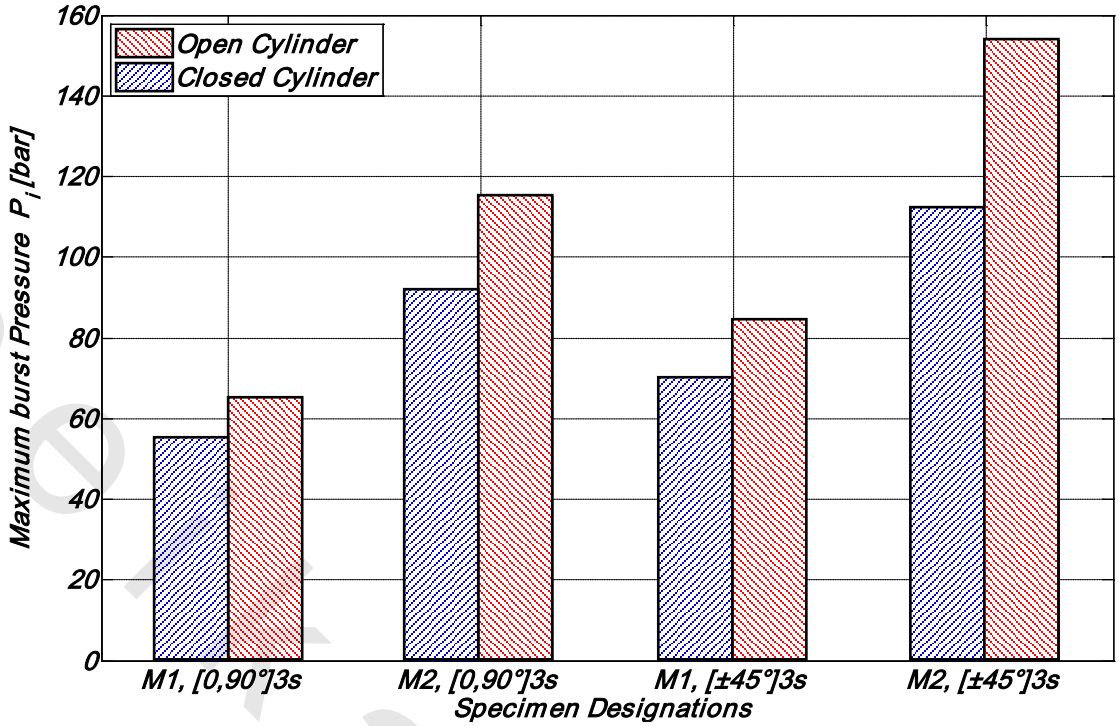

Figure 6.2 Burst Static Pressure for both fiber orientations with both methods of manufacturing

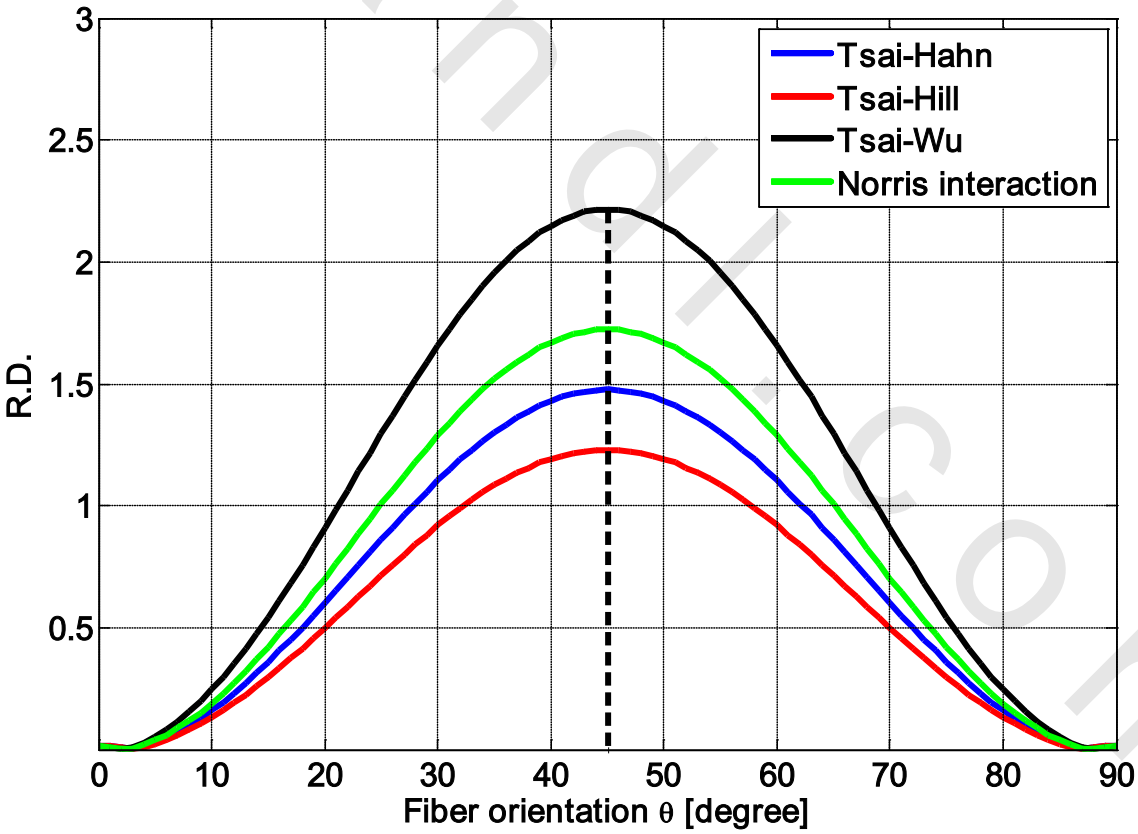

Figure 6.3 The theoretically optimum fiber orientation under pure bending.

(b) Torsion tests

From the results of static torsional tests, we can conclude that the $[\pm 45°]_{3s}$ specimens have the higher torsional strengths than the fiber orientation $[0,90°]_{3s}$ specimens with both method of manufacturing M_1 and M_2. This may be explained by considering the local stress and referring to Table 3.1, the fiber orientation $[0,90°]_{3s}$ has the maximum value of stress component σ_6 which equal to B. This conclusion was found in several works **[83-88], [138]**. Figure 6.4 present the theoretically optimum fiber orientation under torsion, as shown in the figure the fiber orientation $[\pm 45°]_{3s}$ has the failure criterion lower than fiber orientation $[0,90°]_{3s}$ (i.e the R.D. of orientation $[\pm 45°]_{3s}$ is the nearest zero), this mean that, the fiber orientation $[\pm 45°]_{3s}$ is more safe than the fiber orientation $[0,90°]_{3s}$ under torsional loading.

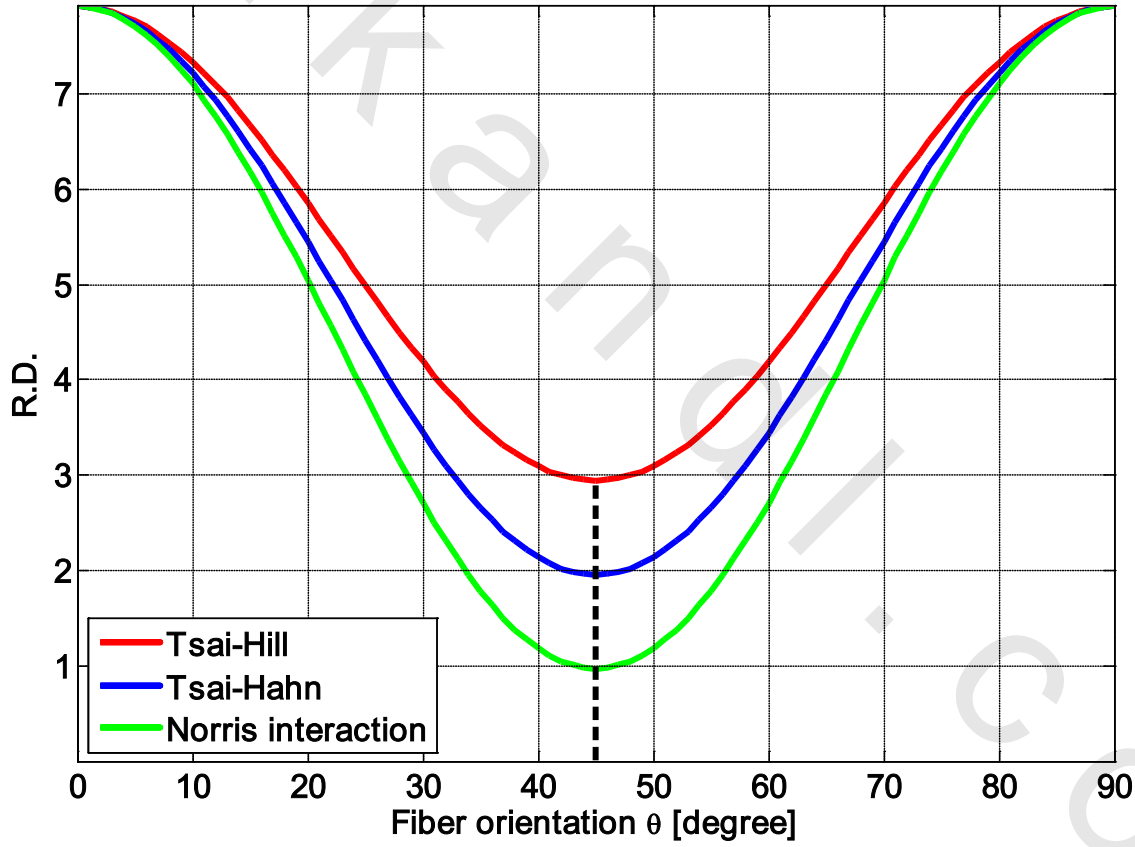

Figure 6.4 The theoretically optimum fiber orientation under pure torsion.

(c) Internal pressure tests

Under hydrostatic pressure tests for closed and open specimens end, the $[\pm 45°]_{3s}$ specimens have the higher burst pressure than the other fiber orientation $[0,90°]_{3s}$

specimens with both method of manufacturing M_1 and M_2. This because the local stresses and referring to Table 3.3, although the fiber orientation $[\pm 45°]_{3s}$ has the highest value of stress component σ_6, it is small compared with the values of normal stress components σ_1 and σ_2, with a value about 33.33% , so that the normal stress components are governed of failure criterion, this conclusion was found in different works **[17-18], [50-59]**. Figure 6.5 present the theoretically optimum fiber orientation under static pressure, as shown in the figure the fiber orientation $[\pm 45°]_{3s}$ has the R.D. lower than fiber orientation $[0,90°]_{3s}$ (i.e the R.D. of orientation $[\pm 45°]_{3s}$ is the nearest zero), this mean the fiber orientation $[\pm 45°]_{3s}$ is more safe than the fiber orientation $[0,90°]_{3s}$ under static internal pressure load.

On the other hand the static pressure tests were conducted with two different end conditions for specimens. The specimens with open end have the higher burst pressure than other specimens under closed end for both fiber orientations and both method of manufacturing. This may be explained by the component of longitudinal stress σ_l which does not appear in open end test. i.e. for any fiber orientation the values of local stresses for open cylinder test are lower than that the values of local stresses for closed end test.

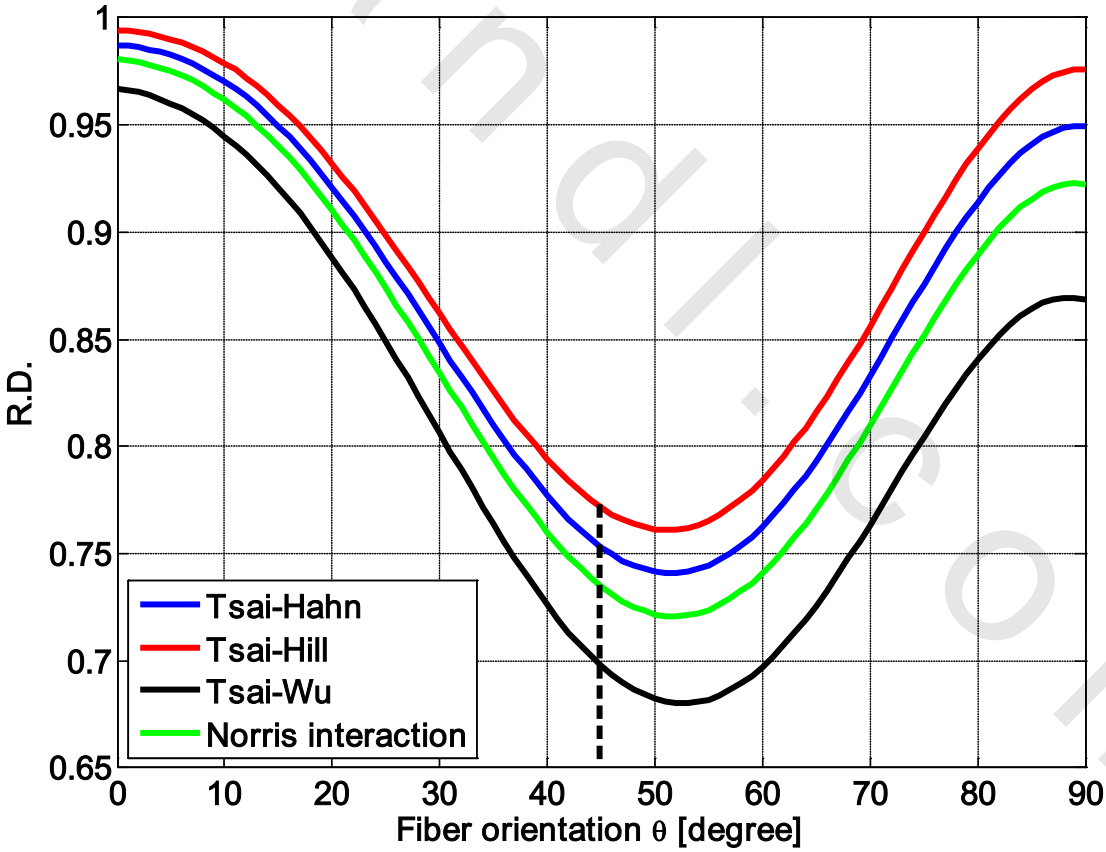

Figure 6.5 The theoretically optimum fiber orientation under hydrostatic pressure.

6.2.1.2 Effect of manufacturing method

The fiber volume fraction by weight (V_f) is defined as the ratio between the weight of fiber to the total weight of the specimen, representing the ductile portion in the composite, and the matrix, which represents the brittle one. Therefore, the volume fraction plays an important role in the mechanical properties of composite materials, resulting in the following:

(a)Bending tests

Under static bending tests, the specimens of method of manufacturing M_2 have the higher bending strength than the method M_1 with percentage about of 8% for both fiber orientations $[0,90°]_{3s}$ and $[\pm45°]_{3s}$. That is because the fiber volume fraction ratio (V_f) of new method of manufacturing M_2 was higher than the other method M_1, Appendix (3). The increase of the fiber volume fraction ratio (V_f) was causes increase the strong of bond interface with higher stiffness and higher static strength, on the other way, increasing the value of fiber volume fraction ratio (V_f) causes increase in the normal and transverse modulus in E-glass fiber/Epoxy, **[82]**.

(b) Torsion tests

Under static torsional tests, the specimens of method of manufacturing M_1 have higher torsional strength than the other method M_2 with percentage more than 60% for both fiber orientations $[0,90°]_{3s}$ and $[\pm45°]_{3s}$. That is because the delamination occurred between the outer layer of the specimens and other layers during torsional tests duo to the matrix cracking, that started and propagated along the circumference surface between them, then the disconnection between the outer layer and other was occurred, i.e. the failure behavior is the same of the one layer specimens.

(c) Internal pressure tests

For both fiber orientations, the specimens of method of manufacturing M_2 have higher burst pressure than the other method M_1 with percentage more than 40% for closed cylinder test and 45% for open cylinder test. This may be explained by the bond interface between the fiber and epoxy for method of manufacturing M_2 becomes stronger due to the increasing of the fiber volume fraction ratio (V_f) and increase in the normal and transverse modulus in E-glass fiber/Epoxy, this conclusion was found in the other study **[82]**.

6.2.1.3 Effect of hydraulic oil absorption

These tests were performed on specimens to study the effect of fiber oil absorption on the ultimate bending and shear strength.

The amount of fiber oil absorption, W (%), absorbed by each specimen was calculated from the relation;

$$W\ (\%) = \left(\frac{W_1 - W_o}{W_o}\right) \times 100$$

Where W (%), is the amount of fiber oil absorption in percentage; W_1 (g) the weight of the wet specimens at a given time, and W_o (g) the initial weight of the specimens. One can notice form the test results that:

1) The amount of fiber oil absorption was very low (~ 0.7%) because the fiber in GFRE specimens were sealed with Epoxy resin and the hydrophobic nature of fibers and the viscosity of the hydraulic oil almost prevent the specimens from oil absorption.
2) The ultimate bending and shear strength of the GFRE specimens were not affected by a small hydraulic oil absorption.

6.2.1.4 Static Failure Modes

The failure modes obtained during the static tests of woven roving GFRE with two fiber orientations, $[0,90°]_{3s}$ and $[\pm45°]_{3s}$ and two methods of manufacturing M_1 and M_2 for each orientation, under bending, torsional and internal pressure were shown in Figure 6.6. We found from the Figure that:

1) The failure modes of specimens under static bending test were shown in the Figures 6.6 (a) and 6.6 (b), one can be notice clearly that, the failure always prefers to propagate along one of bundles at the normal direction of fiber orientation (i.e. 90°), for both fiber orientations, $[0,90°]_{3s}$ and $[\pm45°]_{3s}$ with both methods of manufacturing M_1 and M_2. it was concentrated at the crossover points.
2) Under static torsion test, the failure modes of specimens, i.e. direction of failure propagation were deferent according to the fiber orientations, $[0,90°]_{3s}$ and $[\pm45°]_{3s}$. The failure always prefers to propagate at the same direction of fiber orientation, i.e. at (90°) for $[0,90°]_{3s}$ specimens and (45°) for $[\pm45°]_{3s}$ specimens, Figures 6.6 (c) and 6.6 (d) respectively, for methods of manufacturing M_1 and M_2. Add to that, for the specimens were manufactured with method of manufacturing M_2, the delamination occurred between specimen layers during torsional tests, then the disconnection

between first layer and second layer will cause the failure to occur in first layer only, Figure 6.6 (e).

3) Figure 6.6 (f) shows the failure modes of specimens under static internal pressure test for both fiber orientations, $[0,90°]_{3s}$ and $[\pm45°]_{3s}$, it is noted that, the leakage initiation damage mechanism, since at the high pressure levels, a pin hole formation in the region of effective length. Pin hole, which progresses from the inner surface to the outer surface, when the pin hole reaches the outer surface, the leakage damage begins. The leakage begins at the pin hole region as a small droplet. After a few seconds, the initiation point of intense leakage begins. Add to that, the specimens were manufactured with method of manufacturing M_2, the delamination occurred between specimen layers during internal pressure tests, and the testing oil was filled the gap between specimen layers, Figure 6.6 (g).

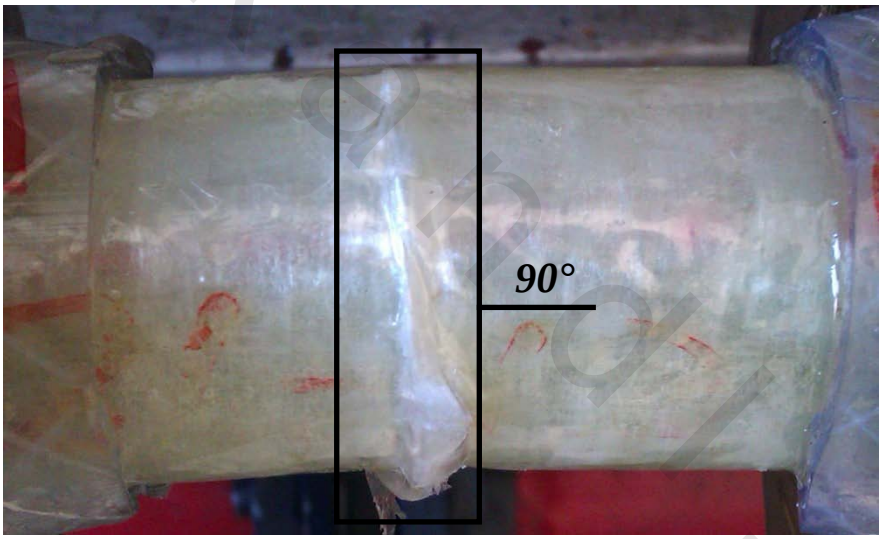

(a) The failure mechanism of M_2, $[0,90°]_{3s}$ specimens under bending

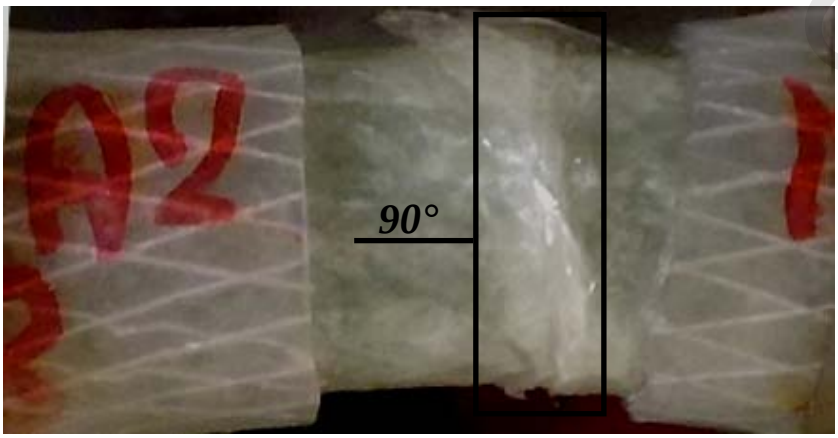

(b) The failure mechanism of M_1, $[\pm45°]_{3s}$ specimens under bending

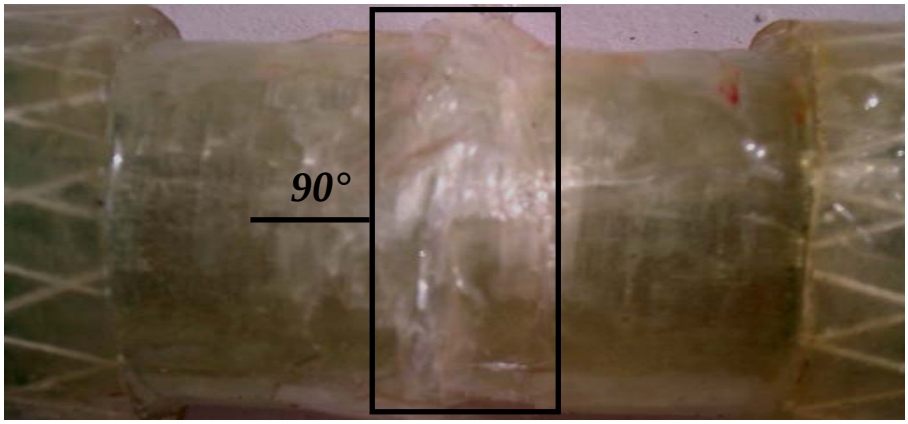

(c) The failure mechanism of M_1, $[0,90°]_{3s}$ specimens under torsion

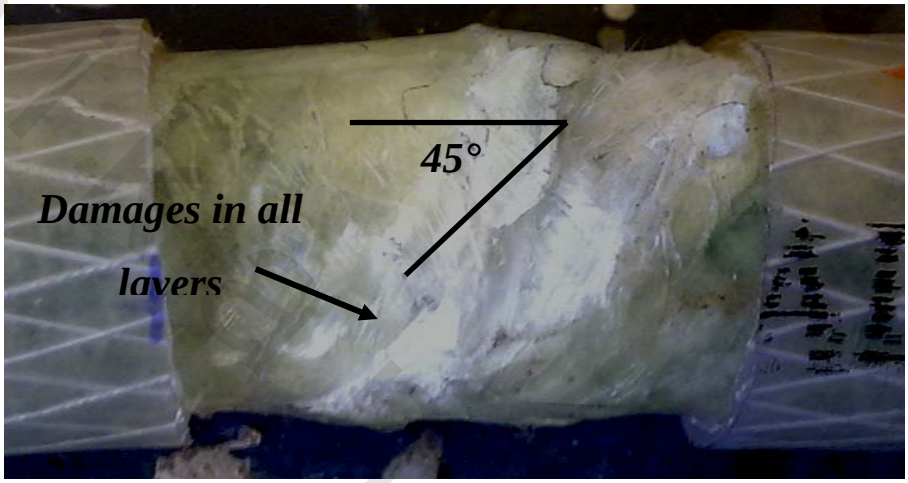

(d) The failure mechanism of M_1, $[\pm 45°]_{3s}$ specimens under torsion

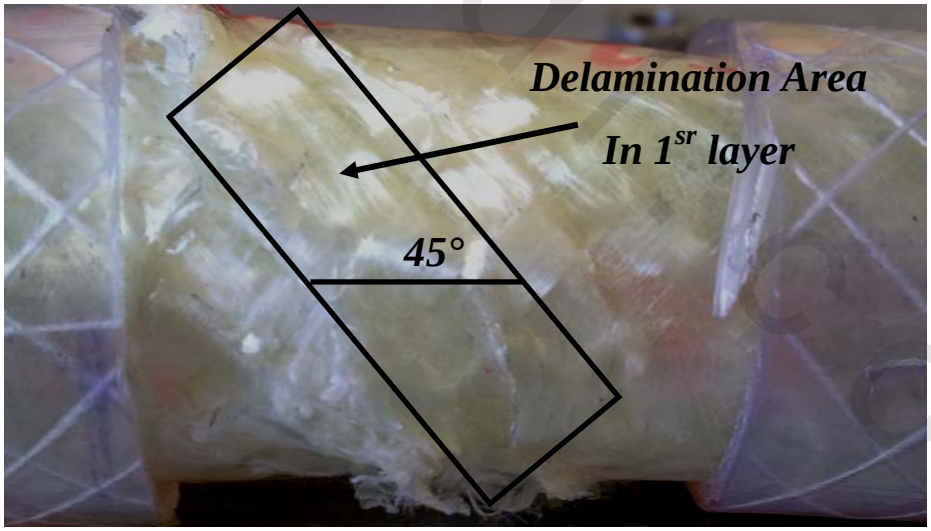

(e) The failure mechanism of M_2, $[\pm 45°]_{3s}$ specimens under torsion

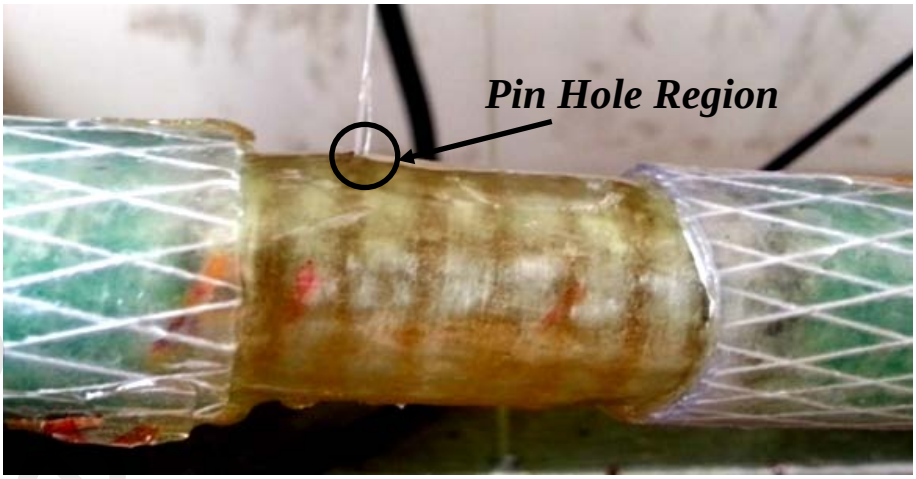

(f) leakage initiation damage mechanism of M_1, $[0,90°]_{3s}$ specimens

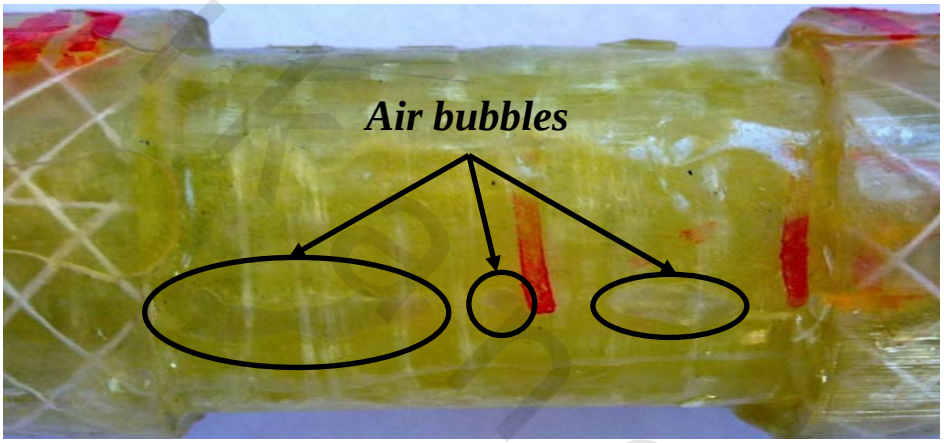

(g) Testing oil was filled the gap between specimen layers of M_2, $[0,90°]_{3s}$ specimens

Figure 6.6 The failure modes of specimens under static tests.

6.2.2 Fatigue tests

6.2.2.1 Completely Reversed Pure Bending or Torsion Tests

Specimens of both fiber orientations, $[0,90°]_{3s}$ and $[\pm45°]_{3s}$ with two methods of manufacturing M_1 and M_2 for each fiber orientation were tested under completely reversed pure bending and completely reversed pure torsion with stress ratio R = -1, Figures 5.5 to 5.9 and 5.12 to 5.16 for pure bending and pure torsion respectively. Using the power formula $\boldsymbol{\sigma_{max} = aN^b}$ for pure bending and $\boldsymbol{\tau_{max} = cN^d}$ for pure torsion have proved its suitability by giving acceptable values for the correlation factor, Tables 5.3 and 5.4.

A comparison between S-N curves for completely reversed pure bending and completely reversed pure torsion of both fiber orientations, $[0,90°]_{3s}$ and $[\pm45°]_{3s}$ with two methods of manufacturing M_1 and M_2, presented in the Figures 6.7 and 6.8 respectively.

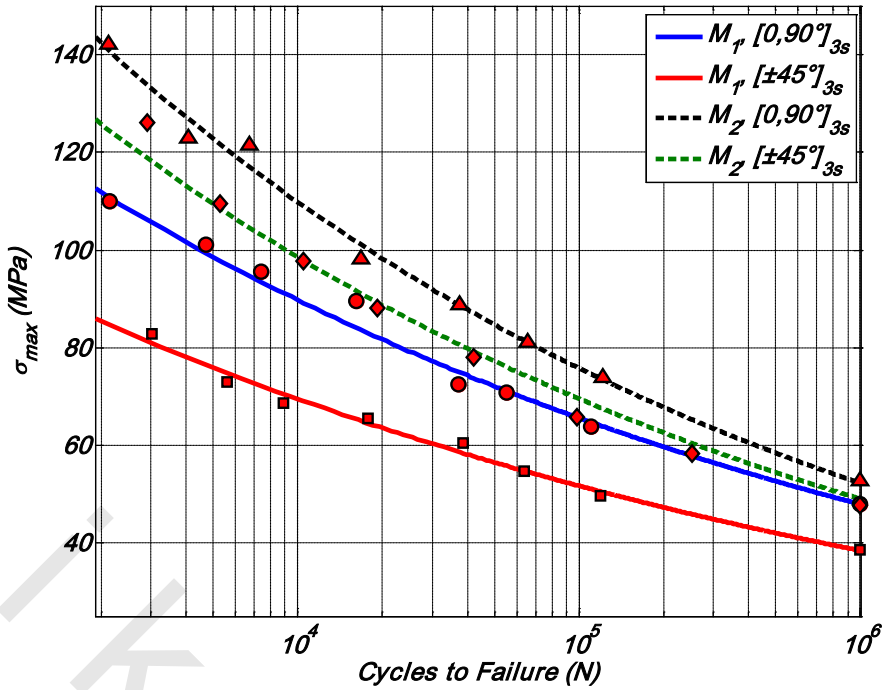

Figure 6.7 The S-N curves for both fiber orientations and both methods of manufacturing under completely reversed pure bending

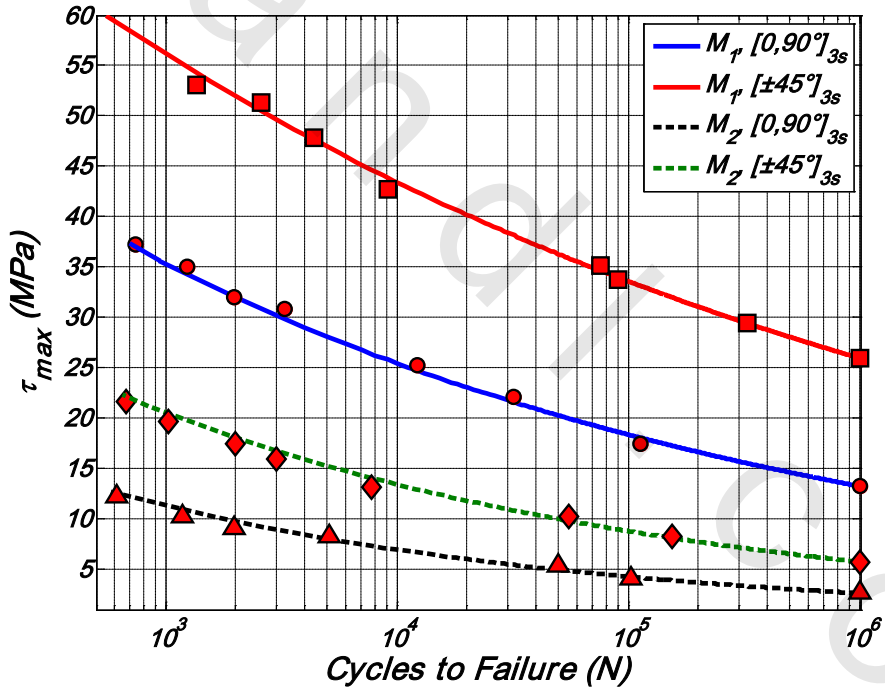

Figure 6.8 The S-N curves for both fiber orientations and both methods of manufacturing under completely reversed pure torsion

The values of fatigue constants (a) and (b) for pure bending and (c) and (d) for pure torsion, presented in Tables 5.3 and 5.4 respectively, were plotted in Figures 6.9 and 6.10 for pure bending, Figures 6.11 and 6.12 for pure torsion for comparison.

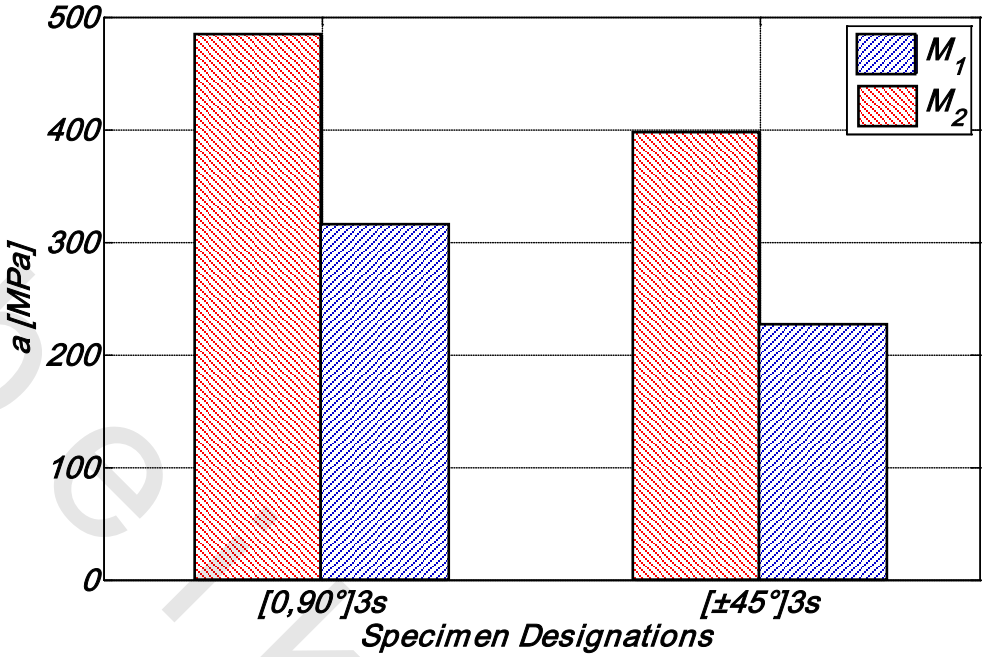

Figure 6.9 The Constant (a) as a function of fiber orientation and Methods of Manufacturing Under $P_r = 0$

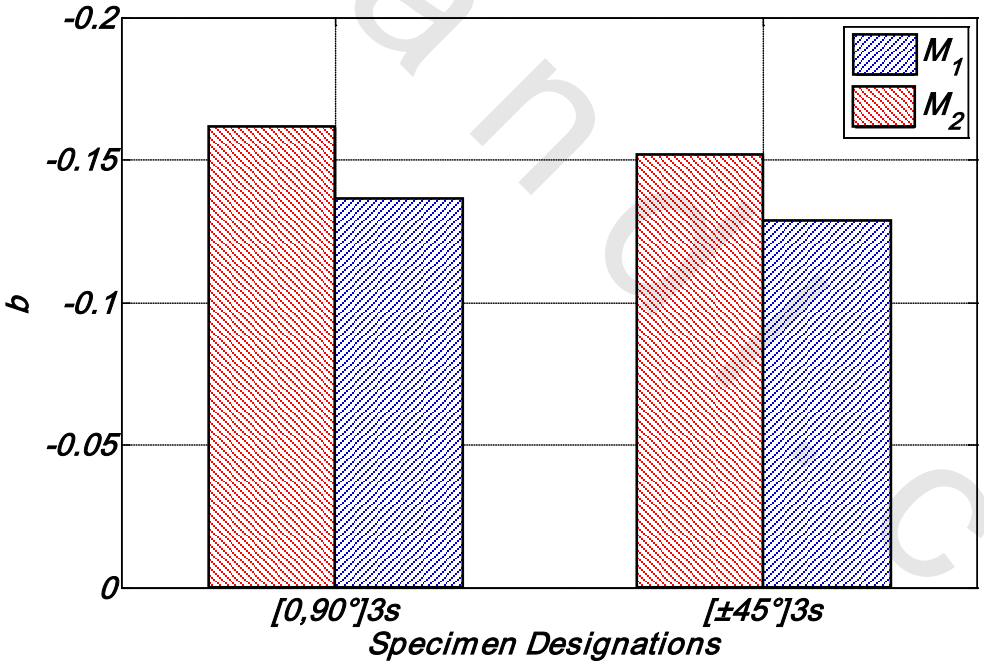

Figure 6.10 The Constant (b) as a function of fiber orientation and Methods of Manufacturing Under $P_r = 0$

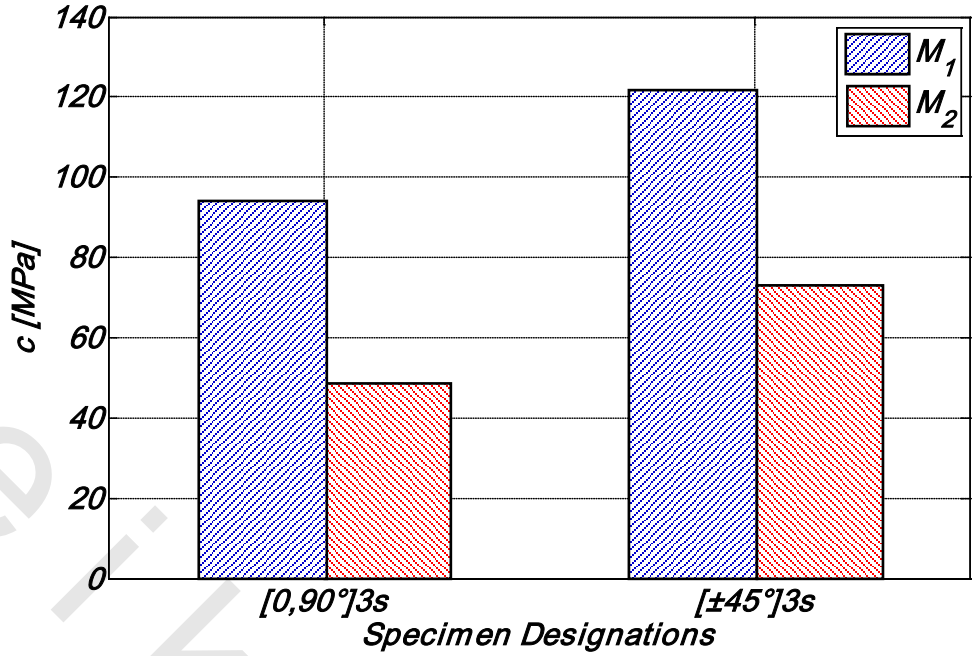

Figure 6.11 The Constant (c) as a function of fiber orientation and Methods of Manufacturing

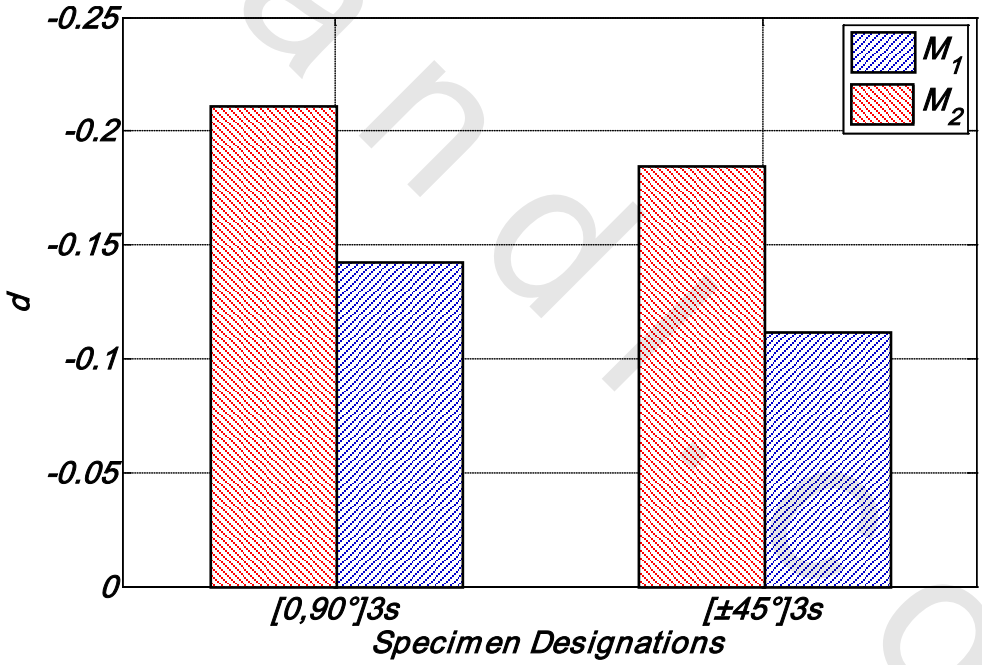

Figure 6.12 The Constant (d) as a function of fiber orientation and Methods of Manufacturing

6.2.2.1.1 Effect of Fiber Orientation

Figures 6.7 and 6.8 presents a comparison between both fiber orientations under completely reversed pure bending and torsion, according to maximum stress σ_{max} and to maximum torsion stress τ_{max}. it is noted that,

1) From the results of completely reversed pure bending, for method of manufacturing M_1 and M_2, the $[0,90°]_{3s}$ specimens have the higher bending stress σ_{max} than the other fiber orientation $[\pm45°]_{3s}$ specimens. This is due to the local stresses of the fiber orientation $[0,90°]_{3s}$ were higher than the local stresses of fiber orientation $[\pm45°]_{3s}$ as the static bending test.
2) Under completely reversed pure torsion, for both method of manufacturing M_1 and M_2, the $[\pm45°]_{3s}$ specimens have the higher torsion stress τ_{max} than the fiber orientation $[0,90°]_{3s}$ specimens. As a result of the local stresses of the fiber orientation $[0,90°]_{3s}$ also were lower than other fiber orientation $[\pm45°]_{3s}$.
3) Referring to Figures 6.9 to 6.12 for completely reversed pure bending and completely reversed pure torsion respectively, it is clear that, the values of fatigue constant (a) or (c) have a great dependence on the fiber orientations, while the deviation in the values of the power (b) or (d) is negligible and it may be considered constant.
4) Also value of fatigue constant (a) for any fiber orientation is higher than the value of fatigue constant (c). That is as a result of for any fiber orientation the values of local stresses under pure bending are lower than the values of local stresses under pure torsion.

6.2.2.1.2 Effect of manufacturing method

Figures 6.13 and 6.14 presents a comparison between methods of manufacturing under completely reversed pure bending and torsion, according to maximum stress σ_{max} or maximum torsion stress τ_{max}. As the steps of analysis show in section 6.2.1.2, we can be resulted in the following:

1) From the results of completely reversed pure bending for both fiber orientations $[0,90°]_{3s}$ and $[\pm45°]_{3s}$, the specimens were manufactured with method of manufacturing M_2 have higher bending stress σ_{max} than the other method M_1 at the same number of cycles to failure (N). This is due to the effect of increasing in the fiber volume fraction ratio (V_f) on increasing in the strong of bond interface and the normal and transverse modulus in E-glass fiber/Epoxy, as the effects were found in the static test.
2) Under completely reversed pure torsion for both fiber orientations $[0,90°]_{3s}$ and $[\pm45°]_{3s}$, the specimens were manufactured with method of manufacturing M_1 have higher torsion stress τ_{max} than the other method M_2. This may be due to delamination and disconnecting effect between the outer layer and other inner layers.

3) According to Figure 6.9 for completely reversed pure bending for both fiber orientations, the values of fatigue constant (a) for method of manufacturing M_2 are higher than the other method M_1.

4) Referring to Figure 6.11 for completely reversed pure torsion for both fiber orientations, the values of fatigue constant (c) for method of manufacturing M_1 are higher than the other method M_2.

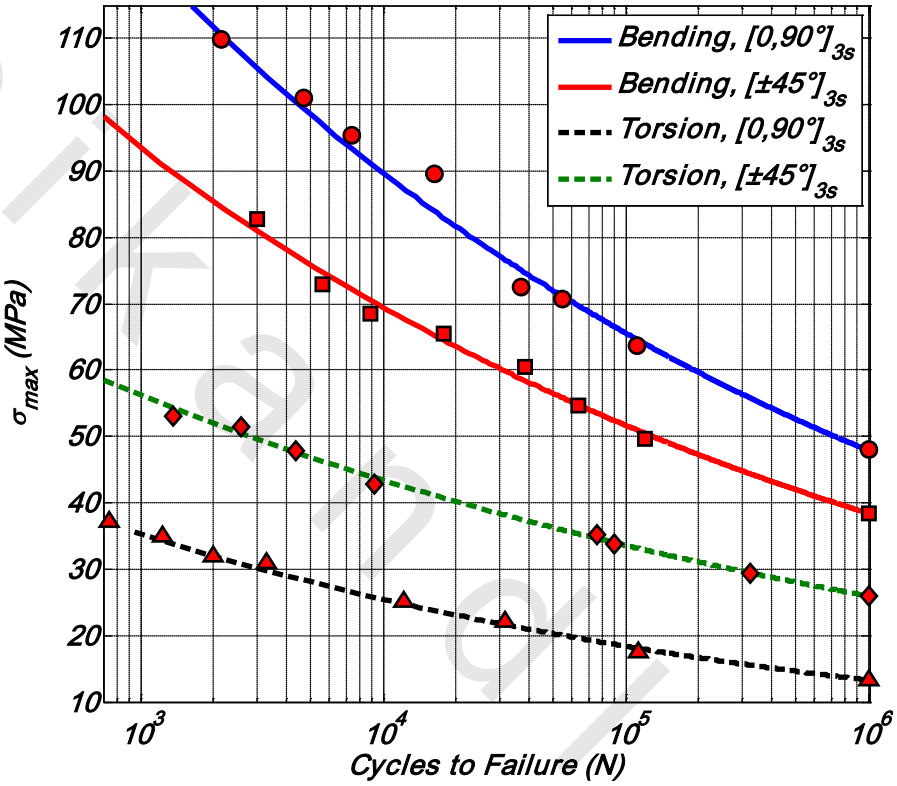

Figure 6.13 The S-N curves for both fiber orientations and method of manufacturing M_1 under completely reversed pure bending and torsion

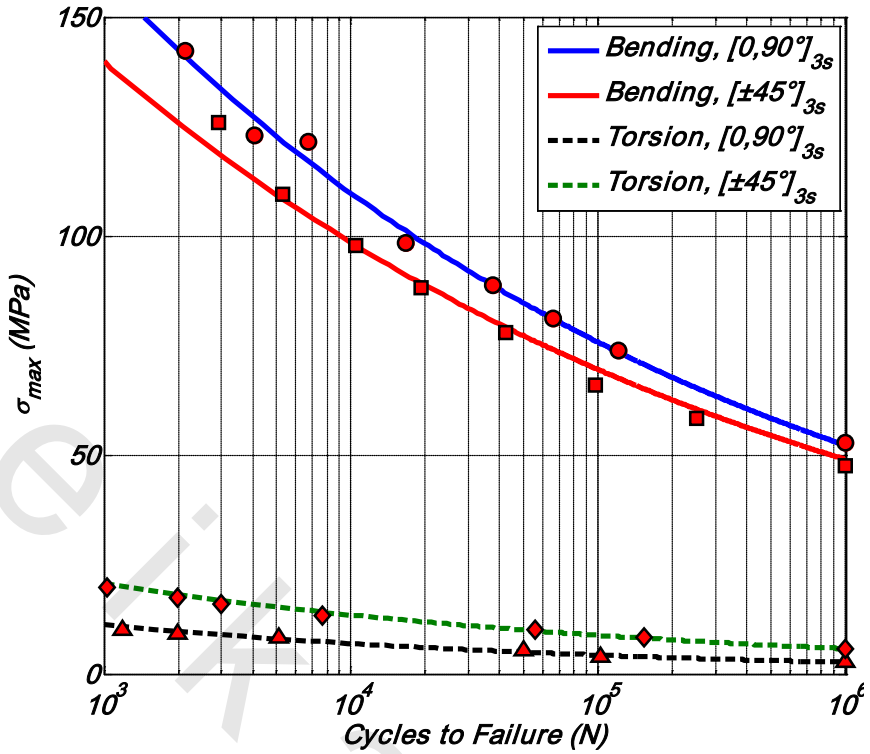

Figure 6.14 The S-N curves for both fiber orientations and method of manufacturing M_2 under completely reversed pure bending and torsion

6.2.2.1.3 Failure Modes

The failure modes obtained during the fatigue tests of woven roving GFRE with two fiber orientations, $[0,90°]_{3s}$ and $[\pm45°]_{3s}$ and two methods of manufacturing M_1 and M_2 for each orientation, under completely reversed pure bending and torsion were shown in Figures 6.15 and 6.16 for completely reversed pure bending and torsion respectively. We showed form the Figure that:

1) For both fiber orientations, $[0,90°]_{3s}$ and $[\pm45°]_{3s}$ and two methods of manufacturing M_1 and M_2 under completely reversed pure bending and torsion, the dispersed whitened area and intensity (i.e. failure area) is depend on the maximum stress levels or cycles to failure (N), i.e. the dispersed whitened area and intensity were decreased when stress level decreased or cycles to failure (N) increased, as shown in the figures 6.15 and 6.16.
2) In Figures 6.15 and 6.16, the dispersed whitened areas, especially concentrated around the fibers. The dispersed whitened areas represent matrix cracking, while those concentrated around the fibers represent debonding. Debonding has started by matrix cracking that reached the interface and overcame the interfacial bond strength **[84]**.
3) In Figure 6.15, the failure modes of both fiber orientations, $[0,90°]_{3s}$ and $[\pm45°]_{3s}$ and two methods of manufacturing M_1 and M_2 under completely reversed pure bending, one

can see clearly the failure always prefers to propagate at the direction of fiber orientation ($90°$) (i.e. in global state), it was concentrated at the crossover points.

4) In Figure 6.16, the failure modes of both fiber orientations, $[0,90°]_{3s}$ and $[\pm45°]_{3s}$ and two methods of manufacturing M_1 and M_2 under completely reversed pure torsion, one can see clearly the failure always prefers to propagate along one of bundles at the same direction of fiber orientation (i.e. in local state), it was concentrated at the crossover points. Add to that, the specimens were manufactured with method of manufacturing M_2, the delamination occurred between specimen layers during torsional tests, then the disconnection between first layer and second layer will cause the failure to occur in first layer only.

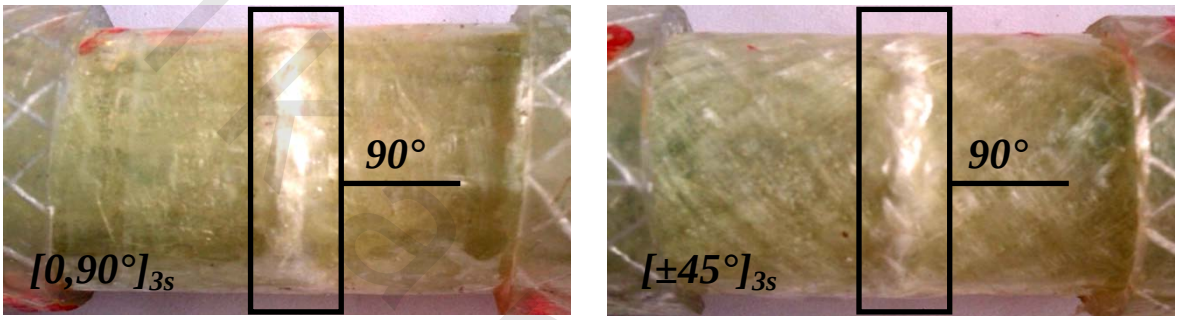

(a) High Stress Level ($10^3 \leq N \leq 10^4$)

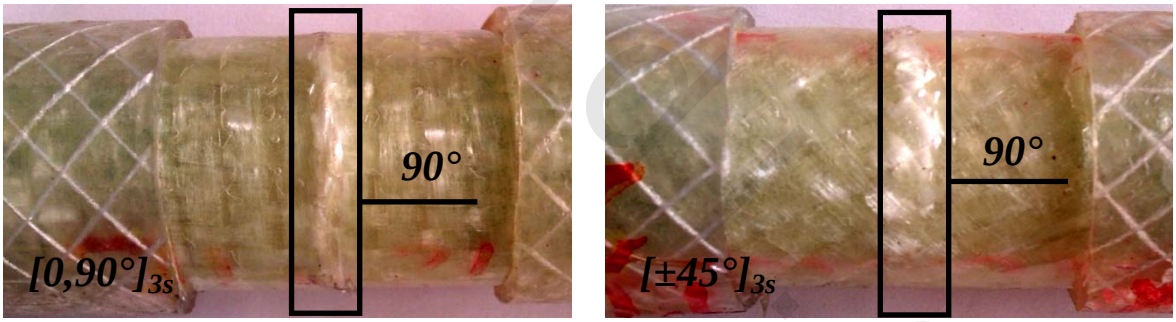

(b) Medium Stress Level ($10^4 \leq N \leq 10^5$)

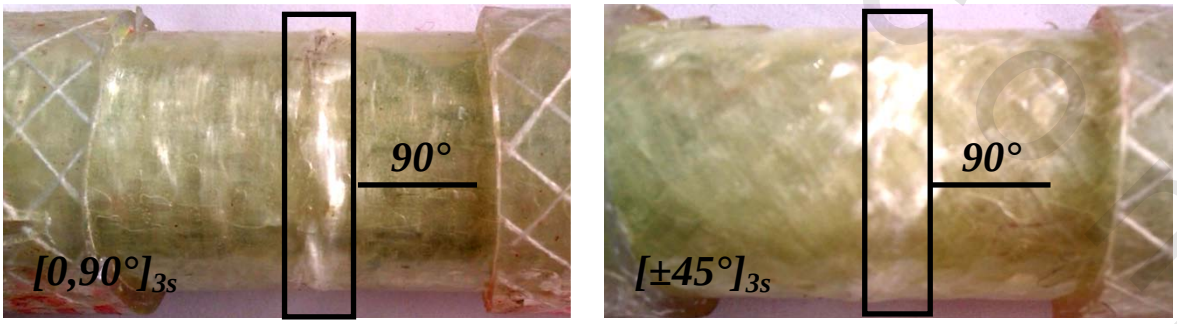

(c) Low Stress Level ($10^3 \leq N \leq 10^4$)

Figure 6.15 The Dispersed Whitened Areas under Completely Reversed Pure Bending for Both Fiber Orientations.

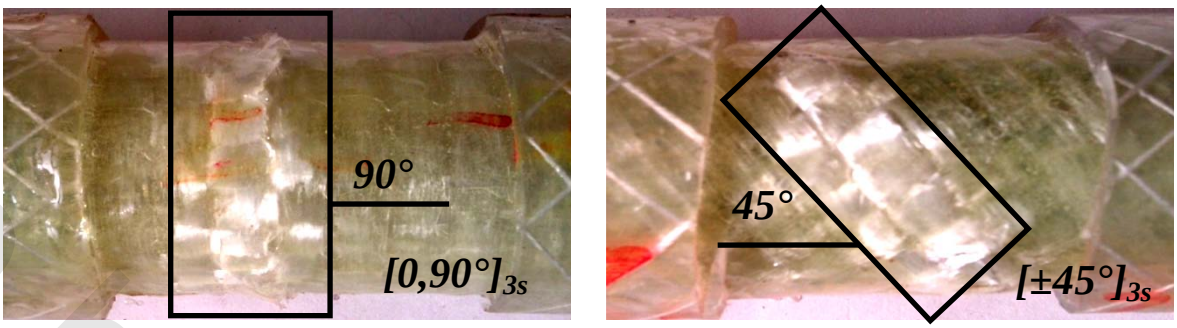

(a) High Stress Level ($10^3 \leq N \leq 10^4$)

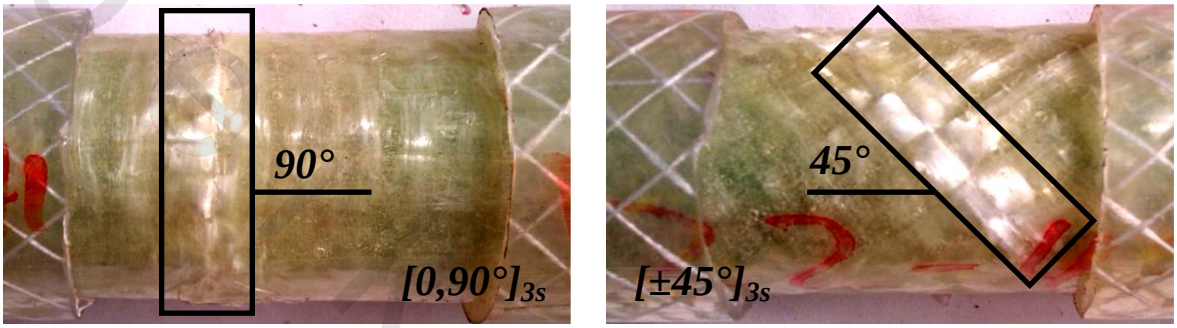

(b) Medium Stress Level ($10^4 \leq N \leq 10^5$)

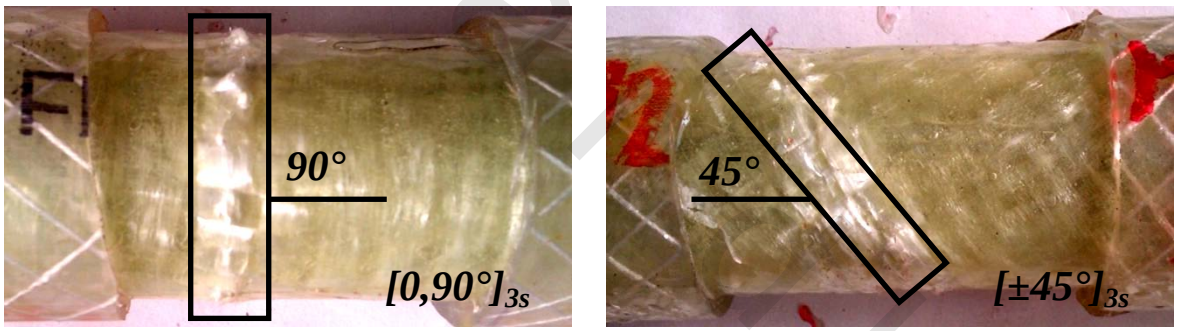

(c) Low Stress Level ($10^3 \leq N \leq 10^4$)

Figure 6.16 The Dispersed Whitened Areas under Completely Reversed Pure Torsion for Both Fiber Orientations.

6.2.2.2 Combined Completely Reversed Bending and Internal Pressure Tests

Specimens with two fiber orientations, $[0,90°]_{3s}$ and $[\pm45°]_{3s}$ and two methods of manufacturing M_1 and M_2 for each fiber orientation, were tested under combined internal hydrostatic pressure and completely reversed bending, (R=-1) with different pressure ratios between the applied pressure and burst pressure ($P_r = P/P_{max} = 0, 0.25, 0.5, 0.75$), Figures 6.17 to 6.20. Using the power formula $\sigma_{max} = aN^b$ have proved its suitability by giving acceptable values for the correlation factor.

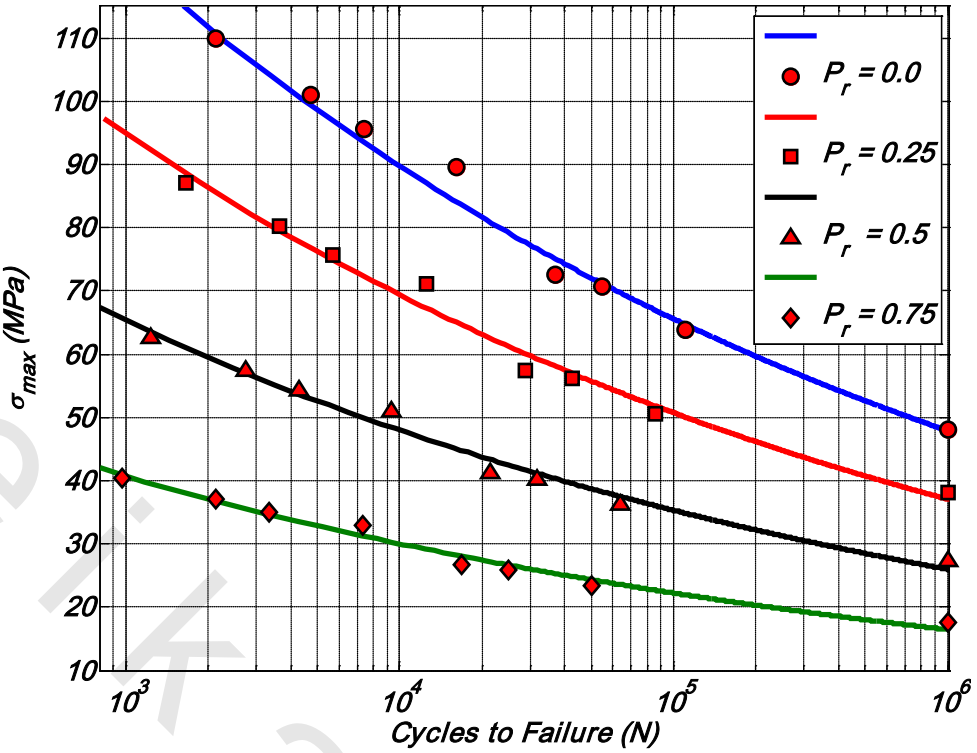

Figure 6.17 S-N Curve for $[0,90°]_{3s}$ and M_1 specimens

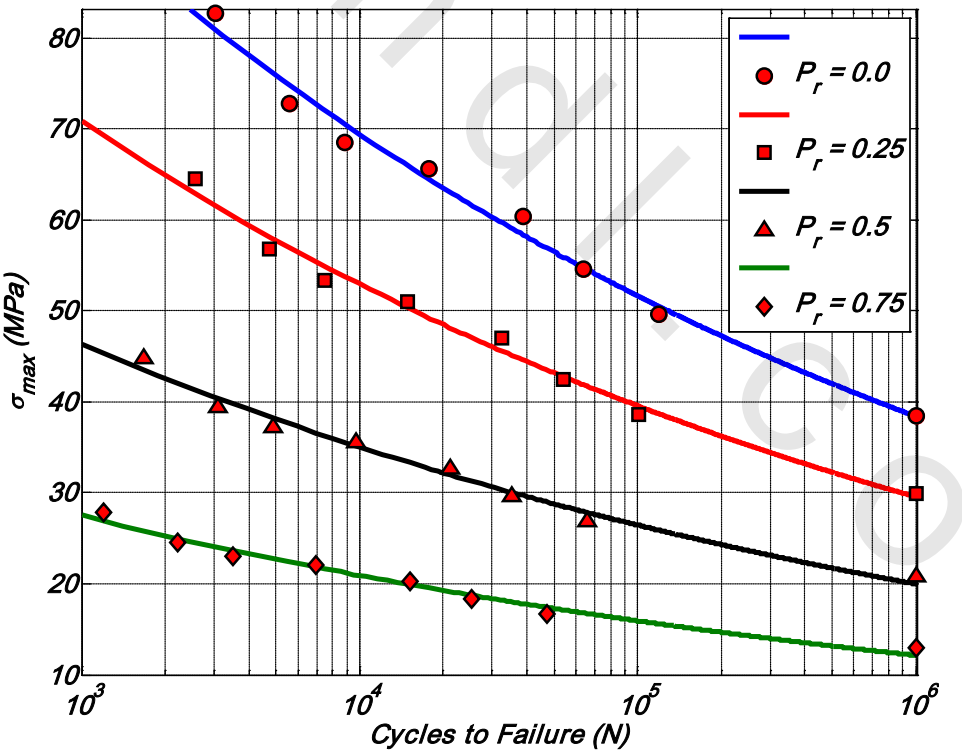

Figure 6.18 S-N Curve for $[\pm 45°]_{3s}$ and M_1 specimens

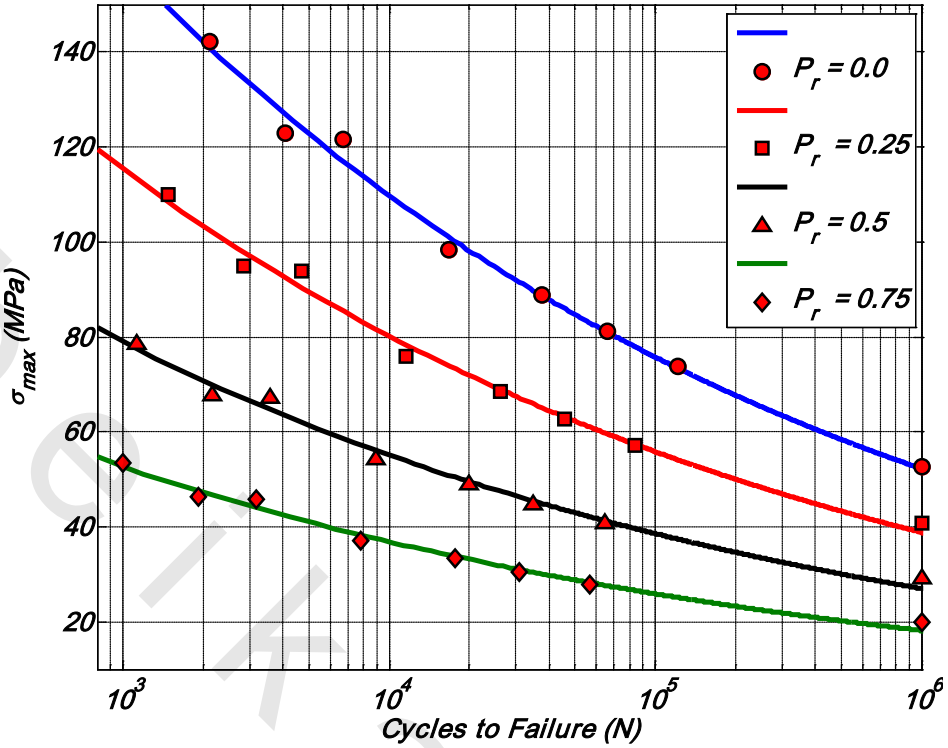

Figure 6.19 S-N Curve for $[0,90°]_{3s}$ and M_2 specimens

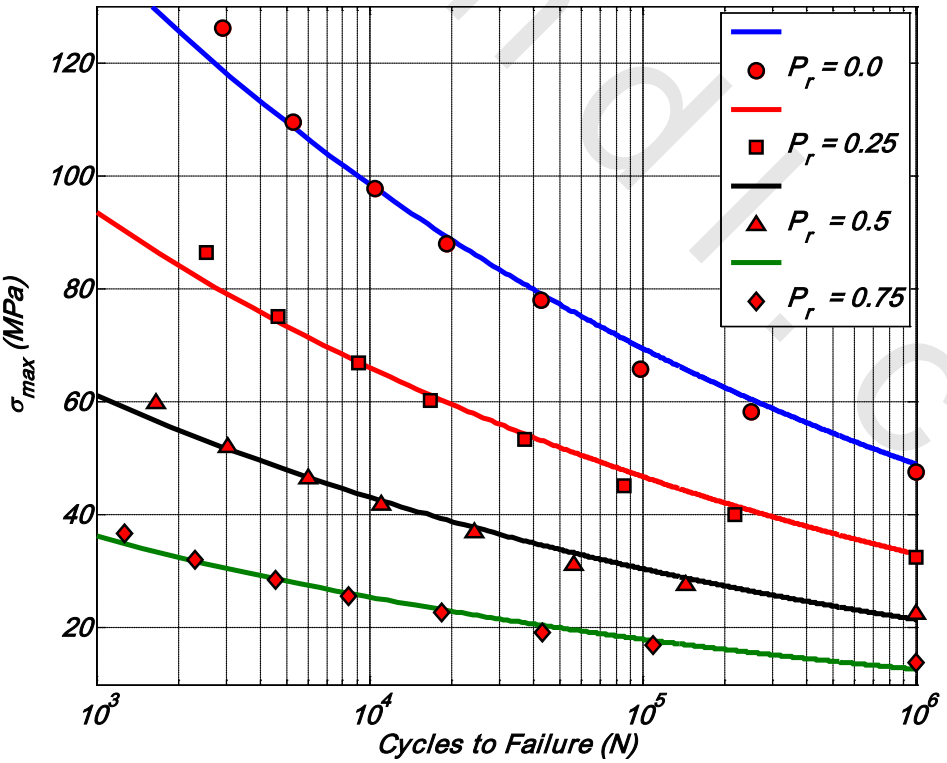

Figure 6.20 S-N Curve for $[\pm 45°]_{3s}$ and M_2 specimens

Tables A3.43 to A3.54 were plotted in Figures 6.21 and 6.22 for $P_r = 0.25$, 6.23 and 6.24 for $P_r = 0.5$, 6.25 and 6.26 for $P_r = 0.75$.

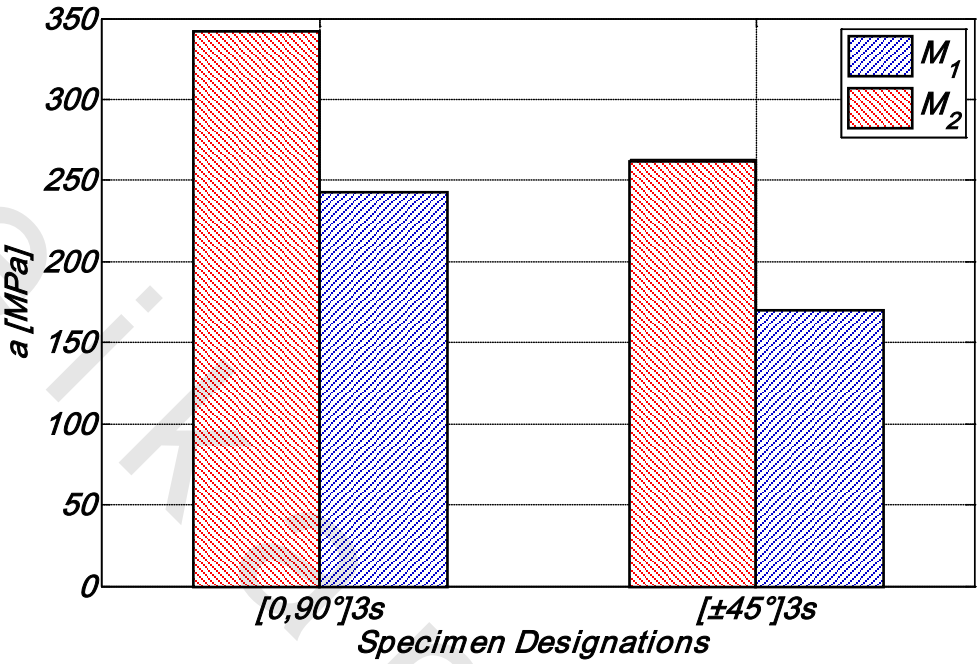

Figure 6.21 The Constant (a) as a function of fiber orientation and Methods of Manufacturing with $P_r = 0.25$

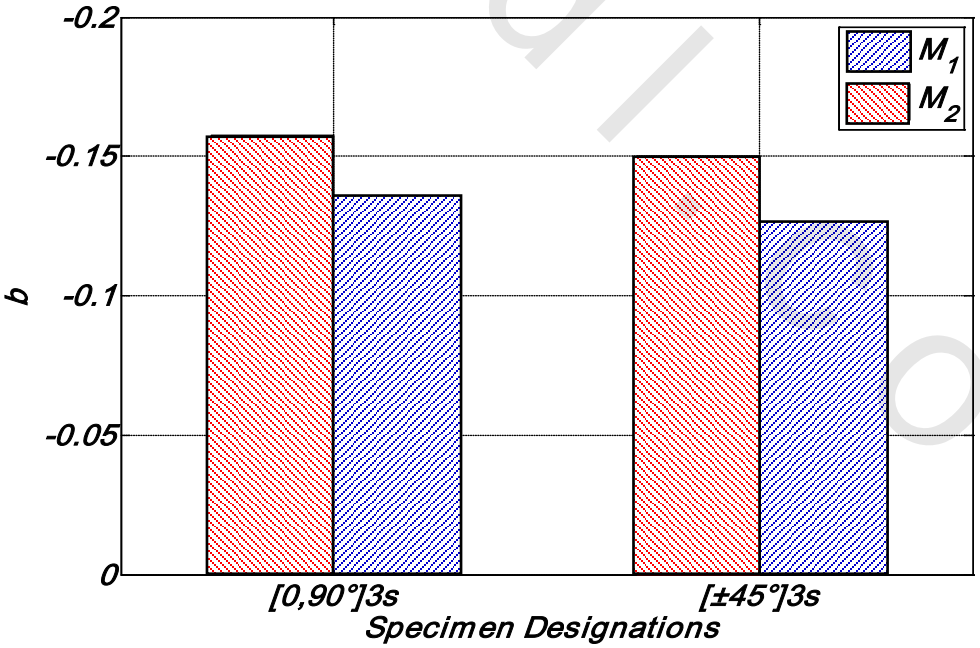

Figure 6.22 The Constant (b) as a function of fiber orientation and Methods of Manufacturing wit

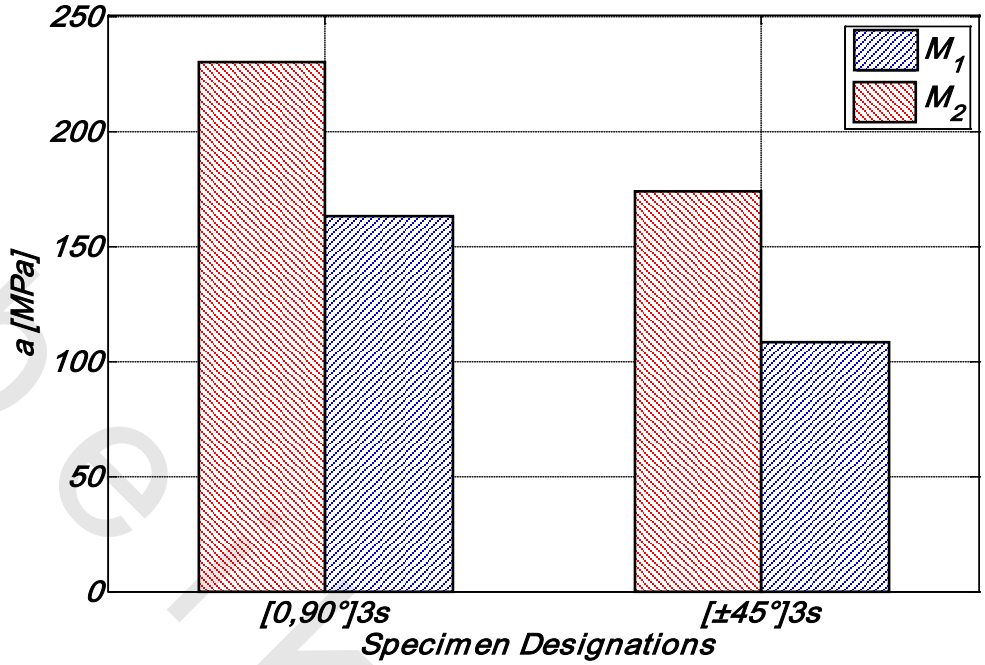

Figure 6.23 The Constant (a) as a function of fiber orientation and Methods of Manufacturing with $P_r = 0.5$

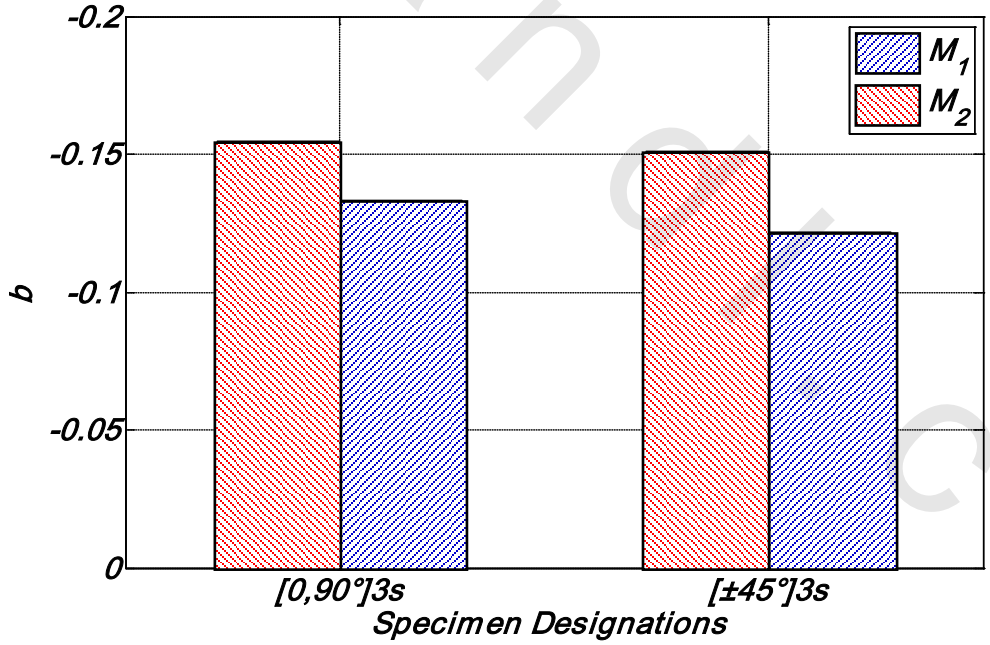

Figure 6.24 The Constant (b) as a function of fiber orientation and Methods of Manufacturing with $P_r = 0.5$

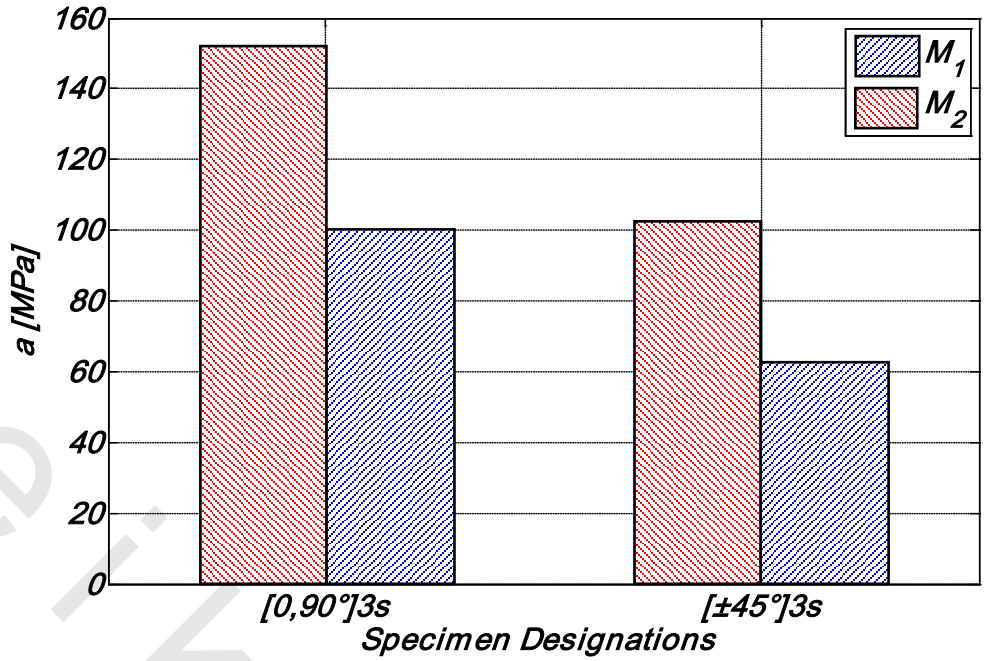

Figure 6.25 The Constant (a) as a function of fiber orientation and Methods of Manufacturing with $P_r = 0.75$

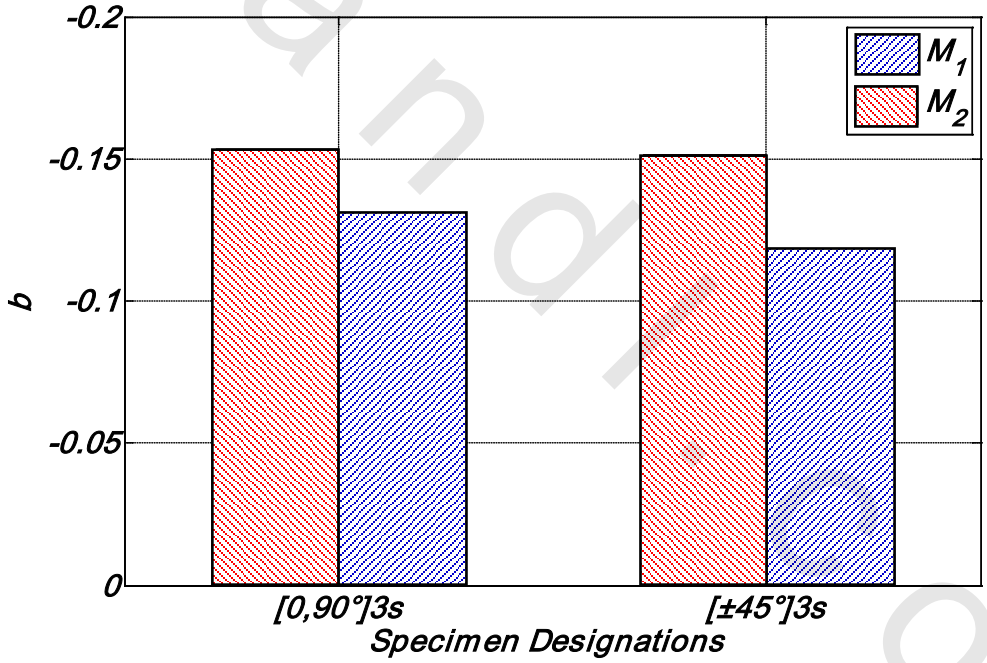

Figure 6.26 The Constant (b) as a function of fiber orientation and Methods of Manufacturing with $P_r = 0.75$

Analyzing the values of two constants (a) and (b) taking into account the variation of fiber orientations, methods of manufacturing, and pressure ratios, and considering Figures 6.17 to 6.20 resulted in the following:

1) For both fiber orientations, $[0,90°]_{3s}$ and $[\pm45°]_{3s}$ and two methods of manufacturing M_1 and M_2, the S-N curves for different pressure ratios (P_r) are almost parallel to each other.
2) For both fiber orientations, $[0,90°]_{3s}$ and $[\pm45°]_{3s}$ and two methods of manufacturing M_1 and M_2, the S-N curves for pressure ratio ($P_r = 0$) has the highest stress, the S-N curves for pressure ratio ($P_r = 0.75$) has the lowest stress, while the other curves for the remaining stress ratios laid in between, with descending order.
3) The deviation in the values of the power (b) at different pressure ratios (P_r) is negligible and it may be considered constant, the average value of (b) was calculated and considered to be used at any pressure ratio (P_r), as the corresponding standard deviation was found to have acceptable values, as shown in Table 6.1.
4) The values of the fatigue constant (a) were found to depend on the pressure ratio (P_r) for all fiber orientations

Table 6.1: Fatigue Constants (a) and Average values of (b) for tested specimens

Fiber orientation	Method of Manufacturing	Average value of (b)	Standard Deviation (%)	a (MPa)			
				$P_r = 0$	$P_r = 0.25$	$P_r = 0.5$	$P_r = 0.75$
[0,90°]	**M_1**	-0.13388	0.002659	314.3	242.5	163.2	99.88
	M_2	-0.15673	0.003395	484.4	341.9	229.2	151.6
[±45°]	**M_1**	-0.12368	0.004631	226.6	169.7	107.5	62.09
	M_2	-0.15095	0.00058	397.2	263.3	173.6	102.7

Where: M_1: The first method of manufacturing

M_2: The second method of manufacturing

6.2.2.2.1 Effect of Fiber Orientation

When dealing with the effect of the fiber orientation with two methods of manufacturing M_1 and M_2, the local stresses must be taken into account, considering the local stresses resulted in the following:

1) As mentioned before, the deviation in the values of the power (b) at different pressure ratios (P_r) is negligible and it may be considered to be constant, i.e., the change in fiber orientations don't affect the values of the power (b).

2) As shown in the Figures 6.21, 6.23 and 6.25, a constant (a) of the $[0,90°]_{3s}$ specimens was higher than the $[\pm45°]_{3s}$ specimens, this means that the value of the constant (a) was found to depend on fiber orientation angle (θ), as the fiber orientation increases the value of (a) will decreases, i.e. the fatigue strength decreased, for different pressure ratios (P_r), According to Figures 6.27 to 6.29, because the $[0,90°]_{3s}$ specimens have local stresses lower than the $[\pm45°]_{3s}$ specimens, Table 3.4.

6.2.2.2.2 Effect of manufacturing method

For both fiber orientations, $[0,90°]_{3s}$ and $[\pm45°]_{3s}$ with different pressure ratios (P_r), the specimens were manufactured with method of manufacturing M_2 have higher maximum stress σ_{max} than the other method M_1 at the same number of cycles to failure (N), Figures 6.27 to 6.29. This was pointed to the values of fatigue constant (a) for method of manufacturing M_2 are higher than the other method M_1, According to Figures 6.21, 6.23 and 6.25. This is due to an increase in the value of fiber volume fraction ratio (V_f) in the new method of manufacturing M_2, this is causes increasing in the strong of bond interface and the normal and transverse modulus in E-glass fiber/Epoxy, this analysis were found in both static and completely reversed bending test.

6.2.2.2.3 Effect of Pressure ratio (Pr)

The values of fatigue constant (a) of the maximum stress equations are obtained as functions of the pressure ratio (P_r), for both fiber orientations, $[0,90°]_{3s}$ and $[\pm45°]_{3s}$ with two methods of manufacturing M_1 and M_2 for each fiber orientation, and given in Tables 6.1 and 6.2. Figure 6.30 showed the relation between the pressure ratio (P_r) and fatigue constant (a) for all testing specimens, it is clear that:

1) The value of fatigue constant (a) was found to depend on the pressure ratio (P_r), for both fiber orientations, with two methods of manufacturing, as the following relations indicated in Table 6.1.
2) Using the exponential law: $\boldsymbol{a = e * exp(f * P_r)}$, have proved its suitability by given acceptable values for the correlation factor, and the constants (e) and (f), of the used exponential law were given in Table 6.2.
3) Increasing the value of pressure ratio (P_r) causes a decrease in the corresponding value of fatigue constant (a), i.e. the pressure ratio (P_r) had a detrimental effect on the fatigue strength. This may be explained by the effect of the tensile mean stress that was coming

from the longitudinal stress component (σ_l) of the applied pressure inside the specimens, where, the tensile mean stress always tends to decrease their fatigue resistance, **[149]**.

Table 6.2: Fatigue Constants (a) as a function of pressure ratio (P_r)

Fiber orientation	Method of Manufacturing	a (MPa)	Correlation factor
$[0,90°]_{3s}$	M_1	$a = 322 * \exp(-1.396 * P_r)$	0.9818
	M_2	$a = 487.9 * \exp(-1.511 * P_r)$	0.9984
$[\pm45°]_{3s}$	M_1	$a = 232.3 * \exp(-1.56 * P_r)$	0.9814
	M_2	$a = 399.3 * \exp(-1.719 * P_r)$	0.9981

Where: M_1: The first method of manufacturing

M_2: The second method of manufacturing

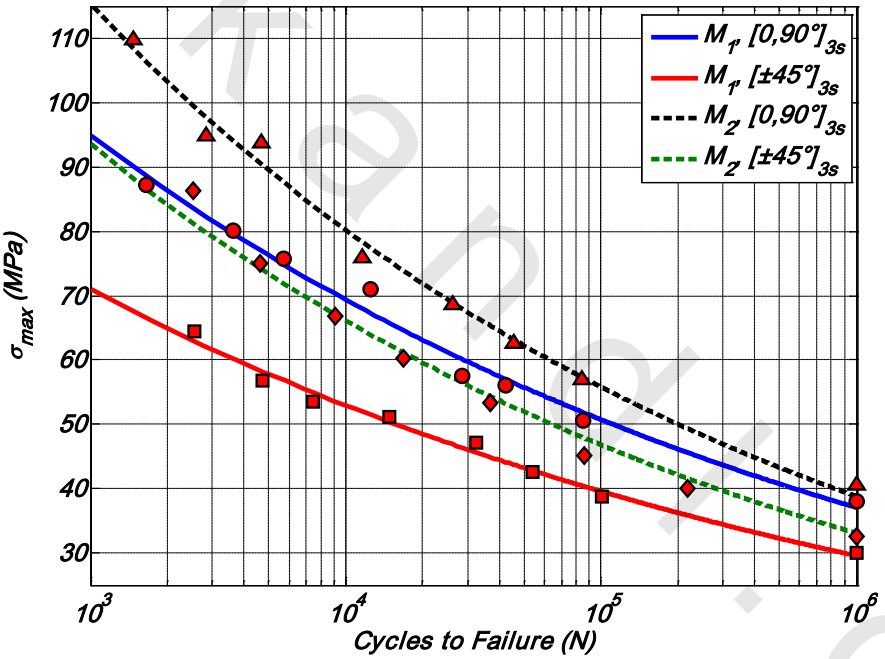

Figure 6.27 The S-N curves for both fiber orientations and both methods of manufacturing under combined completely reversed bending plus internal pressure with $P_r = 0.25$

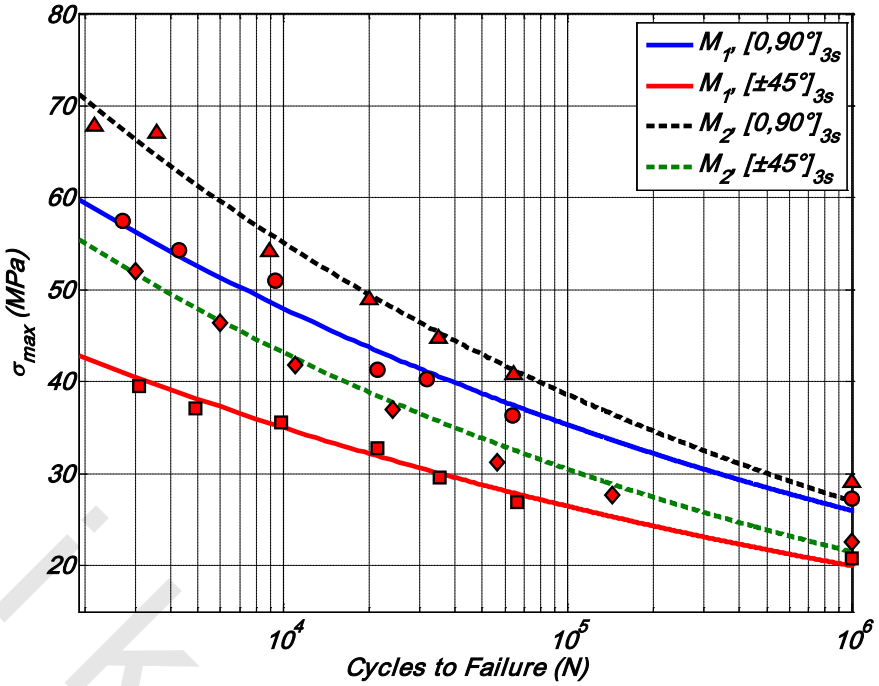

Figure 6.28 The S-N curves for both fiber orientations and both methods of manufacturing under combined completely reversed bending plus internal pressure with $P_r = 0.5$

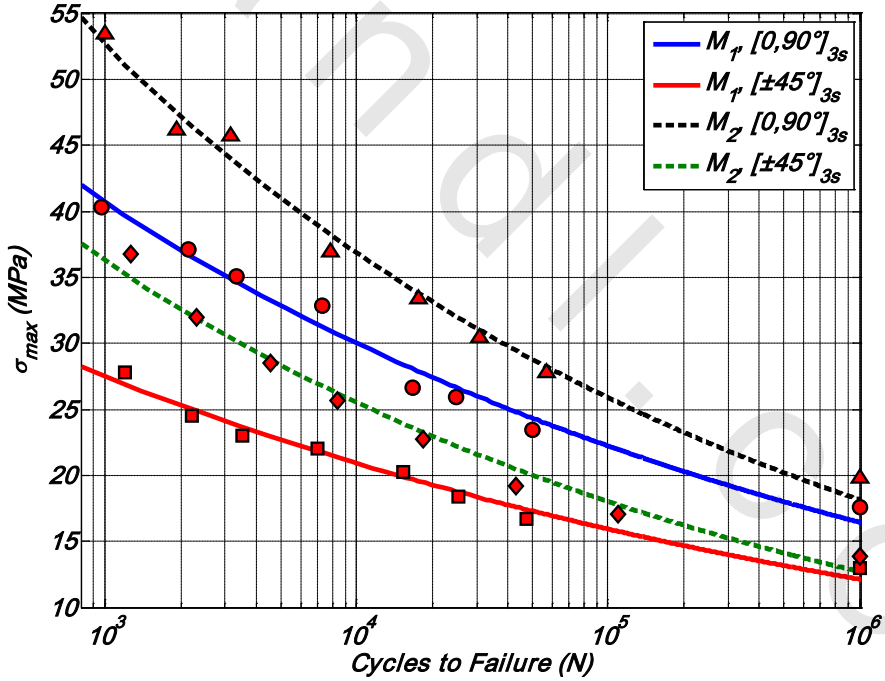

Figure 6.29 The S-N curves for both fiber orientations and both methods of manufacturing under combined completely reversed bending plus internal pressure with $P_r = 0.75$

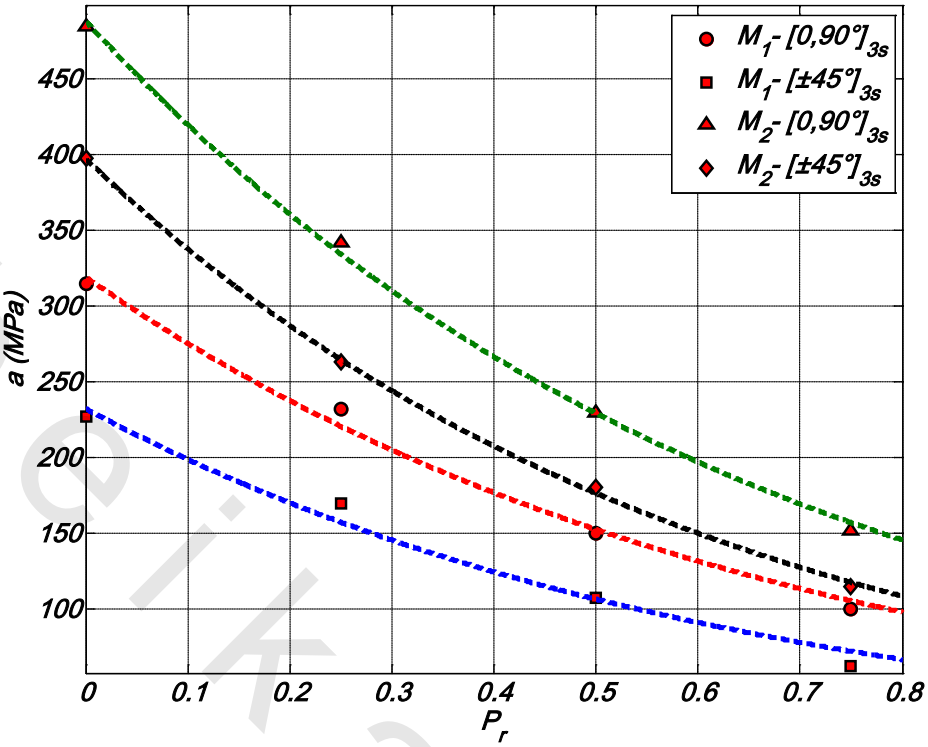

Figure 6.30 Effect of Pressure ratios (P_r) on the fatigue constant (a) for both fiber orientations and both methods of manufacturing

6.2.2.2.4 Failure Modes

The failure modes obtained during the fatigue tests for this group of tests were shown in Figure 6.31. During these tests, three damage mechanisms were observed.

The first damage mechanism was whitening. At this stage debonding and delamination occurred. White zones grew wider and propagate along one of bundles at the fiber direction. As the number of cycles increases, the small cracks are combined as a thin line. These thin lines form the strips and then the strips form the concentrated whitening at the crossover points (whitening initiation).

Especially at the high stress levels, the concentrated whitening region was observed and grewed rapidly. At this region a pin hole formation begins. Due to Pin hole, which progresses from the inner surface to the outer surface, was opened and closed under the effect of tension-compression as a result of bending moment at each loading cycle. When the pin hole reaches the outer surface, the leakage damage begins.

The leakage begins at the pin hole region as a small droplet. After a few number of cycles, the initiation point of intense leakage begins.

At the last stage in the damage progress, fiber breakage or matrix damage takes place. These were an unstable phases in which the specimens start losing its structural integrity.

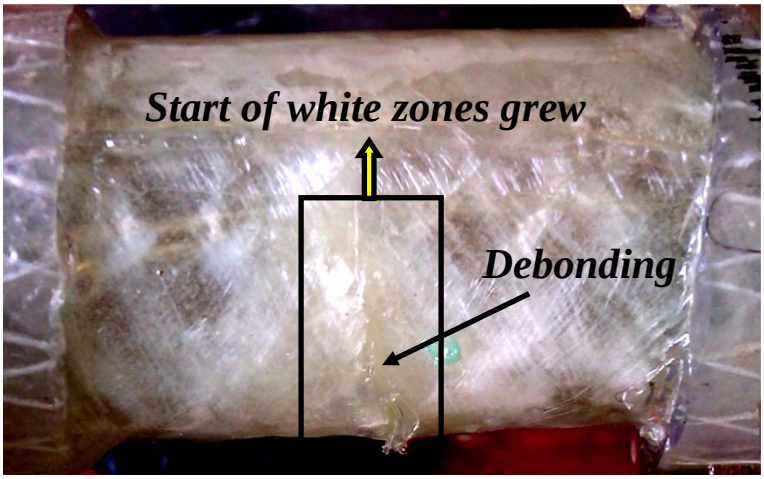

First stage of Damage Mechanism

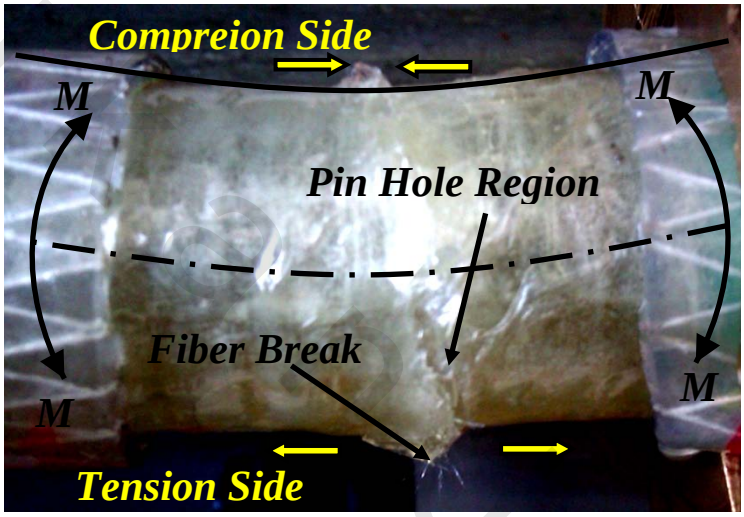

Second stage of Damage Mechanism

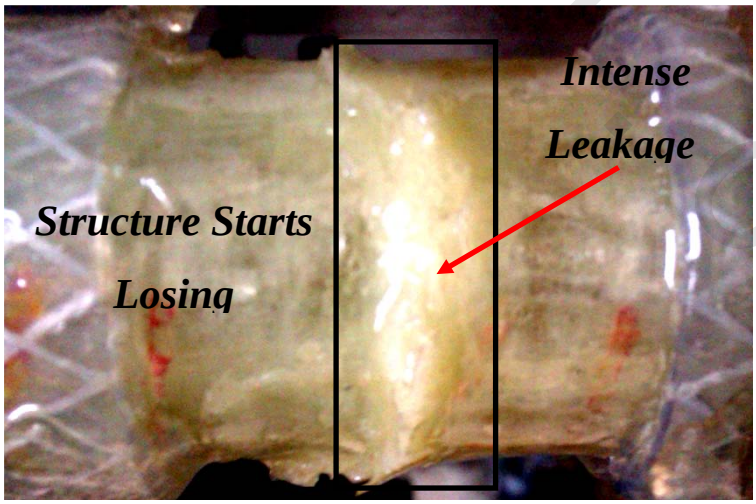

Last stage of Damage Mechanism

Figure 6.31 The Damage Mechanism Under internal hydrostatic pressure and completely reversed bending for both fiber orientations with both methods of manufacturing

6.3 Effect of Mean Stress:

It is well known that, the compressive mean stress has no effect on the fatigue behavior of different metals, which may be beneficial; while the tensile mean stress always tends to decrease their fatigue resistance.

In the present study, although there are no mean stresses produced from bending moment loading, i.e. R = -1, but the internal hydrostatic pressure produce this type of stress. Which has a positing value and must be taken into consideration. In this section, the effect of the mean stress will be discussed.

The effect of mean stresses on the fatigue behavior of Glass Fiber-Reinforced Epoxy (GFRE) is studied via testing closed end, woven-roving specimens with two fiber orientations $[0,90°]_{3s}$ and $[\pm45°]_{3s}$ and two methods of manufacturing M_1 and M_2, with different pressure ratios ($P_r = 0, 0.25, 0.5, 0.75$). For all pressure ratios, the specimens were subjected to tension-compression local and global stress components that are clearly shown in the Figures 6.32, 6.33 for fiber orientation $[0,90°]_{3s}$, and Figures 6.34, 6.35 for fiber orientation $[\pm45°]_{3s}$, according to Table 3.4.

The hoop- amplitude diagrams were plotted at different lives for both fiber orientations, $[0,90°]_{3s}$ and $[\pm45°]_{3s}$ and two methods of manufacturing M_1 and M_2, as shown in the Figures 6.36 to 6.39. The need for groups of specimens, one at each pressure ratio, having exactly the same life; make it impossible to use the actual experimental data in plotting the hoop-amplitude relations. However, the uses of the fitted S-N equations that have a high correlation factors to find out the required points may be a good idea;

Plotting the hoop-amplitude relation for the $[0,90°]_{3s}$ and $[\pm45°]_{3s\ 3s}$ with two methods of manufacturing M_1 and M_2 specimens under the different pressure ratios and using the static pressure point $(S_H, 0)$ gave straight line relations, as shown in Figures 6.36 to 6.39, with high correlation factors. The relations between the hoop and amplitude stresses are given in Tables 6.3 to 6.6.

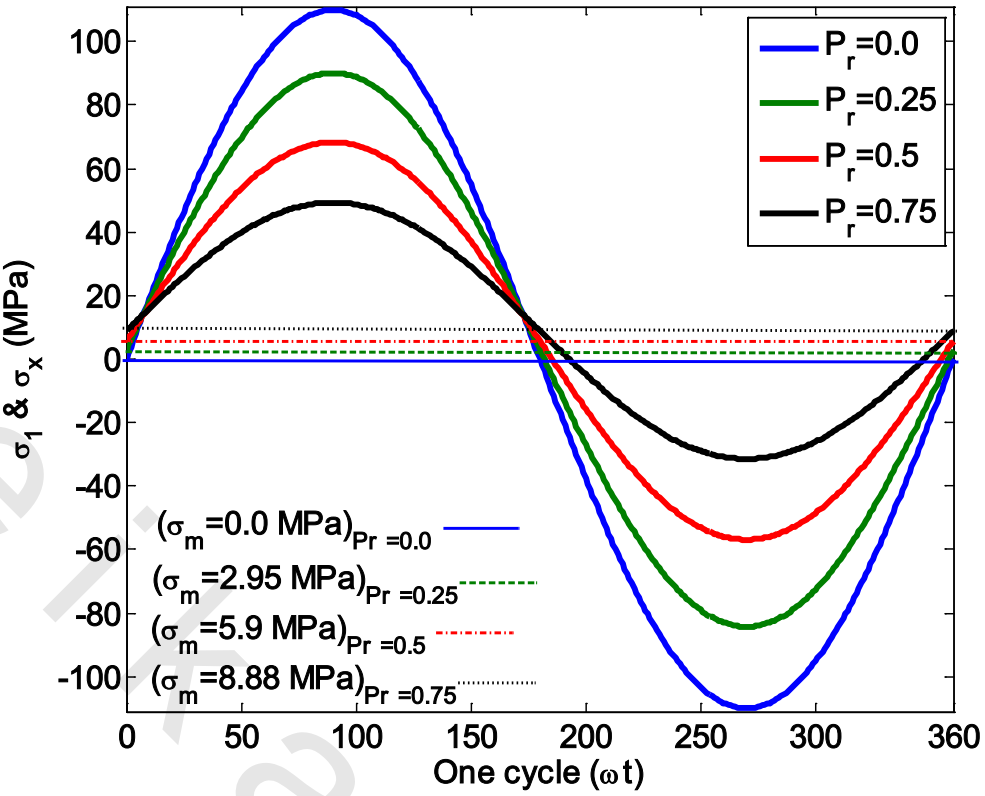

Figure 6.32 Tension-Compression local (σ_1) and global (σ_x) stress components of M_1, $[0,90°]_{3s}$ specimens Under all Pressure ratio (P_r)

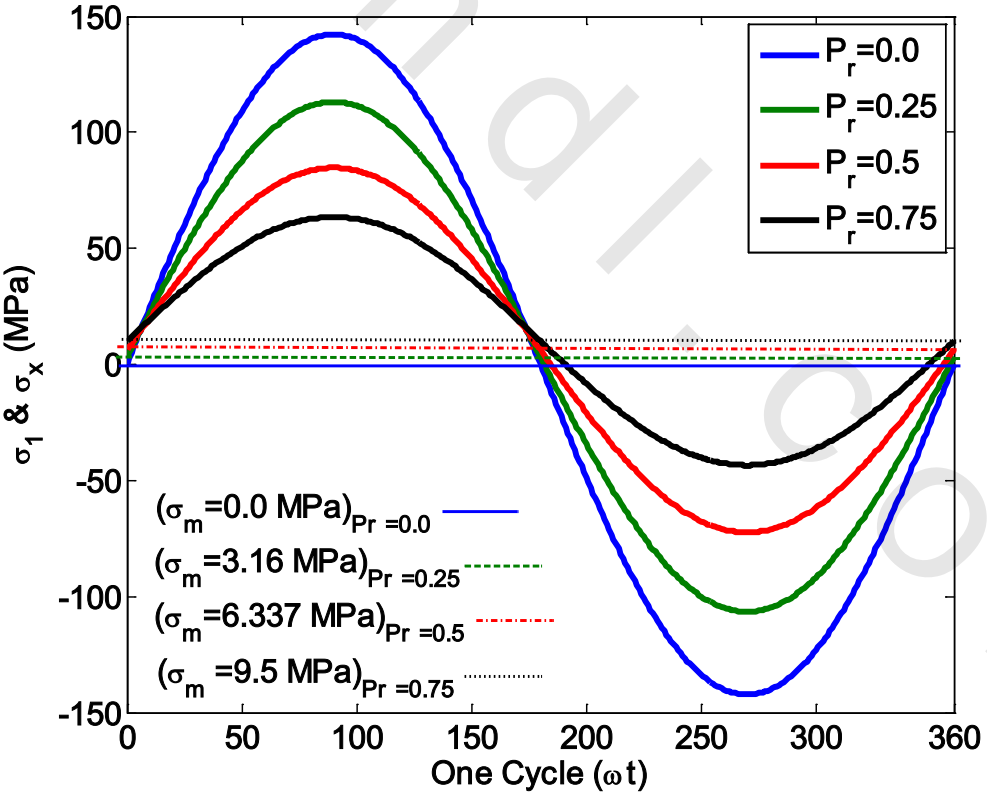

Figure 6.33 Tension-Compression local (σ_1) and global (σ_x) stress components of M_2, $[0,90°]_{3s}$ specimens Under all Pressure ratio (P_r)

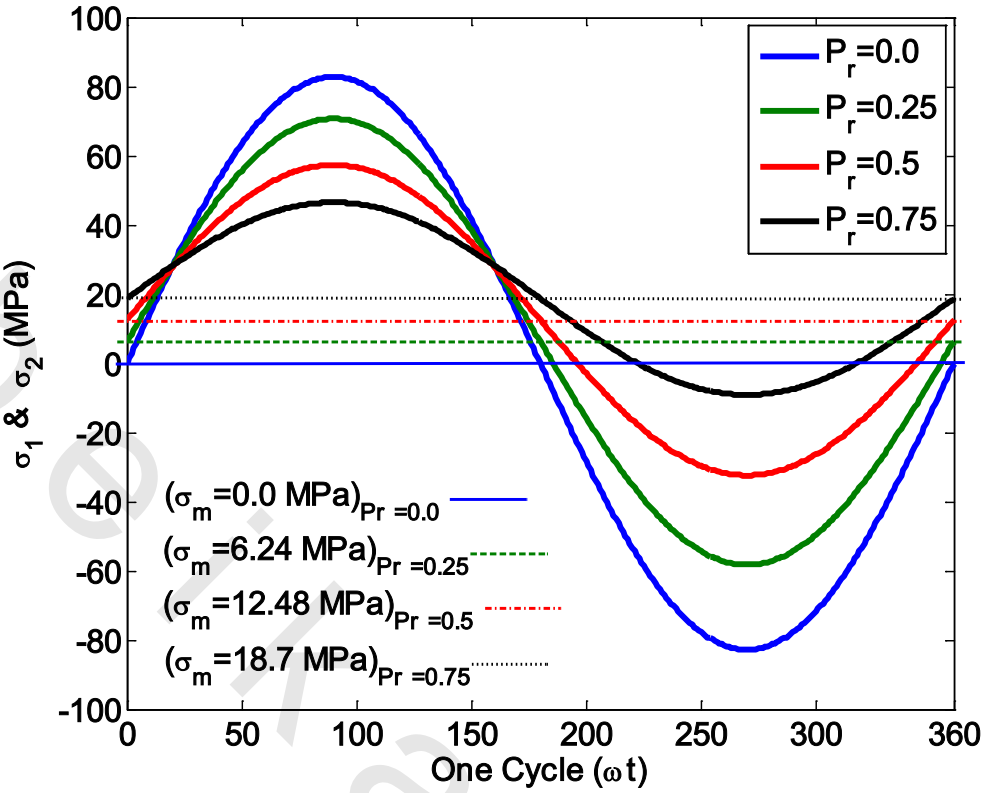

Figure 6.34 (a) Tension-Compression local stress (σ_1 & σ_2) components of M_1, $[\pm 45°]_{3s}$ specimens Under all Pressure ratio (P_r)

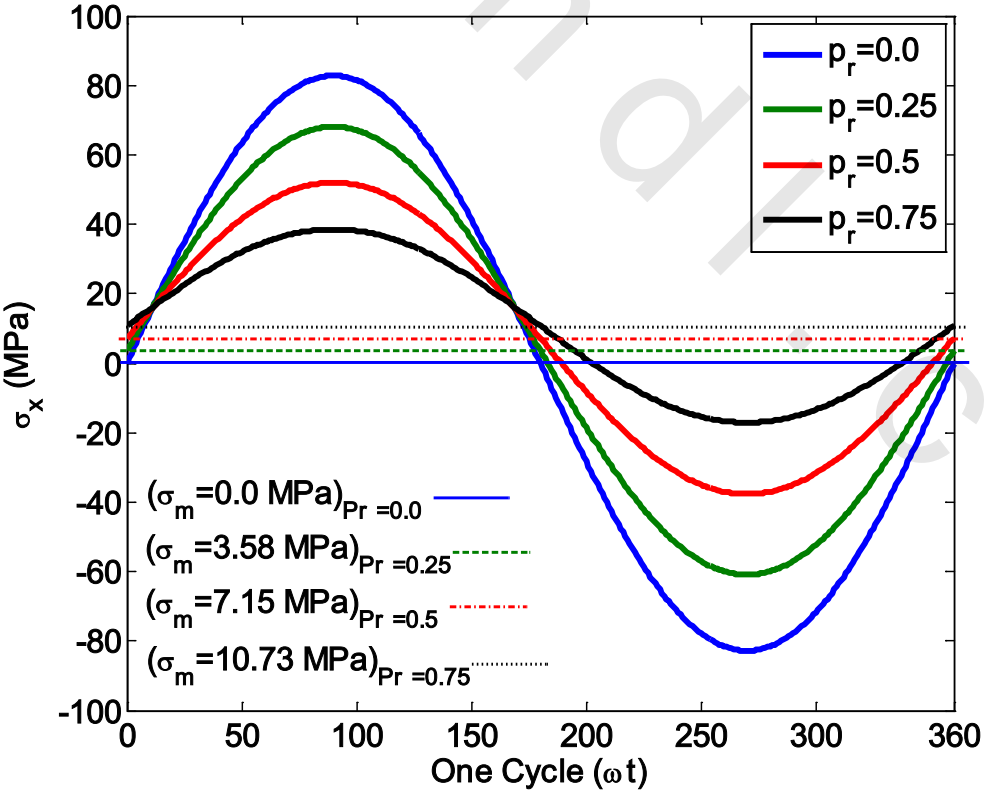

Figure 6.34 (b) Tension-Compression global stress (σ_{max}) components of M_1, $[\pm 45°]_{3s}$ specimens Under all Pressure ratio (P_r)

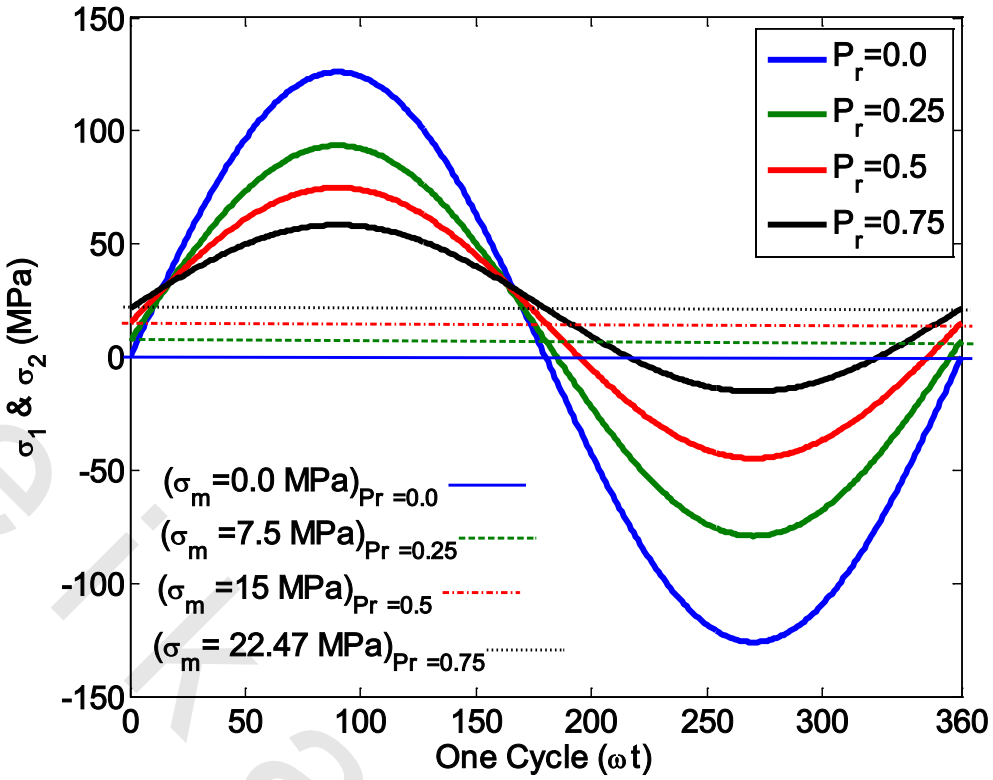

Figure 6.35(a) Tension-Compression local stress (σ_1 & σ_2) components of M_2, $[\pm 45°]_{3s}$ specimens Under all Pressure ratio (P_r)

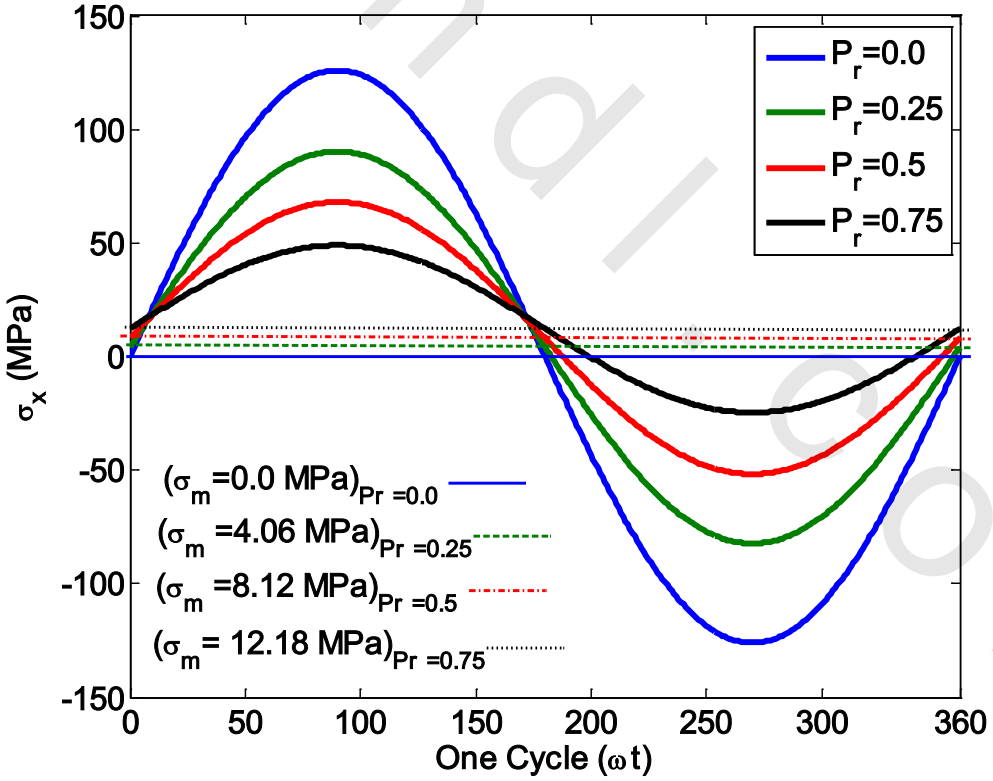

Figure 6.35(b) Tension-Compression global stress (σ_{max}) components of M_2, $[\pm 45°]_{3s}$ specimens Under all Pressure ratio (P_r)

Table 6.3: The Hoop-amplitude relation for M_1, $[0,90°]_{3s}$ specimens

Life (N)	Hoop-amplitude relation	Correlation factor
1E+3	A=-3.019*H+101	0.9999
1E+4	A=-2.908*H+95.88	0.9985
5E+4	A=-2.755*H+90.06	0.9989
1E+5	A=-2.131*H+71.04	0.9993
5E+5	A=-1.921*H+63.84	0.9999
1E+6	A=-1.464*H+48.17	0.9999

Where: A: Amplitude of normal stress (MPa)

H: Hoop stress (MPa)

Table 6.4: The Hoop-amplitude relation for M_1, $[\pm45°]_{3s}$ specimens

Life (N)	Hoop-amplitude relation	Correlation factor
1E+3	A=-2.004*H+73.56	0.9984
1E+4	A=-1.799*H+65.84	0.9989
5E+4	A=-1.625*H+60.68	0.9996
1E+5	A=-1.457*H+54.65	0.9996
5E+5	A=-1.352*H+50.05	0.9983
1E+6	A=-1.048*H+38.68	0.9995

Where: A: Amplitude of normal stress (MPa)

H: Hoop stress (MPa)

Table 6.5: The Hoop-amplitude relation for M_2, $[0,90°]_{3s}$ specimens

Life (N)	Hoop-amplitude relation	Correlation factor
1E+3	A=-3.104*H+122	0.9969
1E+4	A=-2.453*H+97.29	0.9978
5E+4	A=-2.308*H+88.5	0.9997
1E+5	A=-2.112*H+81.03	0.9999
5E+5	A=-1.888*H+73.53	0.9994
1E+6	A=-1.351*H+52.25	0.9967

Where: A: Amplitude of normal stress (MPa)

H: Hoop stress (MPa)

Table 6.6: The Hoop-amplitude relation for M_2, $[\pm45°]_{3s}$ specimens

Life (N)	Hoop-amplitude relation	Correlation factor
1E+3	A=-2.797*H+121.2	0.9812
1E+4	A=-2.446*H+105.6	0.9832
5E+4	A=-2.108*H+93.02	0.9733
1E+5	A=-1.797*H+75.33	0.9861
5E+5	A=-1.267*H+55.85	0.9789
1E+6	A=-1.043*H+45.69	0.9804

Where: A: Amplitude of normal stress (MPa)

H: Hoop stress (MPa)

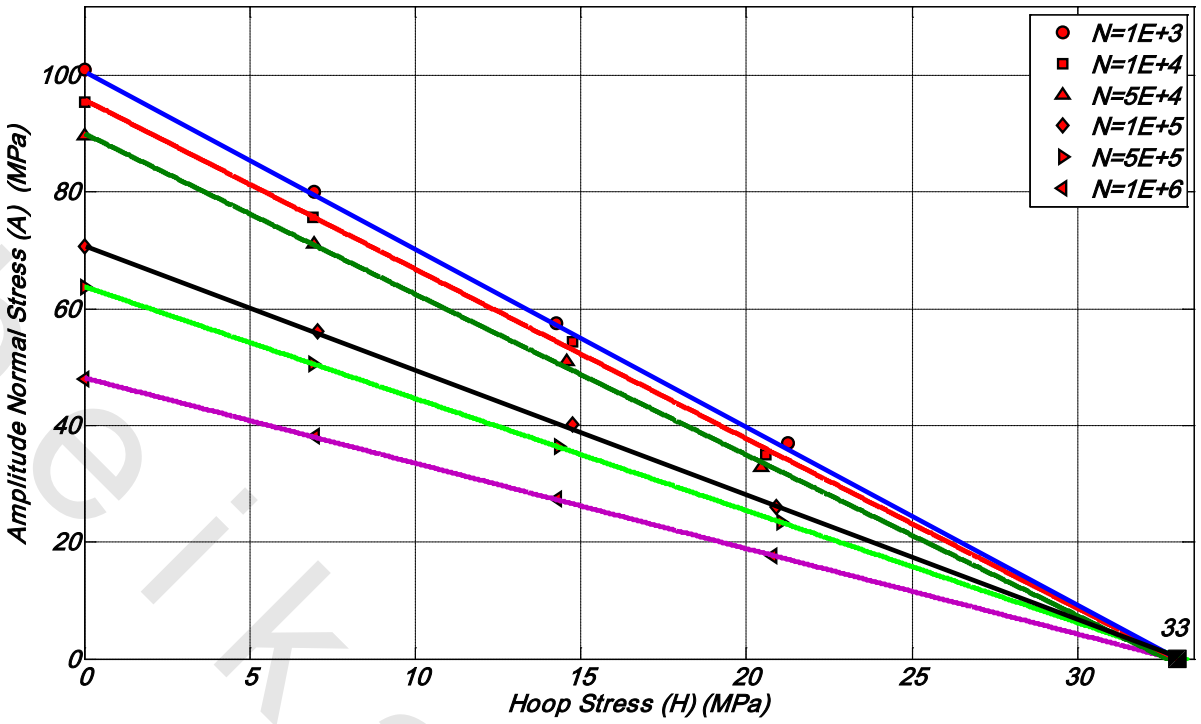

Figure 6.36 Hoop-amplitude relation for M_1, $[0,90°]_{3s}$ specimens

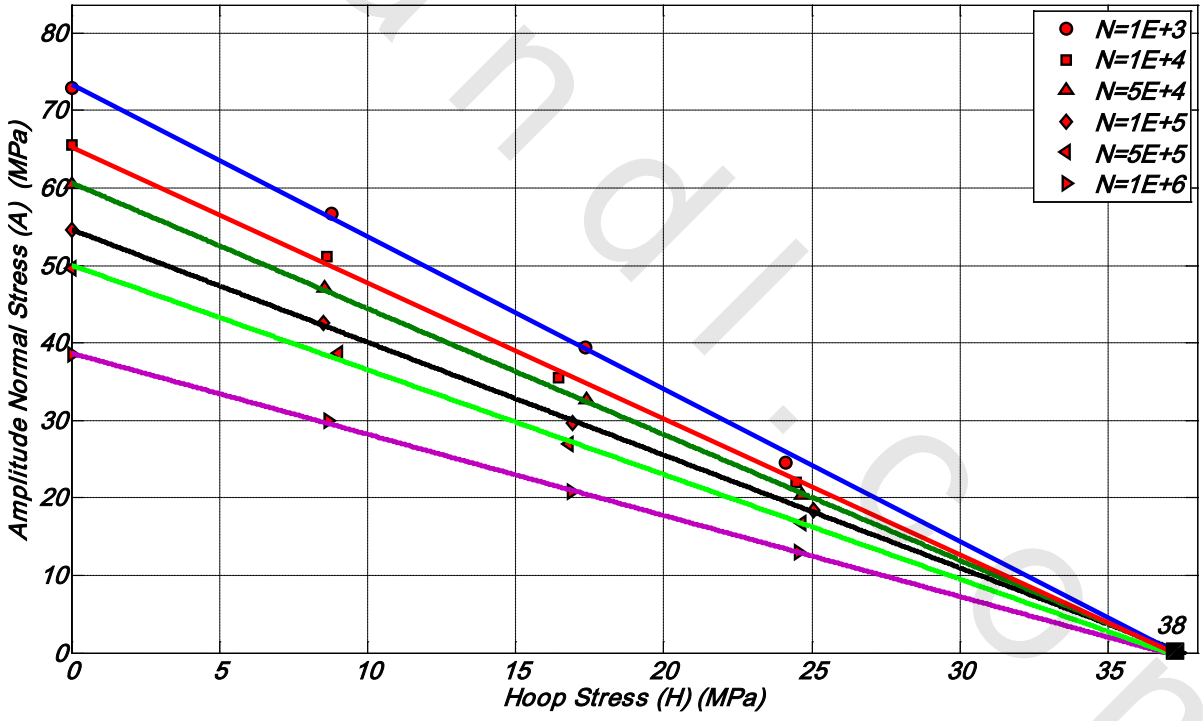

Figure 6.37 Hoop-amplitude relation for M_1, $[\pm 45°]_{3s}$ specimens

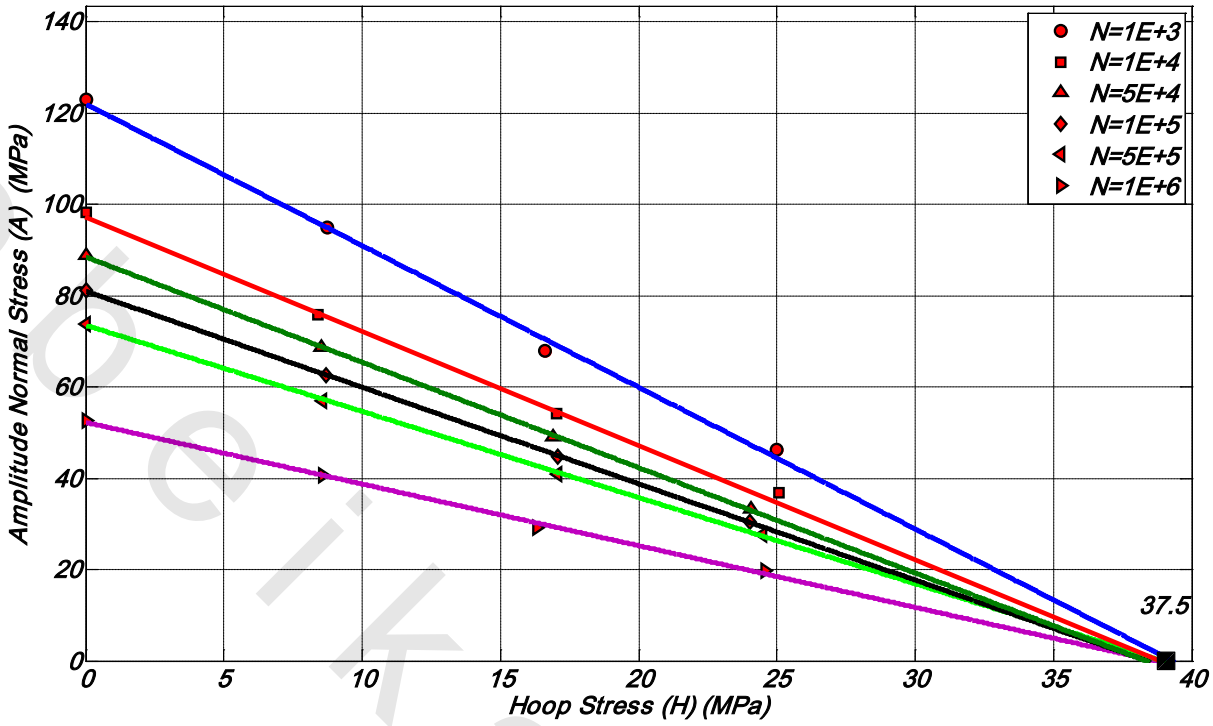

Figure 6.38 Hoop-amplitude relation for M_2, $[0,90°]_{3s}$ specimens

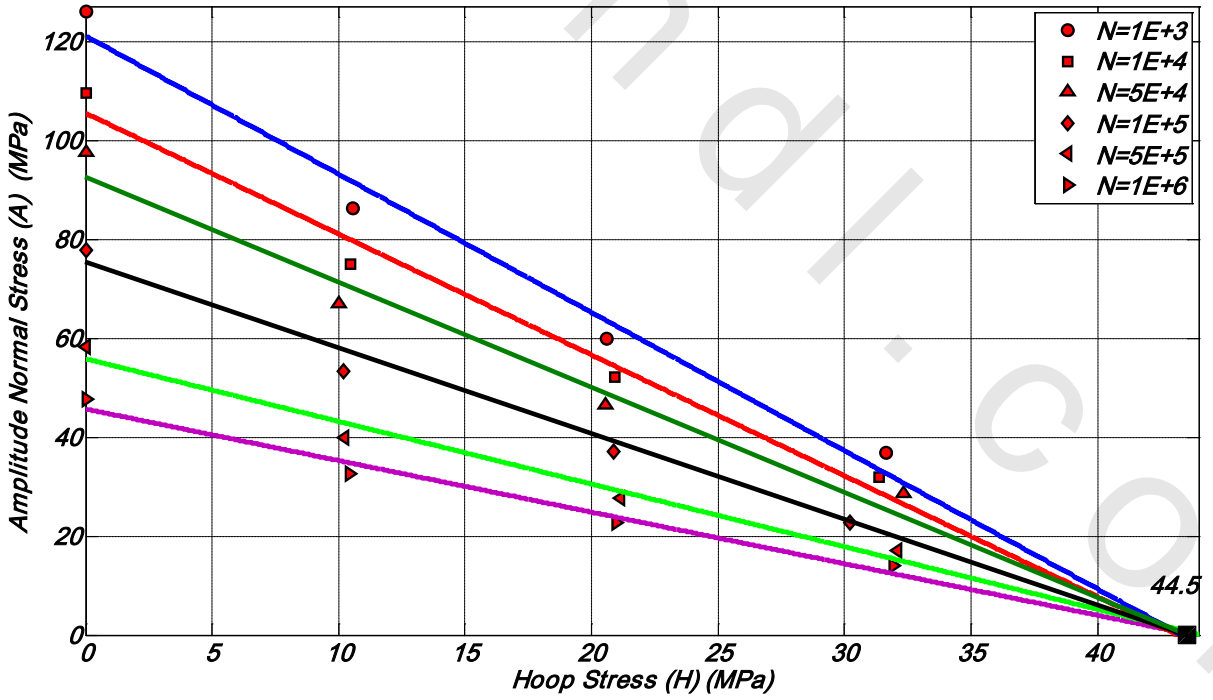

Figure 6.39 Hoop-amplitude relation for M_2, $[\pm 45°]_{3s}$ specimens

Since, at any life, the fitted straight line joints the two points $(S_H, 0)$ and $(0, S_f)$ and passes by the other points with a high correlation factors. This supports the use of an equation in the same form as Goodman's equation for normal stresses to be the governing equation for the hoop-amplitude relation.

The classical form of Goodman's equation for normal stresses $\left\{\frac{\sigma_m}{S_U} + \frac{\sigma_a}{S_f} = 1.0\right\}$ was found not suitable to be the governing equation for the mean-amplitude relation in the present study, that is may be due to the effect of hoop stress σ_H, that not taken into considration.

Myeong et al **[150]** modified the Goodman's equation to study the effect of mean stress in theirs work of limit load interaction of cracked branch junctions under combined pressure and bending, and they found that, the new form of Goodman's equation i.e., $\left\{\frac{P}{P_{max}\ (M=0)} + \frac{M}{M_{max}\ (P=0)} = 1.0\right\}$ was suitable for theirs case.

However, the above equation of Myeong et al **[150]** is also not suitable for present case, that is because the great difference in the type of loading. Similarly the modification to the classical form of Goodman's equation was done here, taken into consideration the type of loading. The new suggested form of Goodman's equation may be as:

$$\left\{\frac{\sigma_H}{S_H(S_f=0)} + \frac{\sigma_{max}}{S_f(S_H=0)} = 1.0\right\}_{\theta,M,P_r} \qquad (6.1)$$

Where: σ_H: the hoop stresses.

S_H : the hoop strength.

σ_{max} : the maximum stress.

S_f: the fatigue strength at completely reversed bending.

To check the suitability of the suggestion form of Goodman's equation (6.1) let the right hand side of the equation equal to Goodman's relative damage, G.R.D., were plotted against the number of cycles to failure under both manufacturing method M_1 and M_2 for all fiber orientations as shown in Figure 6.40.

Figure 6.40 shows that the new form of Goodman's equation is the suitable for representing the effect of the hoop stress for the present work by giving excellent results for both manufacturing method M_1 and M_2 for all fiber orientations and for all pressure

ratios, where, the values of G.R.D. are around the theoretical value of unity. For both manufacturing method M_1 and M_2 for all fiber orientations, the G.R.D. are ranging from 0.9215 as a minimum value to 1.185 as a maximum value with an average value of 1.0303 and standard deviation of 0.05355 which are very near to unity, and the difference may be referred to scatter in experimental data.

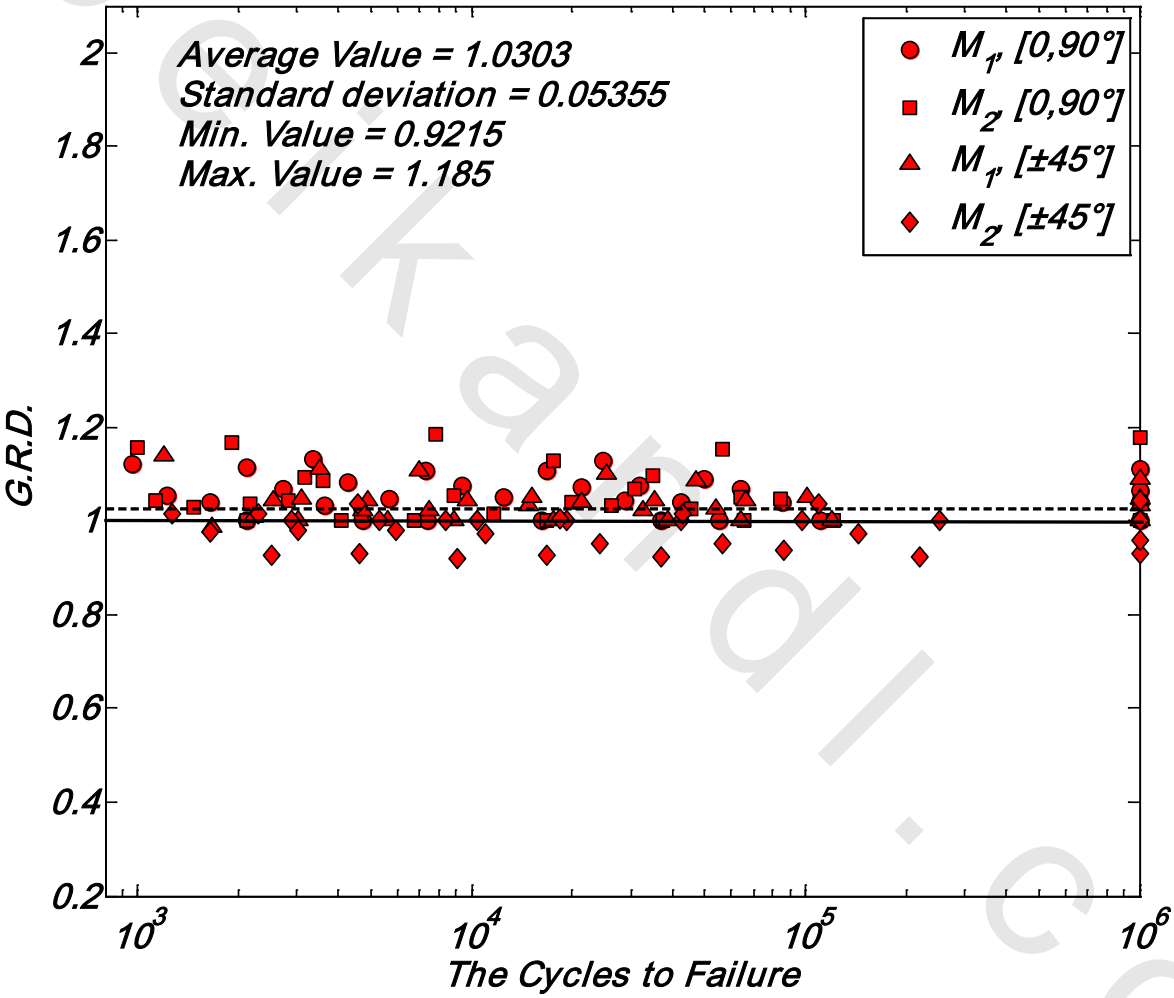

Figure 6.40 The G.R.D. for both manufacturing method M_1 and M_2 for all fiber orientations and all pressure ratios.

6.4 Validity of SWT Parameter

The Smith-Watson-Topper (SWT) parameter ($\sqrt{\sigma_{max}\,\sigma_a}$) proposed by Smith et al. **[125]** has allowed a great reduction in the number of tests required to estimate the effect of mean stress on the fatigue life of metals, and some composites for which it was validated. This is because; if the SWT parameter is found to be valid, then plotting it instead of the maximum or the amplitude stress component against the number of cycles to failure tends to plot a single curve, when having variable mean stresses or stress ratios.

The SWT parameter at different pressure ratios (P_r) were obtained for the present case of combined bending moment and hydrostatic internal pressure from the equation (6.2):

$$SWT = \sqrt{(\sigma_{max} + \sigma_m)\sigma_a} \tag{6.2}$$

Where: $\sigma_m = \sigma_l$, produced by internal pressure.

σ_{max} : maximum normal stress produced by bending moment.

The data of the tested specimens with different pressure ratios (P_r), (Tables A3-33 to A3-52) were used to plot the SWT parameter for both fiber orientation and both methods of manufacturing, against the number of cycles to failure.

Figures 6.41 and 6.42 show these results for $[0,90°]_{3s}$ and $[\pm45°]_{3s}$ of the first method of manufacturing M_1 while Figures 6.43 and 6.44 show the results of the second method of manufacturing M_2. The power-law form: $\boldsymbol{SWT = a_1 N^{b_1}}$ was used for fitting these data points that gave acceptable results when having good correlation factors, but the values of the constants ($\boldsymbol{a_1}$) and ($\boldsymbol{b_1}$) were obtained from equation (6.2) had small correlation factors, Table 6.7, although this values were gave a valid SWT parameter, where the comparison between the values of two constants ($\boldsymbol{a_1}$) and ($\boldsymbol{b_1}$) and the corresponding two constants (a) and (b) for completely reversed pure bending of the corresponding fiber orientation and methods of manufacturing were gave a good promising result. The degradation of the correlation factors was explained by the large scatter of data points, as shown in the Figures 6.41 to 6.44. This degradation of the correlation factors was found also in several works **[69, 73, 83, 151]**.

To improve the correlation factor and increase the reliability of the uses SWT parameter for the present study a modification for SWT parameter equation, (6.2), should be done by taken into account the effect of hoop stress σ_h in the SWT parameter.

Equation (6.3) shows the suggested modification for SWT parameter taken into account the effect of the hoop stress σ_h, and Table 6.7 gives the results after modification.

$$SWT^* = \sqrt{(\sigma_{max} + \sigma_m)(\sigma_a + K\sigma_h)} \quad (6.3)$$

Where: $K = \left(\frac{[S_H]_{[\theta,M]}}{[S_L]_{[\theta,M]}}\right)$,

$[S_H]_{[\theta,M]}$: The maximum hoop strength corresponding to its fiber orientations and manufacturing method.

$[S_L]_{[\theta,M]}$: The maximum longitudinal strength corresponding to its fiber orientations and manufacturing method.

The values of the constants ($\boldsymbol{a_1}$) and ($\boldsymbol{b_1}$) for equation (6.2) and equation (6.3), are given in Table 6.7.

Table 6.7: Values of constants ($\boldsymbol{a_1}$) and ($\boldsymbol{b_1}$) for the (SWT) parameter, $\boldsymbol{SWT = a_1 N^{b_1}}$

Fiber orientation	Method of Manufacturing	($\boldsymbol{a_1}$) MPa	($\boldsymbol{b_1}$)	Correlation factor	Bending Fatigue Constants at R=-1	
					($\boldsymbol{a}$) MPa	($\boldsymbol{b}$)
$[0,90°]_{3s}$	**M_1**	303	-0.1574	0.4155	*314.3*	*-0.1361*
		290*	-0.1291*	0.9053*		
$[\pm45°]_{3s}$		219	-0.1508	0.237	*226.6*	*-0.1284*
		230*	-0.1217*	0.775*		
$[0,90°]_{3s}$	**M_2**	477	-0.1891	0.4894	*484.4*	*-0.1612*
		470*	-0.1613*	0.8627*		
$[\pm45°]_{3s}$		386	-0.1807	0.4216	*397.2*	*-0.1514*
		400*	-0.1491*	0.8814*		

Where: M_1: The first method of manufacturing
M_2: The second method of manufacturing
****The data of SWT^* [Equation (6.3)]***

Figures 6.45 and 6.46 show the modified SWT parameter for *$[0,90°]_{3s}$* and *$[\pm45°]_{3s}$* of the first method of manufacturing *M_1* while Figures 6.47 and 6.48 show these results for *$[0,90°]_{3s}$* and *$[\pm45°]_{3s}$* of the second method of manufacturing *M_2*, respectively. Using the power law: $\boldsymbol{SWT^* = a_1 N^{b_1}}$ this notice that, the results obtained for modified SWT parameter had acceptable values of correlation factors. This because the data points of the modified SWT parameter in Equation (6.3) were plotted in small point distributed area around the same fitting curve of SWT parameter in Equation (6.2).

As given in Table 6.8, the constant ($\boldsymbol{b_1}$) for both fiber orientation and both methods of manufacturing are approximately equal and may be considered as material constant. Furthermore, the ratio between the constant ($\boldsymbol{a_1}$) to the static ultimate strength (S_u) of the

corresponding fiber orientation and methods of manufacturing resulted in good promising results. This ratio was found to be nearly constant for all fiber orientation with the same method of manufacturing.

Table 6.8: The ratio between the constant ($\boldsymbol{a_1}$) to the static ultimate strength (S_u)

Fiber orientation	Method of Manufacturing	$\boldsymbol{a_1/S_u}$
$\mathbf{[0,90°]_{3s}}$	$\mathbf{M_1}$	*1.5934*
$\mathbf{[\pm45°]_{3s}}$		*1.4465*
$\mathbf{[0,90°]_{3s}}$	$\mathbf{M_2}$	2.3737
$\mathbf{[\pm45°]_{3s}}$		2.3121

Finally Tables 6.7 and 6.8 show that:

1) The ratio between the constant ($\boldsymbol{a_1}$) to the static ultimate strength (S_u) of the corresponding to fiber orientation and methods of manufacturing are nearly equal for both fiber orientation at different methods of manufacturing, this conclusion was found by literatures **[84-88]**.
2) Comparing the values of two constants ($\boldsymbol{a_1}$) and ($\boldsymbol{b_1}$) to the corresponding two constants (a) and (b) of the corresponding fiber orientation and methods of manufacturing resulted in a good promising result.

This means the modified SWT parameter ($SWT = \sqrt{(\sigma_{max} + \sigma_m)(\sigma_a + K\sigma_h)}$) can be used for woven-Roving GFRE with $[0,90°]_{3s}$ and $[\pm45°]_{3s}$ orientations under combined completely reversed bending moment and static internal pressure with different pressure ratios (P_r). Performing only the completely reversed bending moment (R=-1) fatigue test and using the SWT parameter will be sufficient to find out the strength of the material.

6.4.1 Validity of modified SWT Parameter

In this section we will check the validity of modified SWT parameter ($K_{Wafa}\sqrt{\sigma_{max}\,\sigma_a}$) presented by Mohamed **[88]**. In this new form of SWT parameter they found that, the modified SWT parameter equals constant and simple to use with comparison to the original form. The modified SWT parameter for different pressure ratios (P_r) were obtained for the present case of combined bending moment and hydrostatic internal pressure from the equation:

$$SWT = K_{Wafa}\sqrt{(\sigma_{max} + \sigma_m)(\sigma_a + K\sigma_h)}$$

Where: $K_{Wafa} = \frac{1}{A_\theta}$, A_θ = the strength of the specimen under completely reversed pure bending moment corresponding to its fiber orientation. Plotting the modified SWT parameter against the number of cycles to failure (N) for both fiber orientation and both methods of manufacturing, Figure 6.49 shows that:

1) The modified SWT parameter can be drawn in the same diagram for both fiber orientation and both methods of manufacturing.
2) The modified SWT parameter values can be considered to be constant of 0.25489 with applicable value of slandered deviation of 0.065913 for both fiber orientation and both methods of manufacturing. So that, the modified SWT parameter of Mohamed **[88]** is valid for the present study.

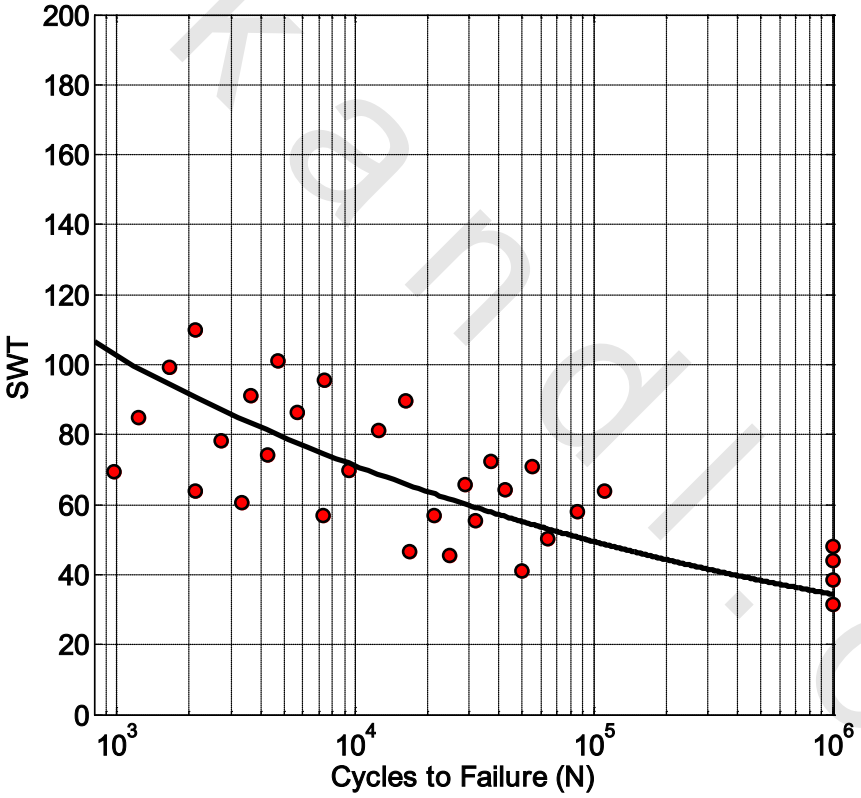

Figure 6.41 The SWT parameter for M_1, $[0,90°]_{3s}$ specimens

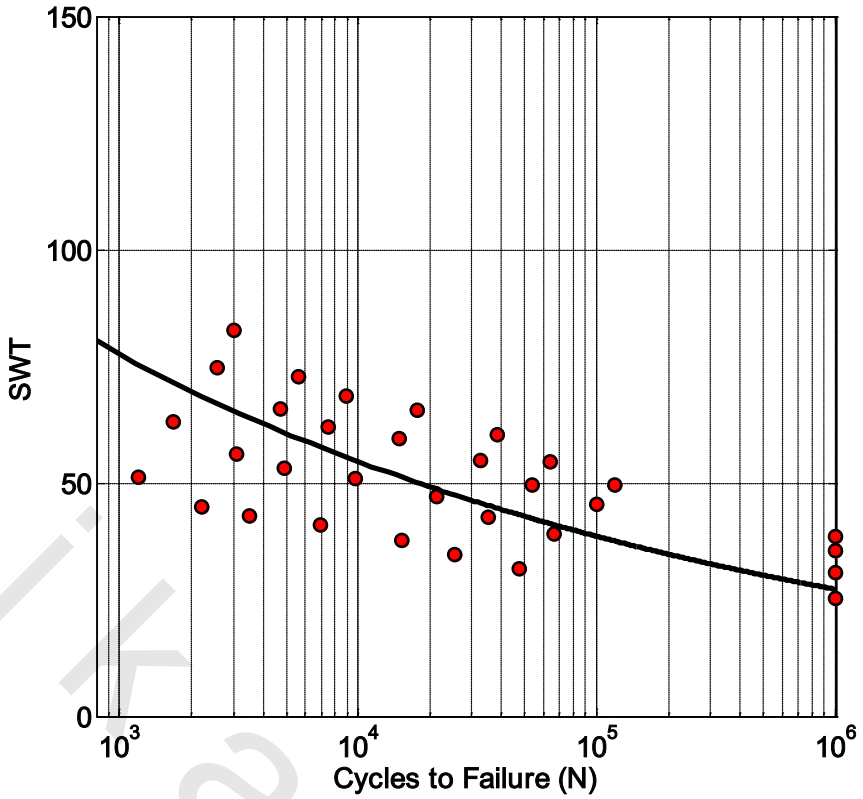

Figure 6.42 The SWT parameter for M_1, $[\pm 45°]_{3s}$ specimens

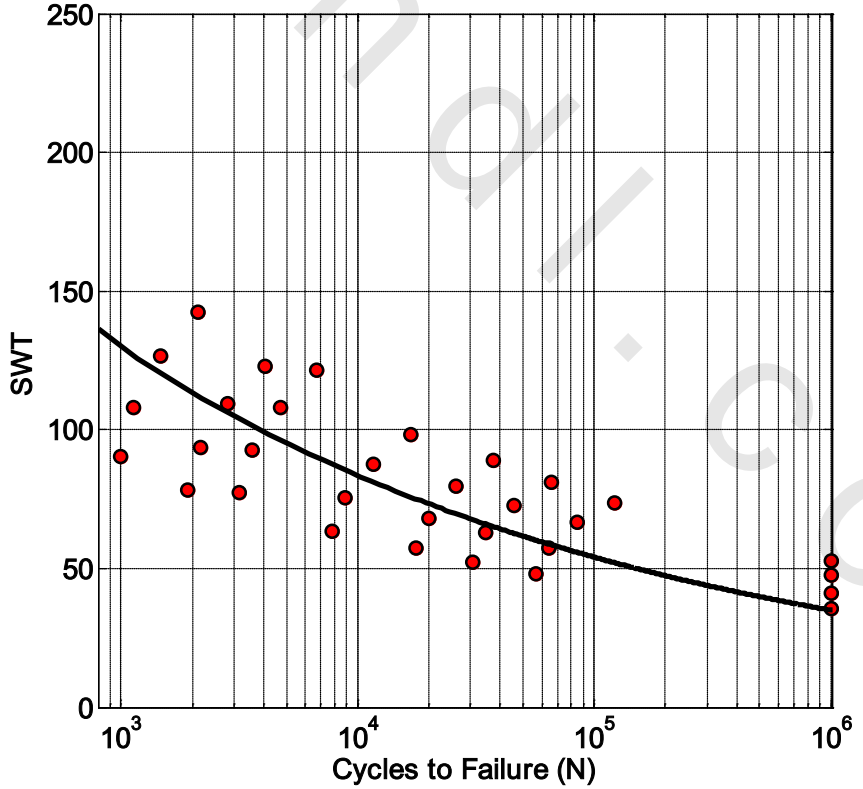

Figure 6.43 The SWT parameter for M_2, $[0,90°]_{3s}$ specimens

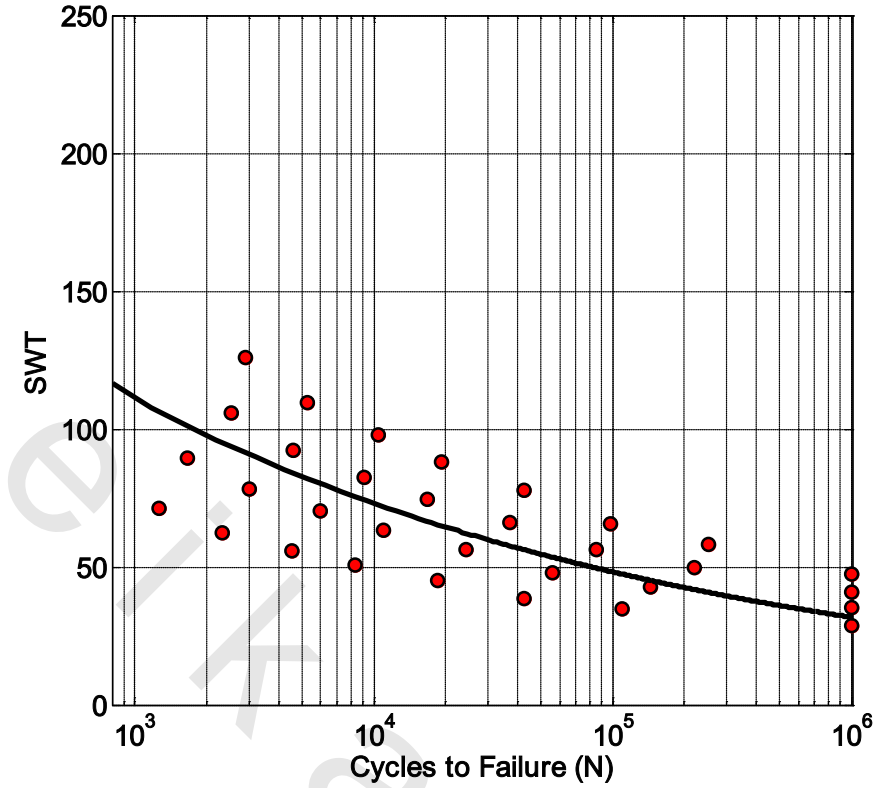

Figure 6.44 The SWT parameter for M_2, $[\pm 45°]_{3s}$ specimens

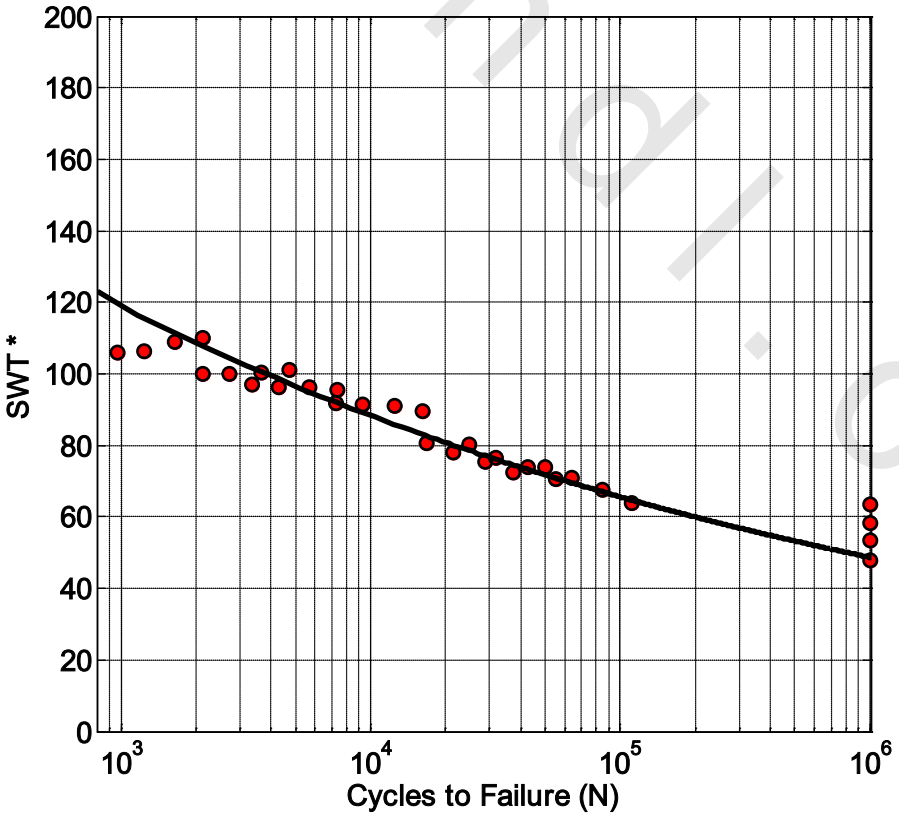

Figure 6.45 The SWT^* parameter for M_1, $[0,90°]_{3s}$ specimens

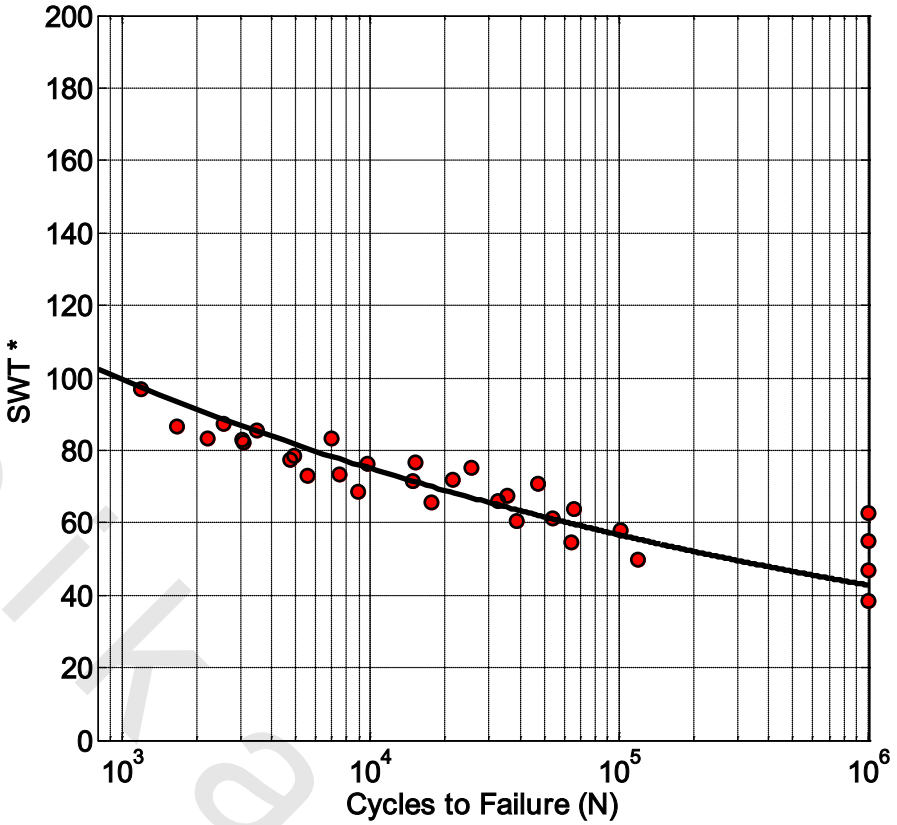

Figure 6.46 The SWT* parameter for M_1, $[\pm 45°]_{3s}$ specimens

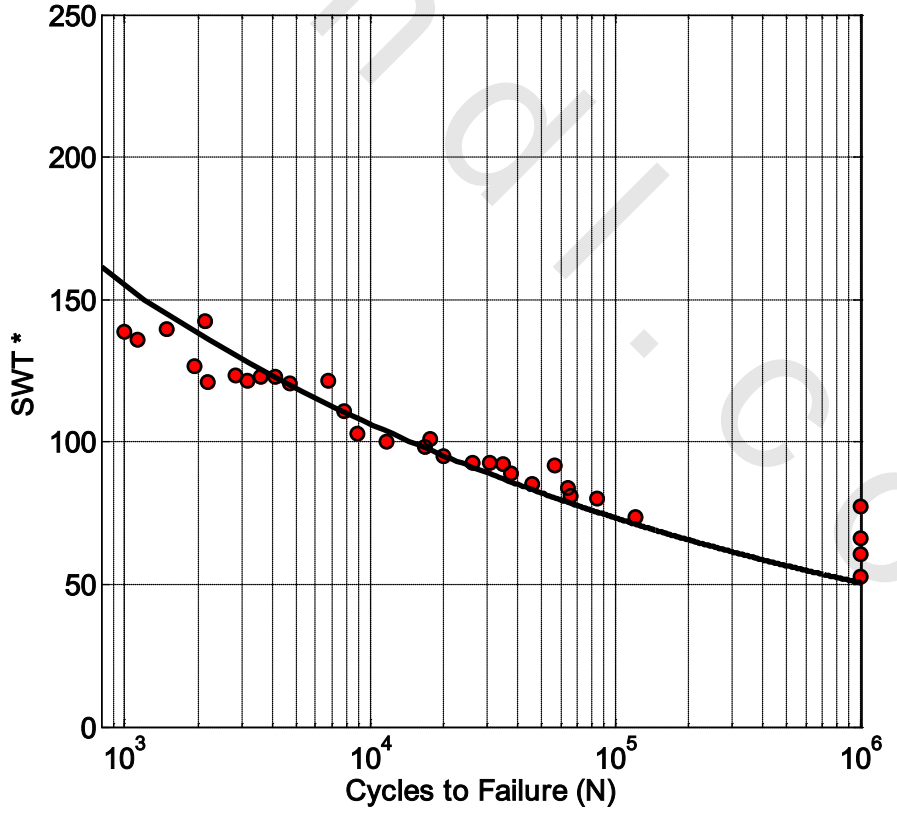

Figure 6.47 The SWT* parameter for M_2, $[0,90°]_{3s}$ specimens

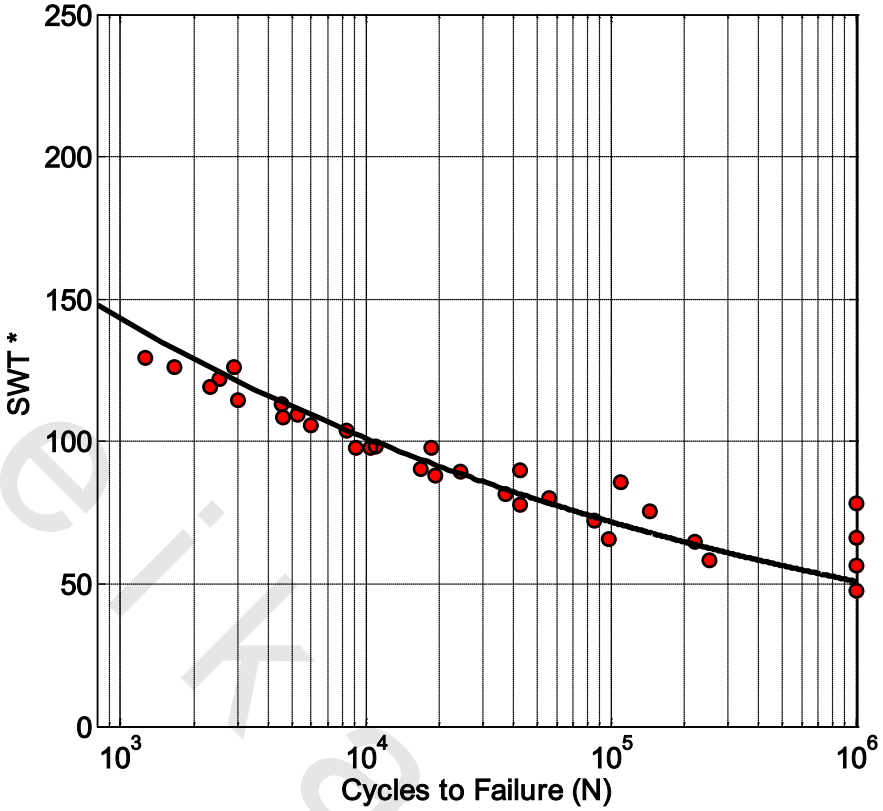

Figure 6.48 The SWT* parameter for M_2, $[\pm 45°]_{3s}$ specimens

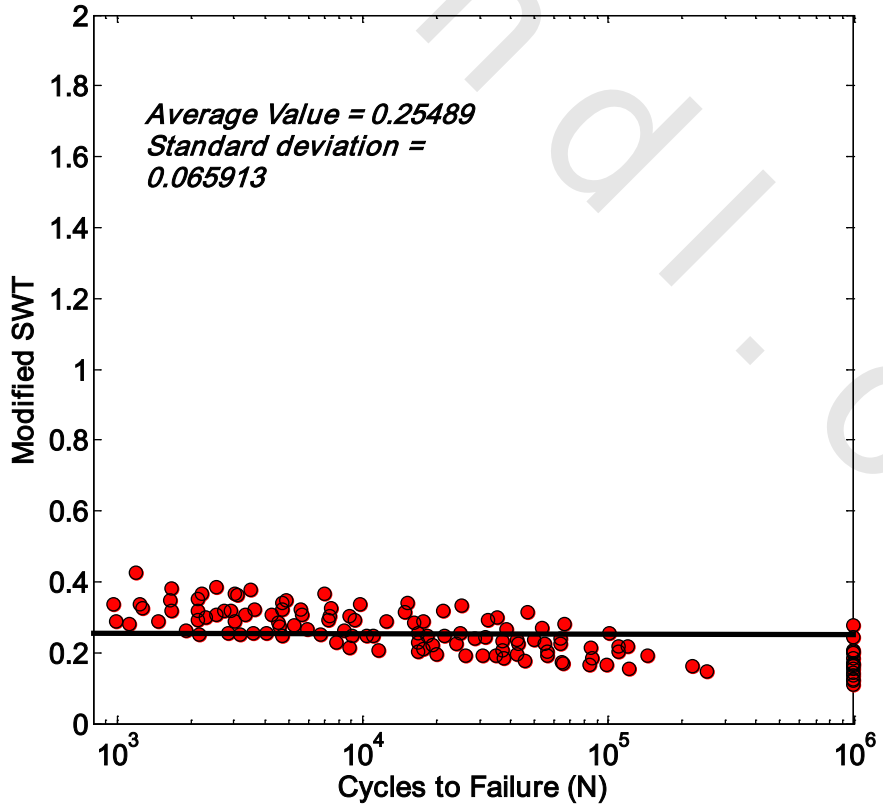

Figure 6.49 The modified SWT parameter for both fiber orientation and both methods of manufacturing

6.5 Validity of Modified Fatigue Strength Ratio (Ψ)

As indicated in the section (2.7), the S-N curves plotted using the maximum fatigue stress $\boldsymbol{\sigma_{max}}$ depends on both fiber orientation, both methods of manufacturing and pressure ratios. Using the modified fatigue strength ratio (Ψ), we can substantially eliminate the fiber orientation dependence, as well as the stress ratio dependence of the off-axis fatigue data to obtain an experimental master S-N curves. However, one of the aims of this study is to check the validity of the modified fatigue strength ratio (Ψ) for woven-Roving GFRE with $[0,90°]_{3s}$ and $[\pm45°]_{3s}$ orientations under combined completely reversed bending moment and hydrostatic internal pressure with different pressure ratios (P_r)

The data of the tested specimens with different pressure ratios (P_r), (Tables A3-33 to A3-52) were used to plot the modified fatigue strength ratio (Ψ) for both fiber orientation and both methods of manufacturing, against the number of cycles to failure.

Figures 6.50 and 6.51 show these results for $[0,90°]_{3s}$ and $[\pm45°]_{3s}$ of the first method of manufacturing M_1 while Figures 6.52 and 6.53 show these results for $[0,90°]_{3s}$ and $[\pm45°]_{3s}$ of the second method of manufacturing M_2, respectively; and the power-law form: $\boldsymbol{\Psi = a_2 N^{b_2}}$ was used for fitting these data points. Table 6.9 gives the values of the constants $(\boldsymbol{a_2})$ and $\boldsymbol{(b_2)}$ with acceptable correlation factors.

Table 6.9: Values of constants $(\boldsymbol{a_2})$ and $\boldsymbol{(b_2)}$ for Modified Fatigue Strength Ratio (Ψ), $\boldsymbol{\Psi = a_2 N^{b_2}}$

Fiber orientation	Method of Manufacturing	$(\boldsymbol{a_2})$ MPa	$(\boldsymbol{b_2})$	$\boldsymbol{a/S_u}$	Correlation factor
$\boldsymbol{[0,90°]_{3s}}$	$\boldsymbol{M_1}$	1.718	*-0.1347*	*1.7269*	*0.9775*
$\boldsymbol{[\pm45°]_{3s}}$		1.486	*-0.13*	*1.4251*	*0.9516*
$\boldsymbol{[0,90°]_{3s}}$	$\boldsymbol{M_2}$	2.45	*-0.1637*	*2.4464*	*0.9746*
$\boldsymbol{[\pm45°]_{3s}}$		2.381	*-0.1542*	*2.2959*	*0.9829*

From Table 6.9, the following conclusions can be obtained:

1) The deviation in the values of constant $\boldsymbol{(b_2)}$, for both fiber orientation with different methods of manufacturing is negligible and may be considered to be material constant with average value of -0.13235 and standard deviation 0.003323 for method of manufacturing M_1 and with average value of -0.15895 and standard deviation 0.006718 for method of manufacturing M_2.
2) The values of constant $(\boldsymbol{a_2})$ was found to be nearly equal to the ratio $\boldsymbol{a/S_u}$. this conclusion was found in similar **[84-88]**.

Where:

S_u: the static ultimate strength,

a: the constant of ($\sigma_{max} = aN^b$) for completely reversed pure bending and its value is determined according to the type of fiber orientation and methods of manufacturing.

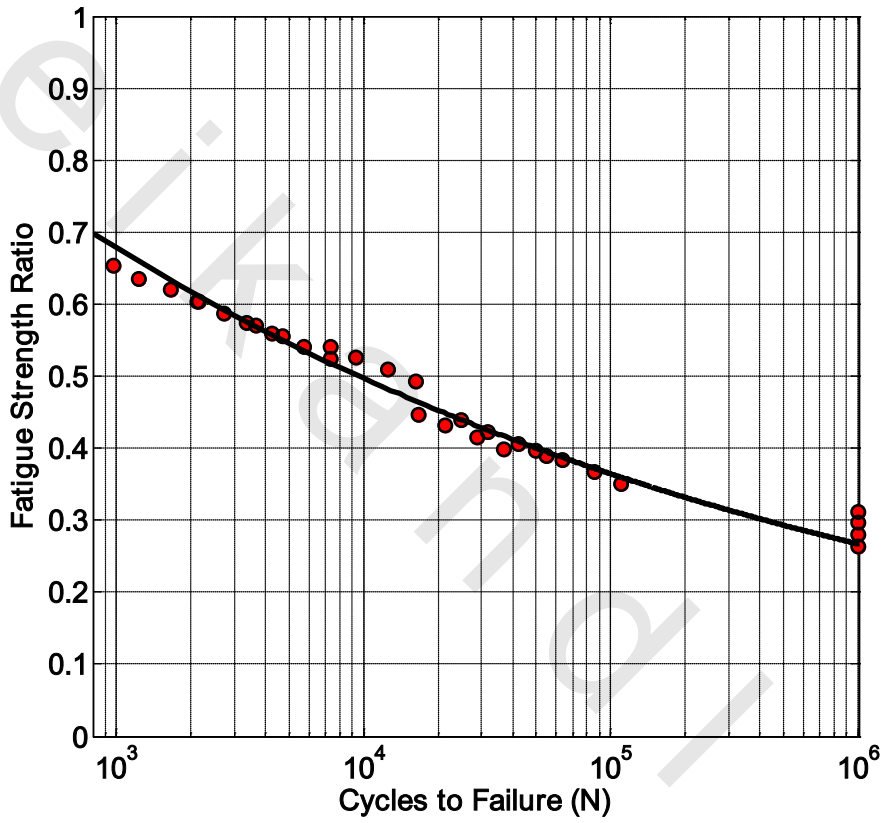

Figure 6.50.The Modified Fatigue Strength Ratio (Ψ) for M_1& $[0,90°]_{3s}$ specimens

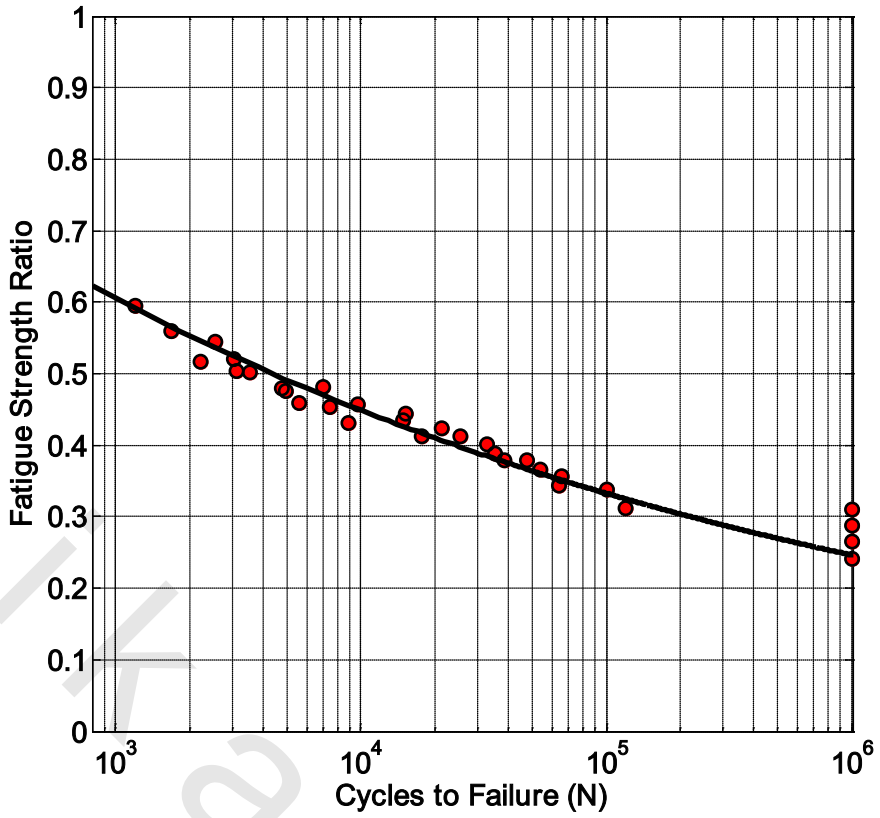

Figure 6.51.The Modified Fatigue Strength Ratio (Ψ) for M_1& $[\pm 45°]_{3s}$ specimens

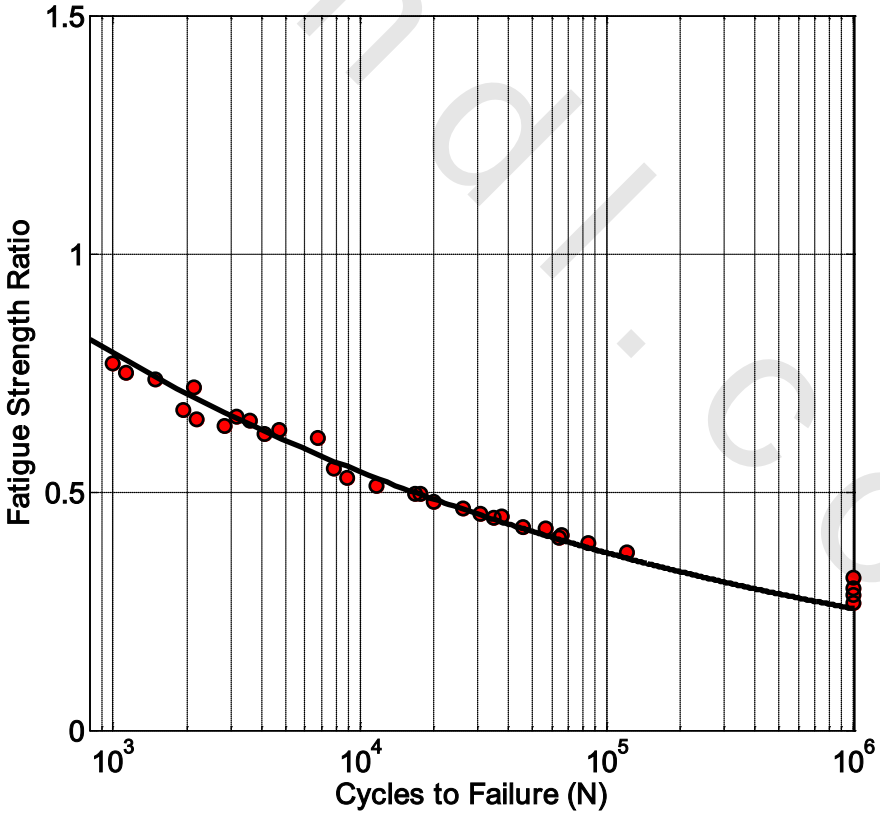

Figure 6.52.The Modified Fatigue Strength Ratio (Ψ) for M_2& $[0,90°]_{3s}$ specimens

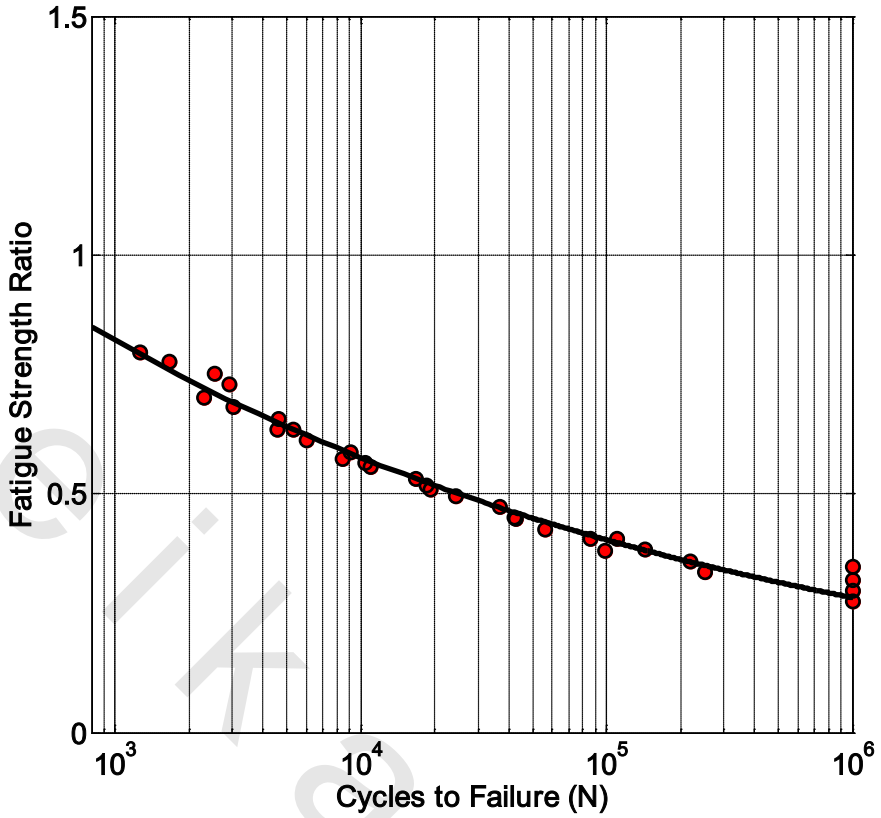

Figure 6.53.The Modified Fatigue Strength Ratio (Ψ) for M_2& $[\pm 45°]_{3s}$ specimens

6.6 Applicability of failure criteria:

The suitability of a certain criterion differs greatly according to the tested material, and its stress state. All failure criteria have their right hand side to be unity, and their left hand side contains the local stress components divided by their corresponding strengths. Therefore, the left hand side of any criterion was named to be its Relative Damage (R.D.)

The corresponding values of R.D. were plotted against the number of cycles to failure was constructed, then a comparison was conducted for the value of the R.D. to unity, the criterion is suitable if its R.D. has a value near unity. If it is less than unity, then the criterion is predicting a specimen life more than the actual life of the experiment.

6.6.1 Selecting Suitable Failure Criteria

Working with failure criteria were done through three steps. First, selecting some of the known failure criteria suitable to be used for the present material, second, reforming them according to the local stress components, for both fiber orientations and methods of manufacturing. Finally, the most suitable criteria for each orientation will be selected, checked and modified if required.

Many previous works considered the suitability of failure criteria to similar materials. Considering these works, **[83-88]**, **[138]** it was found that the most widely used and suitable criteria for GFR under different loading conditions were the following criteria:

1. Hill,
2. Tsai-Hill,
3. Tsai-Wu,
4. Tsai-Hahn,
5. Norris interaction and
6. Norris distortional energy.

6.6.2 Failure Criteria for The Present Work

The local stress components of both fiber orientations specimens *[0, 90°]*$_{3s}$ and *[±45°]*$_{3s}$ are used for substitution in the selected six criteria. This substitution has shown that all failure criteria have different form for both fiber orientations specimens according to the failure criterion, as shown in Table 6.10.

Table 6.10: Selected Failure criteria for *[0, 90°]*$_{3s}$ and *[±45°]*$_{3s}$ specimens Subjected to combined completely reversed pure bending plus internal pressure Stresses

Failure criteria	**[0,90°]$_{3s}$ specimens**	**[±45°]$_{3s}$ specimens**
Hill	$\left(\frac{\sigma_1}{F_1}\right)^2+\left(\frac{\sigma_2}{F_2}\right)^2-2\left(\frac{\sigma_1\sigma_2}{F_1F_2}\right)=1$	$\left(\frac{\sigma_6}{F_6}\right)^2=1$
Tsai-Hill Norris distortional Tsai-Hahn	$\left(\frac{\sigma_1}{F_1}\right)^2+\left(\frac{\sigma_2}{F_2}\right)^2-\left(\frac{\sigma_1\sigma_2}{F_1F_2}\right)=1$	$\left(\frac{\sigma_1}{F_1}\right)^2+\left(\frac{\sigma_6}{F_6}\right)^2=1$
Tsai-Wu	$\left(\frac{\sigma_1}{F_1}\right)^2+\left(\frac{\sigma_2}{F_2}\right)^2+2\left(\frac{\sigma_1\sigma_2}{F_1F_2}\right)=1$	$4\left(\frac{\sigma_1}{F_1}\right)^2+\left(\frac{\sigma_6}{F_6}\right)^2=1$
Norris interaction	$\left(\frac{\sigma_1}{F_1}\right)^2+\left(\frac{\sigma_2}{F_2}\right)^2=1$	$2\left(\frac{\sigma_1}{F_1}\right)+\left(\frac{\sigma_6}{F_6}\right)^2=1$

6.6.3 The relative damage for [0,90°]$_{3s}$ specimens

The relative damage (R.D.) were calculated according to selected suitable failure criteria presented in Table 6.10, for the *[0,90°]*$_{3s}$ specimens under completely reversed pure bending, completely reversed pure torsion and combined completely reversed bending

moment and hydrostatic pressure with two methods of manufacturing M_1 and M_2 with different pressure ratio ($P_r = 0, 0.25, 0.5, 0.75$). Figures 6.54 to 6.61 shows the relative damage for the $[0,90°]_{3s}$ specimens against the number of cycles to failure. The values of (R.D.) are far from unity. This means that, the available different failure criteria are not suitable under these conditions and must be modified to best suit the studied case.

6.6.4 The relative damage for $[\pm 45°]_{3s}$ specimens

Figures 6.62 to 6.69 represent the relative damage for the $[\pm 45°]_{3s}$ specimens under completely reversed pure bending, completely reversed pure torsion and combined completely reversed bending moment and hydrostatic pressure with two methods of manufacturing M_1 and M_2 with different pressure ratio ($P_r = 0, 0.25, 0.5, 0.75$) against the number of cycles to failure. From these Figures, it can be noticed that these failure criteria are not valid and must be modified.

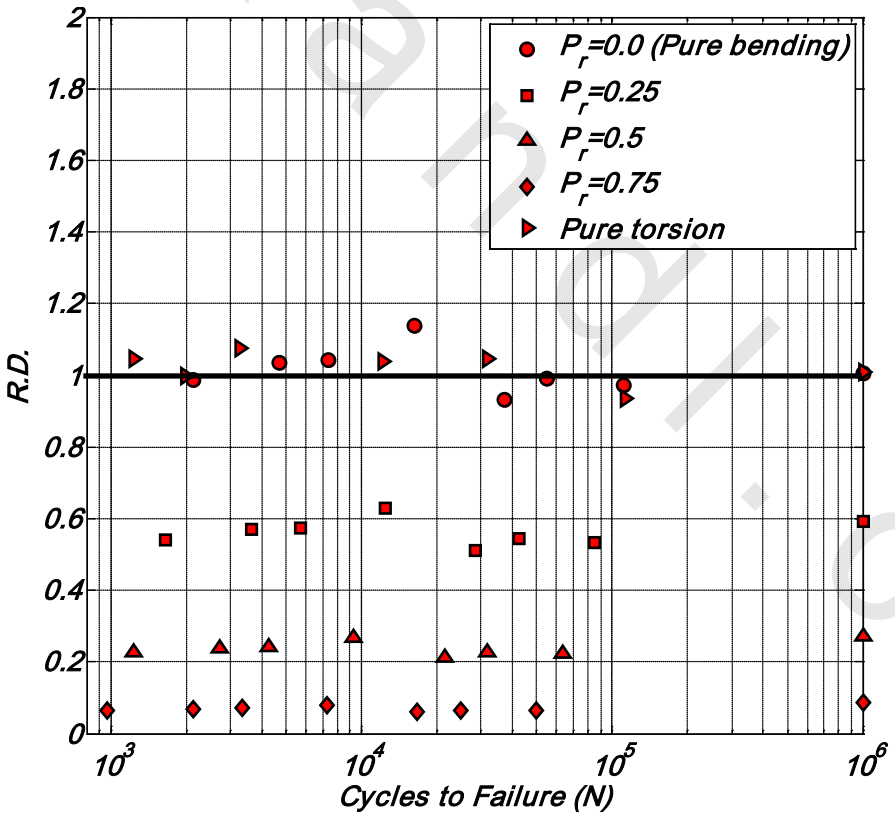

Figure 6.54 Relative damage (R.D.) applying Hill failure criterion for the M_1& $[0,90°]_{3s}$ specimens

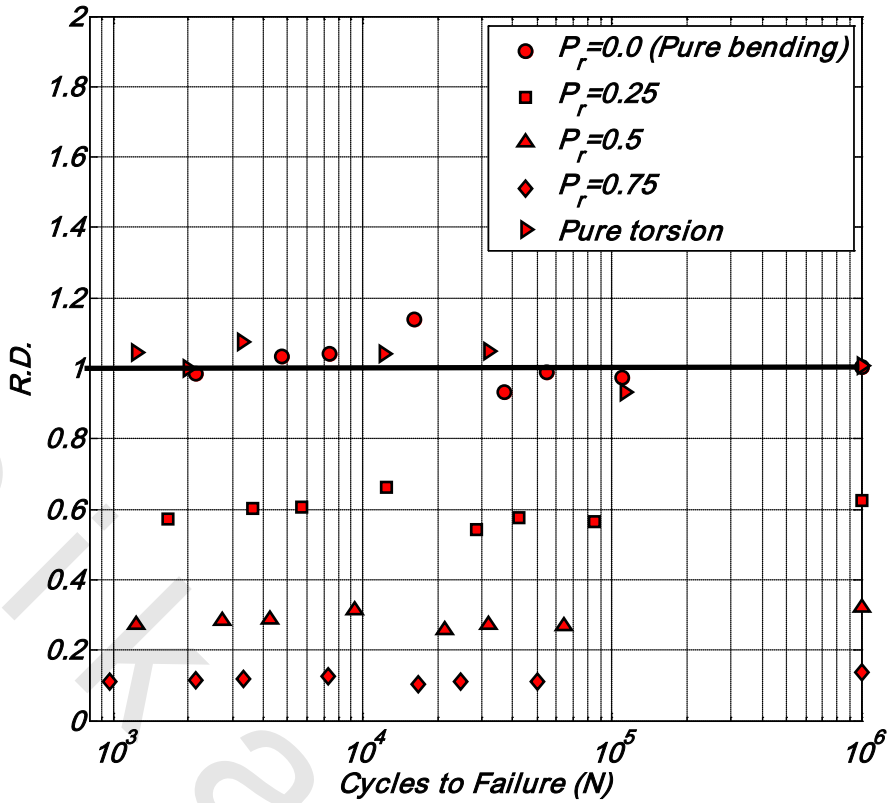

Figure 6.55 Relative damage (R.D.) applying Tsai-Hahn failure criterion for the M_1& $[0,90°]_{3s}$ specimens

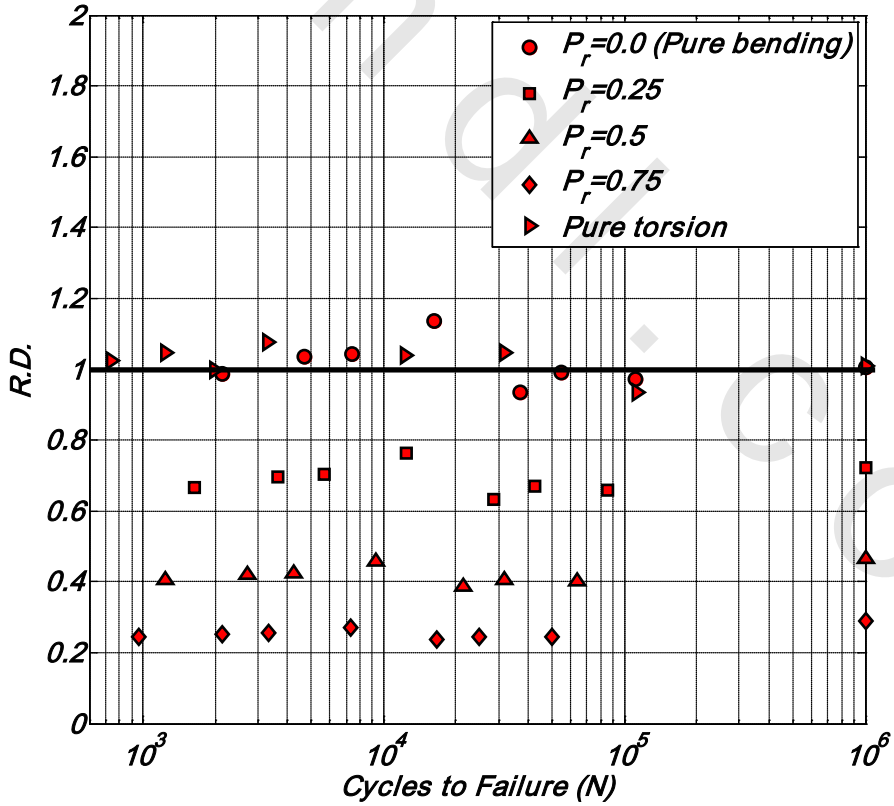

Figure 6.56 Relative damage (R.D.) applying Tsai-Wu failure criterion for the M_1& $[0,90°]_{3s}$ specimens

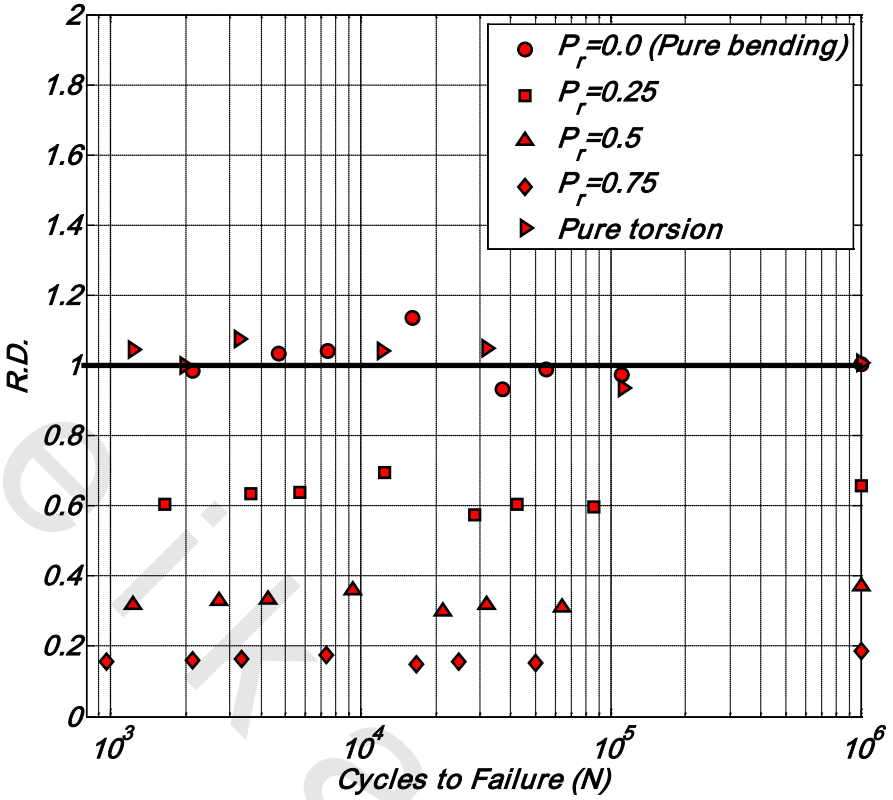

Figure 6.57 Relative damage (R.D.) applying Norris & Mckinnon failure criterion for the M_1& $[0,90°]_{3s}$ specimens

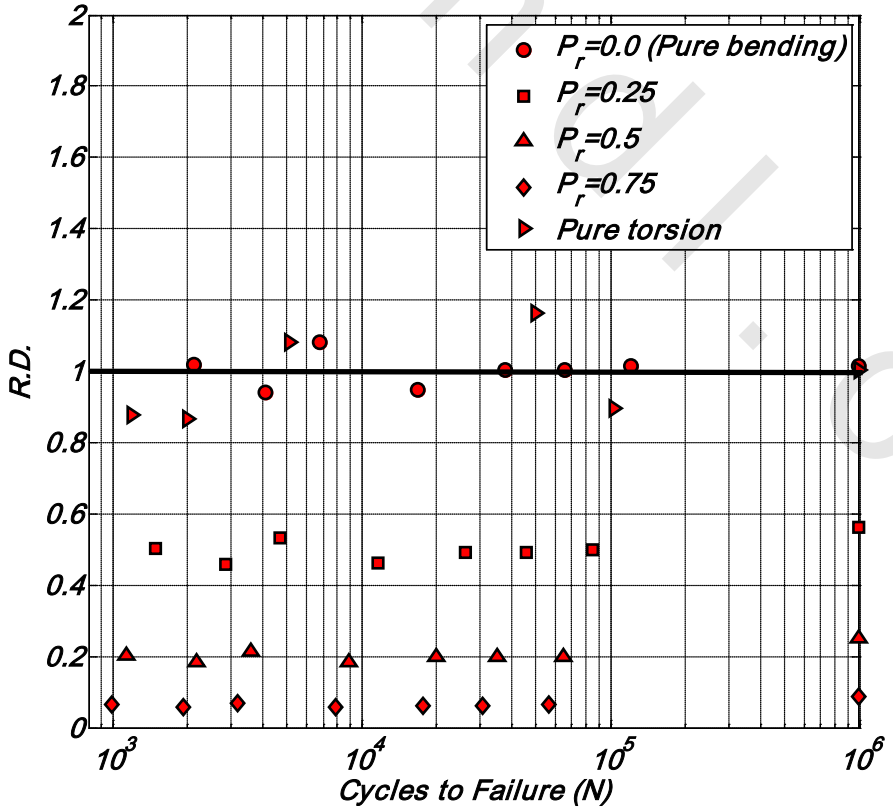

Figure 6.58 Relative damage (R.D.) applying Hill failure criterion for the M_2& $[0,90°]_{3s}$ specimens

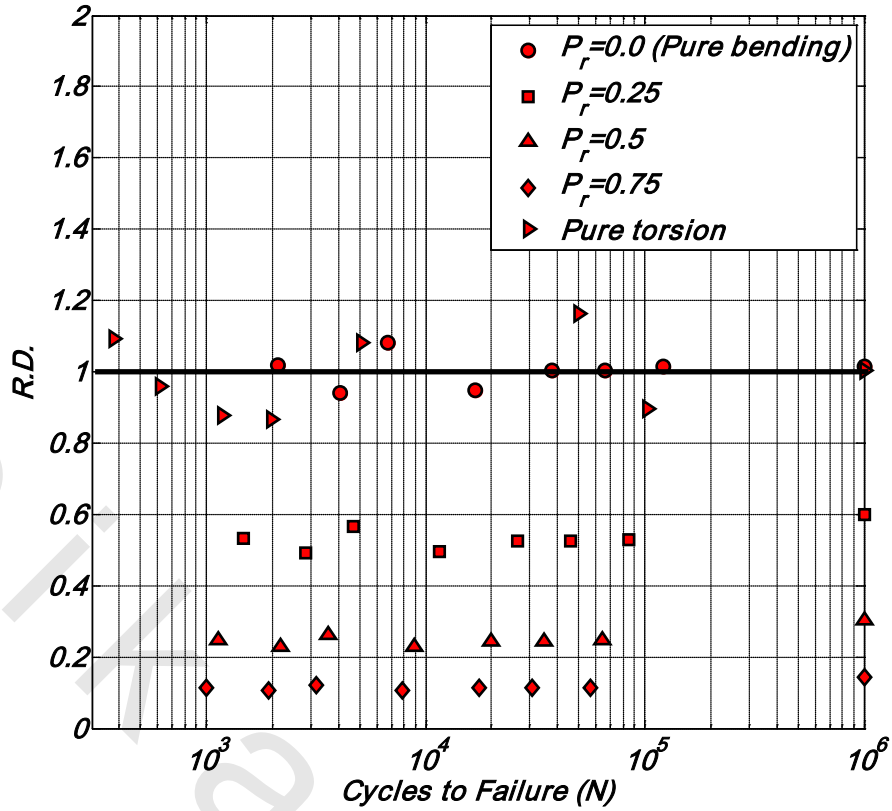

Figure 6.59 Relative damage (R.D.) applying Tsai-Hahn failure criterion for the M_2& $[0,90°]_{3s}$ specimens

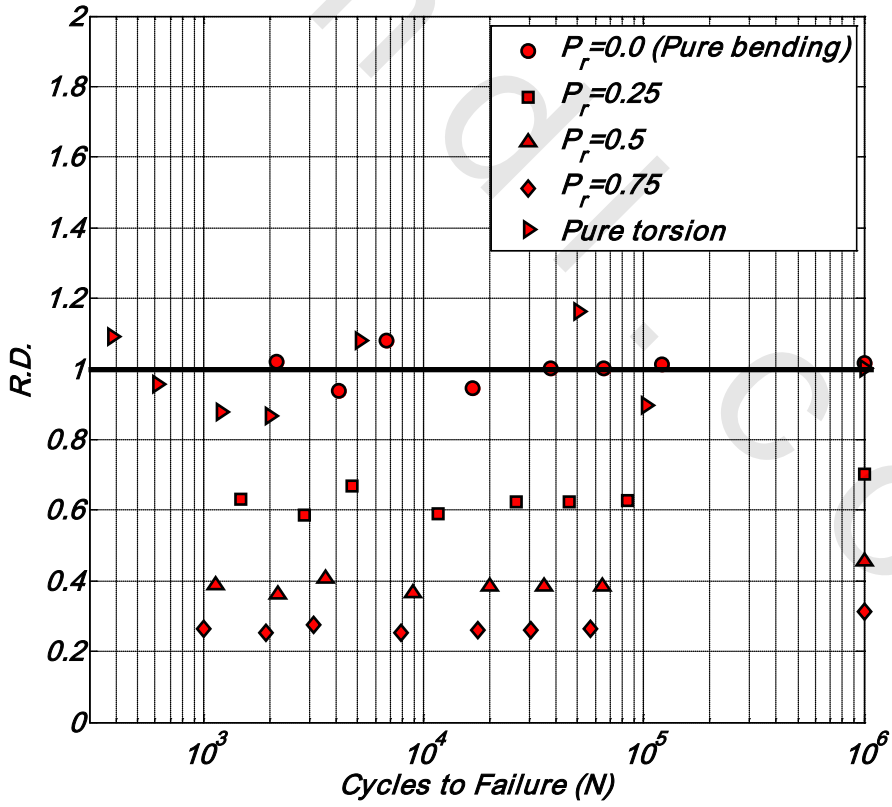

Figure 6.60 Relative damage (R.D.) applying Tsai-Wu failure criterion for the M_2& $[0,90°]_{3s}$ specimens

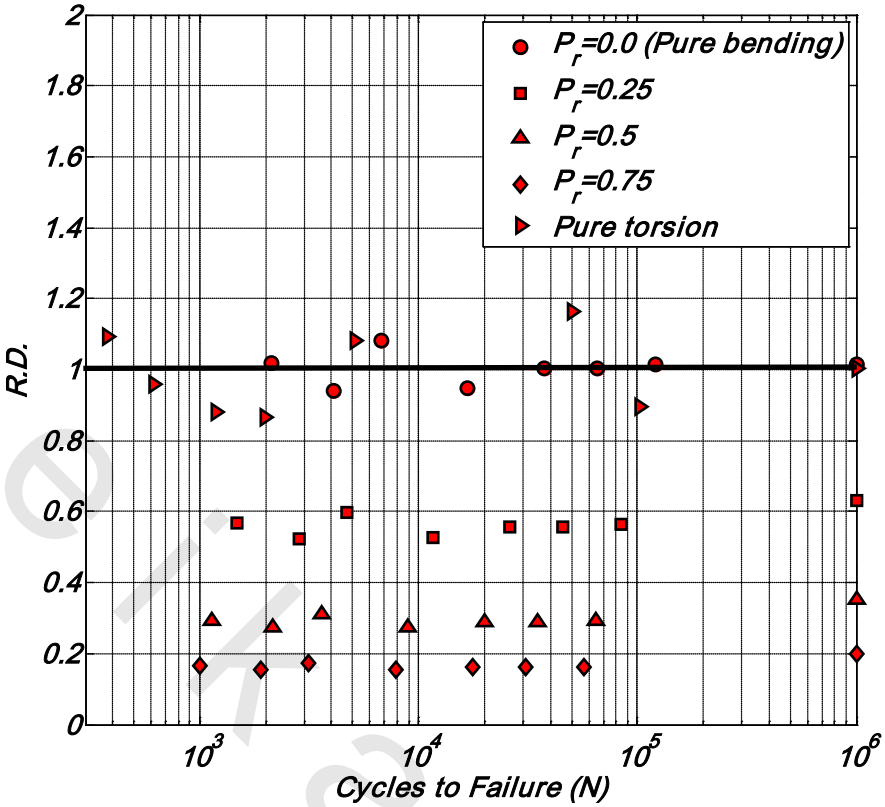

Figure 6.61 Relative damage (R.D.) applying Norris & Mckinnon failure criterion for the M_2 & $[0,90°]_{3s}$ specimens

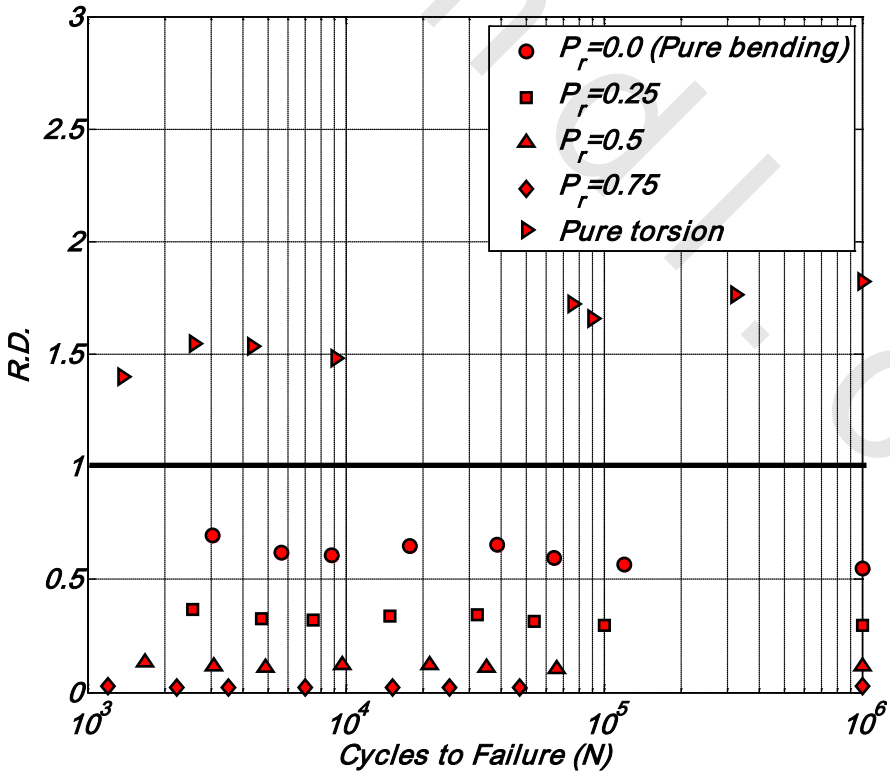

Figure 6.62 Relative damage (R.D.) applying Hill failure criterion for the M_1& $[\pm 45°]_{3s}$ specimens

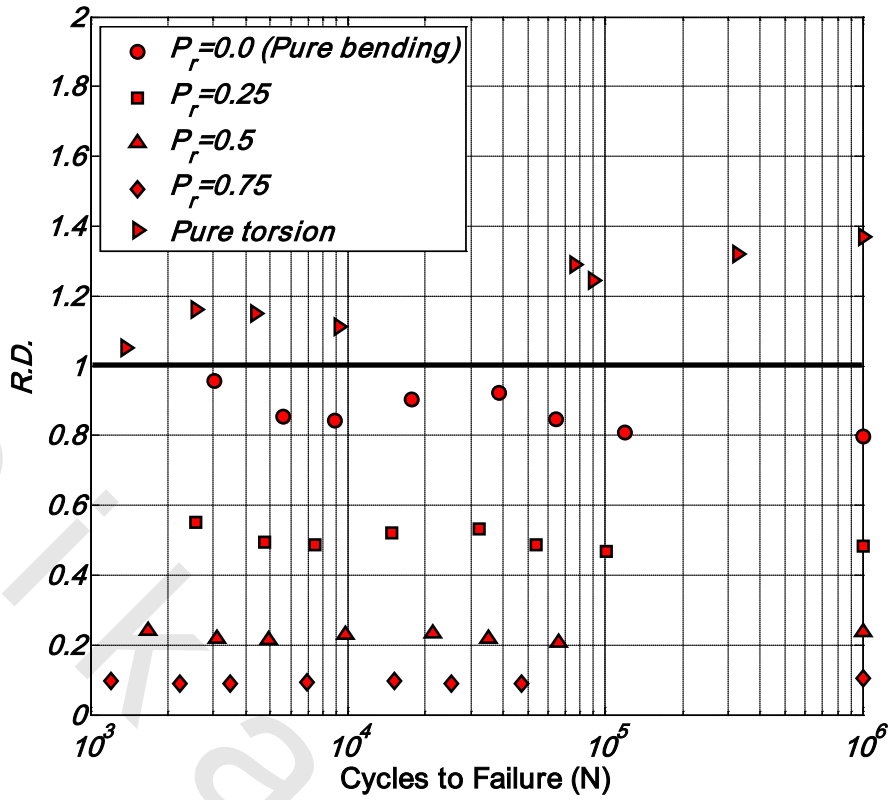

Figure 6.63 Relative damage (R.D.) applying Tsai-Hahn failure criterion for the M_1& $[\pm 45°]_{3s}$ specimens

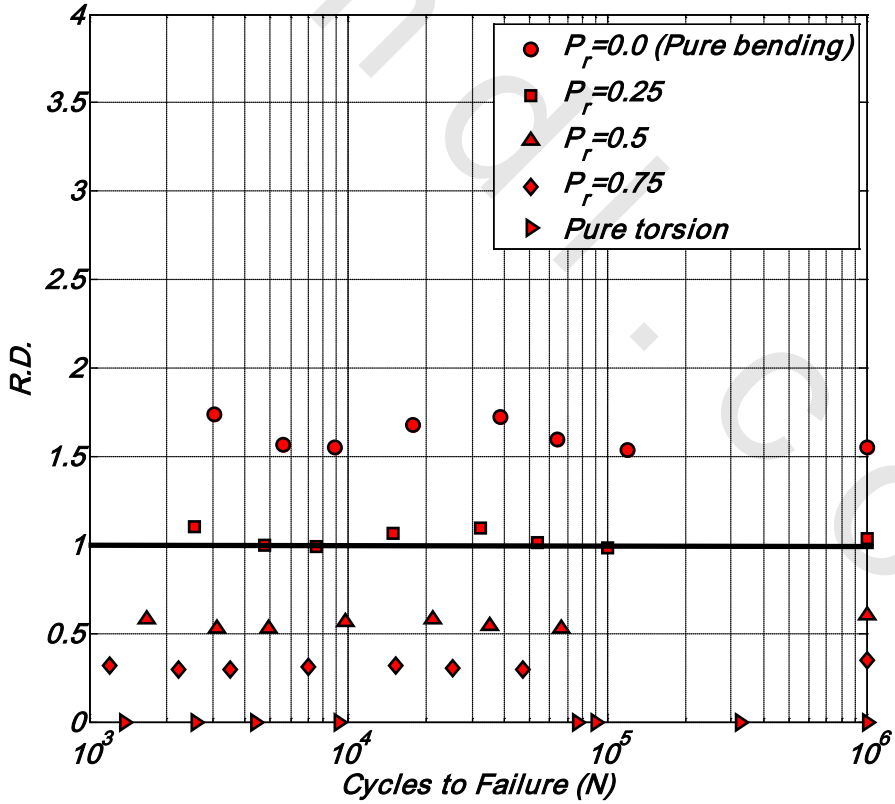

Figure 6.64 Relative damage (R.D.) applying Tsai-Wu failure criterion for the M_1& $[\pm 45°]_{3s}$ specimens

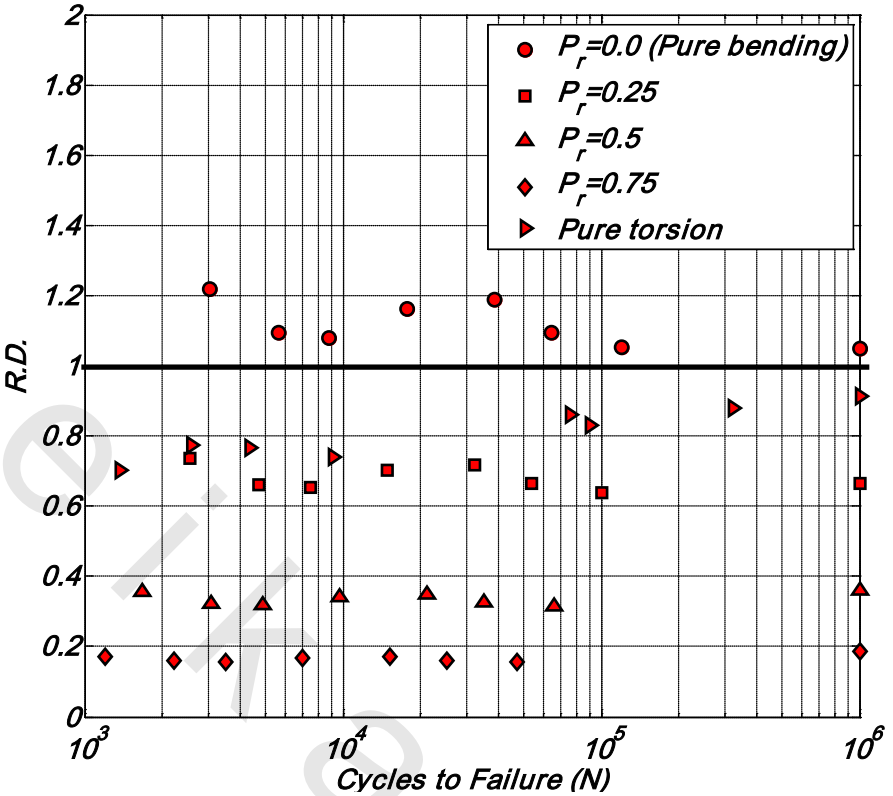

Figure 6.65 Relative damage (R.D.) applying Norris & Mckinnon failure criterion for the M_1& $[\pm 45°]_{3s}$ specimens

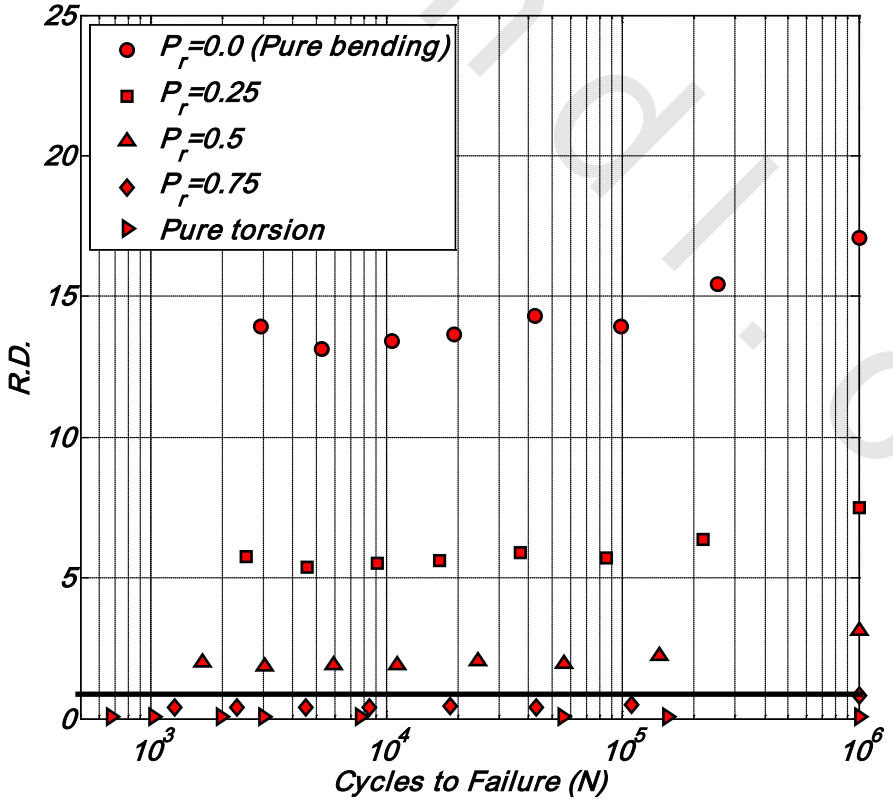

Figure 6.66 Relative damage (R.D.) applying Hill failure criterion for the M_2& $[\pm 45°]_{3s}$ specimens

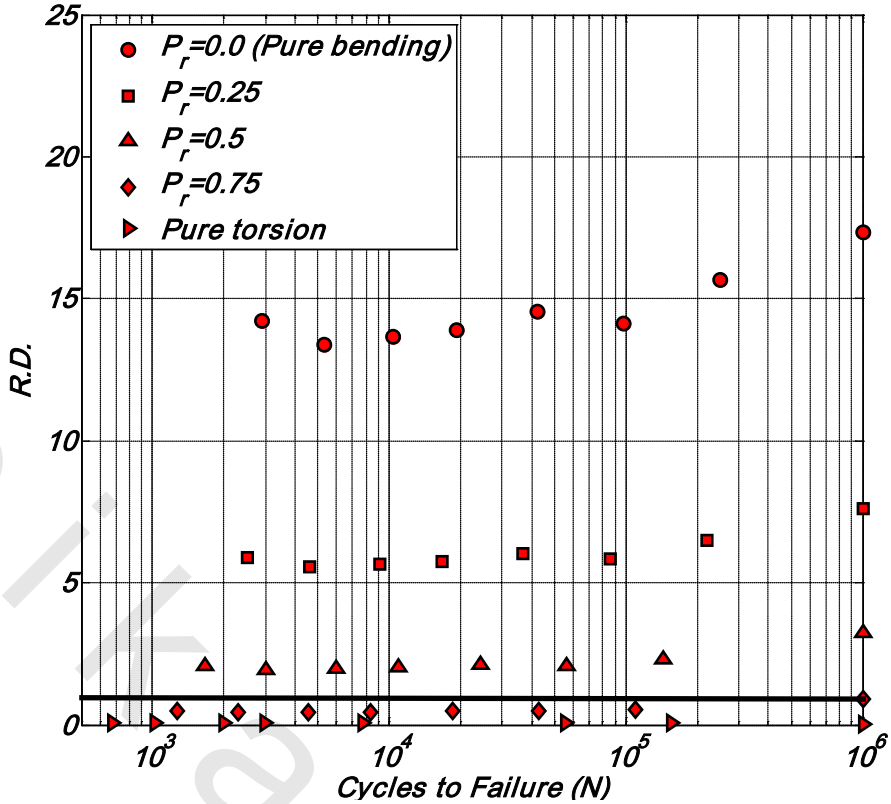

Figure 6.67 Relative damage (R.D.) applying Tsai-Hahn failure criterion for the M_2& $[\pm 45°]_{3s}$ specimens

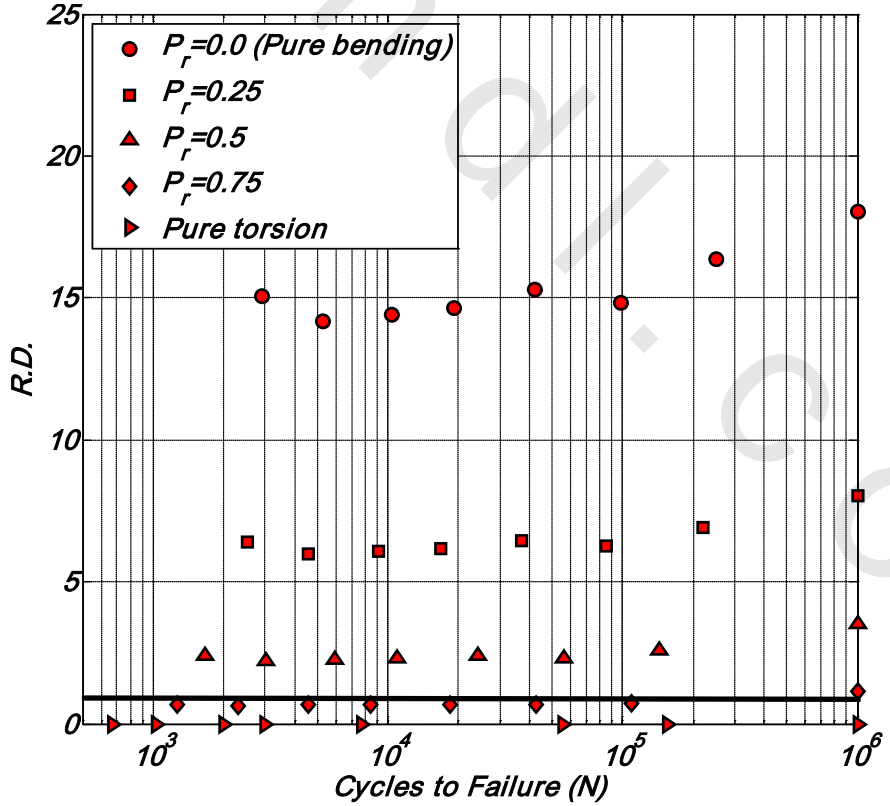

Figure 6.68 Relative damage (R.D.) applying Tsai-Wu failure criterion for the M_2& $[\pm 45°]_{3s}$ specimens

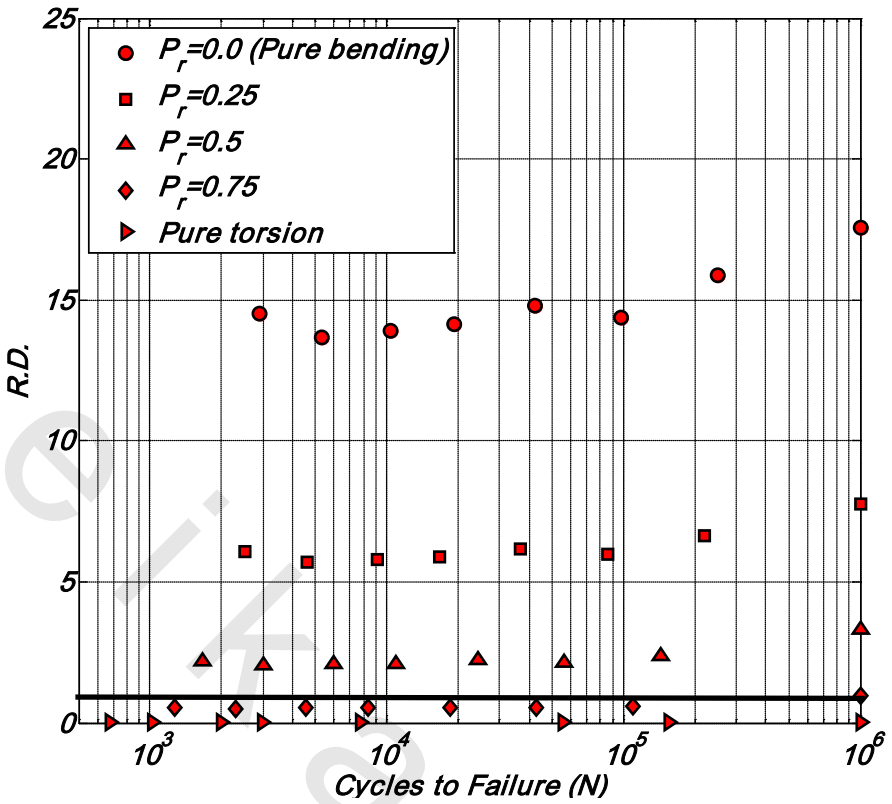

Figure 6.69 Relative damage (R.D.) applying Norris & Mckinnon failure criterion for the M_2& $[\pm 45°]_{3s}$ specimens

6.6.5 Modification of Failure Criteria

Choosing the suitable failure criterion represents the main target for many researchers working with materials, and it represents the first step for new materials before being used in the field. Considering composite materials, specifically, makes it more challenging, because of their very special behavior and characteristics. Besides, it must be noted that, the suitability of a certain criterion differs greatly according to the tested material, and its stress state. All failure criteria have their right hand side to be unity, and their left hand side contains the local stress components divided by their corresponding strengths. Therefore, the left hand side of any criterion was named to be its Relative Damage (R.D.) Secondly, a comparison was conducted for the value of the R.D. to unity, the criterion is suitable if its R.D. has a value near unity.

From the previous Figures 6.54 to 6.69, it is noted that; the relative damage R.D. values calculated from Tsai-Wu criterion at pure torsion for $[\pm 45°]_{3s}$ are equal zero. Therefore, we excluded it from our work; i.e. it is not suitable for the present case, Figure 6.64 and Figure 6.68. On other hand, all remaining theories of failure have very small values of R.D.

for all pressure ratios P_r and for both manufacturing method M_1 and M_2 with all fiber orientation accept fiber orientation $[\pm 45°]_{3s}$ in method M_2 only for all pressure ratios P_r, they have the values of R.D. far from unity. This may be explained by considering the drop in the values of fatigue constant c in $\tau_{max} = cN^d$, Figure 6.9, and local stresses due to the delamination failure mode during torsional tests of specimens from method M_2 (see section (6.2.1.2)), but this reason was not appear in values of R.D. for fiber orientation $[0,90°]_{3s}$ because, it had local stress σ_6 equal zero for all pressure ratio P_r.

El-Midany **[83]** modified the Tsai-Hahn criterion for the tension-tension stress state, this equation was valid only for *[±45°]* fiber orientation in pure bending; the modified equation was presented in form:

$$\left(\frac{\sigma_1}{F_1}\right)^2 + \left(\frac{\sigma_2}{F_2}\right)^2 + \left(\frac{\sigma_6}{F_6}\right)^2 + 2(\sigma_1\sigma_2)\left(\frac{2}{A_{45}^2} - \frac{1}{F_1^2} - \frac{1}{2F_6^2}\right) = R.D$$

Where, A_{45} is the strength of the *[±45°]* specimens under pure bending test.

The values of R.D. after modification, according to Tsai-Hahn modification of El-Midany **[83]**, were plotted for the present work against the number of cycles to failure under both manufacturing method M_1 and M_2 with both fiber orientations as shown in Figure 6.70.

Figure 6.70 shows that El-Midany **[83]** modifying criterion was not suitable for present study where, the values of R.D. were far from the theoretical value of unity for both manufacturing method M_1 and M_2 with both fiber orientations. This also because the value of the fatigue constant (c) in the completely reversed pure torsion tests for manufacturing method M1 were decreased as all previous failure Criteria.

El-hadary **[86]** modified the Tsai-Hahn criterion for in-phase negative stress ratios (R), this equation was formed for two fiber orientations only *[±45°]* and *[0,90°]* .

$$\left(\frac{\sigma_1}{F_1}\right)^2 + \left(\frac{\sigma_2}{F_2}\right)^2 + \left(\frac{\sigma_6}{F_6}\right)^2 + K_1\left(\frac{\sigma_1\sigma_2}{F_1F_2}\right) + K_2\left(\frac{\sigma_1\sigma_6}{F_1F_6}\right) + K_3\left(\frac{\sigma_2\sigma_6}{F_2F_6}\right) = R.D$$

Where:

$$K_1 = -0.003\left(\frac{A}{B}\right) + 12.5(R) + 10\ ,$$

$$K_2 = -1.97\left(\frac{A}{B}\right)^2 + 5.27\left(\frac{A}{B}\right) - 0.37(R) - 2.6,$$

$$K_3 = -0.33\left(\frac{A}{B}\right) - 11.4(R) - 8$$

El-hadary **[87]** modified the Tsai-Hahn criterion for out-in-phase negative stress ratios (R), this equation was formed for two fiber orientations only *[±45°]* and *[0,90°]* .

$$\left(\frac{\sigma_1}{F_1}\right)^2 + \left(\frac{\sigma_2}{F_2}\right)^2 + \left(\frac{\sigma_6}{F_6}\right)^2 - \left(\frac{\sigma_1\sigma_2}{F_1F_2}\right) + H_{16}\left(\frac{\sigma_1\sigma_6}{F_1F_6}\right) = R.D$$

Where:

$H_{16} = \frac{Z+R}{Z+q}$, $q = \left(\frac{A}{B}\right)$,

$\left(\frac{A}{B}\right)$: The ratio between bending and torsional stresses,

z : The phase angle between bending and twisting moment

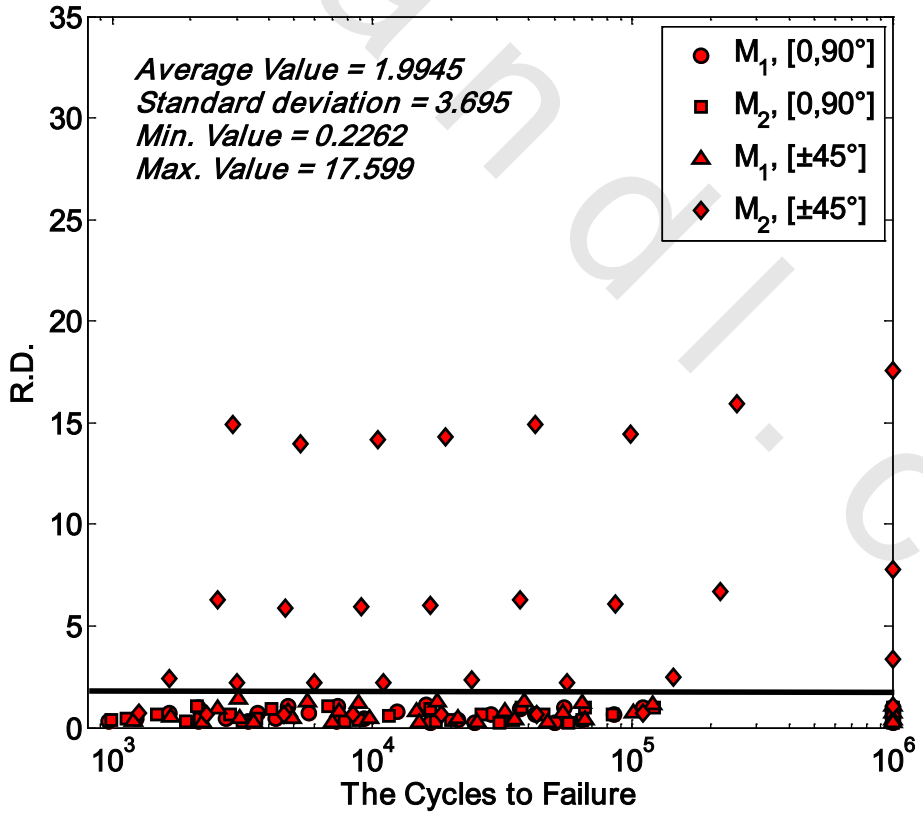

Figure 6.70.Relative damage (R.D.) applying El-Midany **[83]** failure criterion for both manufacturing method M_1 and M_2 for all fiber orientations and all pressure ratios.

Mohamed **[88]** modified the Tsai-Hahn criterion for in-phase negative and positive stress ratios (R), he was modified two equations one for negative stress ratio and the other for positive stress ratios, both equations were formed for four fiber orientations *[±45°]*, *[0,90°]*, *[30º,-60°]* and *[60º,-30°]* as:

$$\left(\frac{\sigma_1}{F_1}\right)^2+\left(\frac{\sigma_2}{F_2}\right)^2+\left(\frac{\sigma_6}{F_6}\right)^2-K_1\left(\frac{\sigma_1\sigma_2}{F_1F_2}\right)+K_2\left(\frac{\sigma_1\sigma_6}{F_1F_6}\right)=R.D \qquad \text{(for negative stress ratios)}$$

$$\left(\frac{\sigma_1}{F_1}\right)^2+\left(\frac{\sigma_2}{F_2}\right)^2+\left(\frac{\sigma_6}{F_6}\right)^2-\left(\frac{\sigma_1\sigma_2}{F_1F_2}\right)+K_3\left(\frac{\sigma_1\sigma_6}{F_1F_6}\right)=R.D \qquad \text{(for positive stress ratios)}$$

Where:

$$K_1=\theta\left(\frac{S_{us}}{S_{es\ (pure\ \ torsion\ )}}\right),$$

$$K_2=\left(\frac{(\theta-R)}{\left(\theta-\left(\frac{A}{B}\right)\right)}\right)\left(\frac{S_{us}}{S_u}\right)_{[0,90°]},$$

$$K_3=R\left(\theta^2+\frac{1}{\left(\frac{A}{B}\right)}\right)\left(\frac{S_u^2}{A_\theta\ S_{es\ (pure\ \ torsion\ )}}\right),$$

θ: Fiber orientation angle in rad,

A_θ: The strength of specimen corresponding to its fiber orientation.

S_{es}: The endurance limit in shear strength.

The values of R.D. were calculated for present work according to Tsai-Hahn modification of Mohamed **[88]** for negative stress ratio, and plotted against the number of cycles to failure under both manufacturing method M_1 and M_2 with both fiber orientations as shown in Figure 6.71.

Figure 6.71 shows that Mohamed **[88]** modifying criterion was not valid for present work where, the values of R.D. were far from the theoretical value of unity for both manufacturing method M_1 and M_2 with both fiber orientations. This also due to the drop in value of the fatigue constant (c) in the completely reversed pure torsion tests for manufacturing method M1, this conclusion was found also when apply the other failure Criteria.

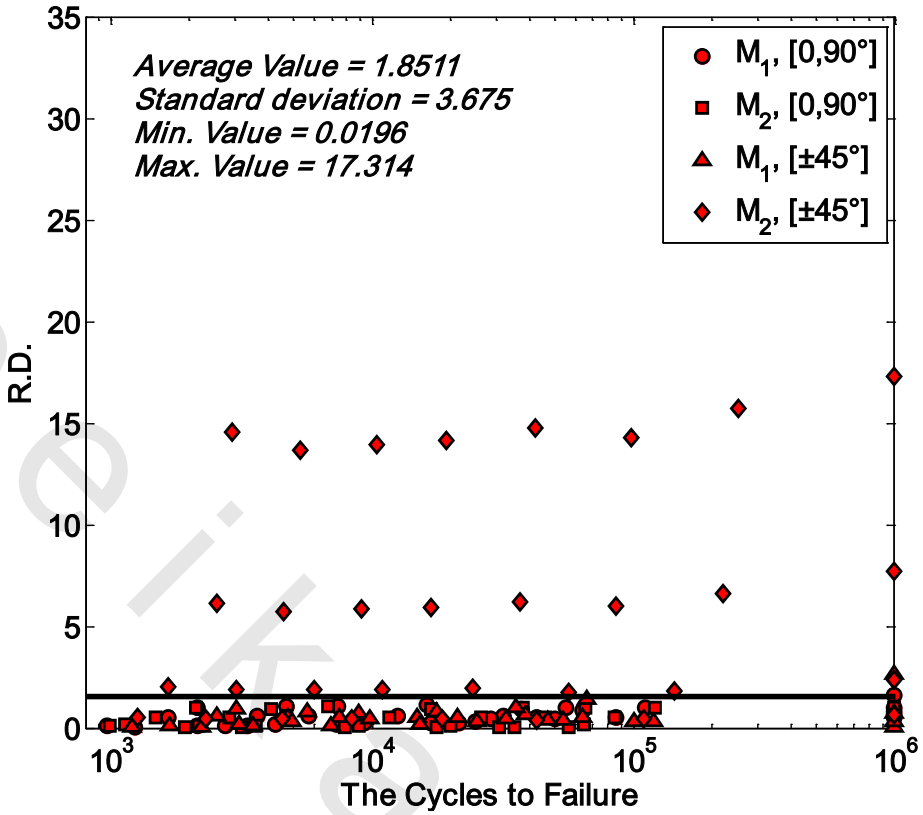

Figure 6.71.Relative damage (R.D.) applying Mohamed **[88]** failure criterion for both manufacturing method M_1 and M_2 for all fiber orientations and all pressure ratios.

Taking the previous works of **[83-88]** , **[125]** into consideration, it is obvious that, the Tsai-Hahn is more suitable failure criteria for the tension-compression stress state and it may be modified to best suit the present work; i.e. making the R.D.

Consequently, a new procedure was proposed for adapting these two criteria to best fit the tested case. The suggested procedure was based mainly on introducing a new term to increase the correlation between the experimental data and the theoretical equations.

6.6.5.1 The main principals for selecting the new term

1. It must reflect the effect of both, hoop and amplitude stress components.
2. It must depend on the local stress and strength components and not the global ones.
3. It should contain a minimum number of variables, as possible, for simplicity and ease of use.
4. It must be dimensionless.

The previous principals led us to suggest the following forms of failure criterion for all pressure ratios under both manufacturing method M_1 and M_2 for all fiber orientations:

$$\left(\frac{\sigma_1}{F_1}\right)^2 + \left(\frac{\sigma_2}{F_2}\right)^2 + W_1\left(\frac{\sigma_6}{F_6}\right)^2 - W_2\left(\frac{\sigma_1\sigma_2}{F_1F_2}\right) + W_3\left(\frac{\sigma_1}{F_1}\right) + W_4\left(\frac{\sigma_2}{F_2}\right) = 1$$

Where:

$$W_1 = \left(\frac{[S_{us}]_{[\theta,M]}}{[S_{us}]_{[\pm 45°,M_1]}}\right)^{\left[\frac{n^2\theta}{2}\right]}$$

$$W_2 = \left(\frac{[S_{us}]_{[\theta,M]}}{[S_u]_{[\theta,M]}}\right)$$

$$W_3 = (P_r)\left(\frac{[S_H]_{[\theta,M]}}{[S_L]_{[\theta,M]}}\right)\left(\frac{[S_u]_{[\pm 45°,M_2]}}{[S_u]_{[\theta,M]}}\right)$$

$$W_4 = (P_r)\left[\left(\frac{[S_{us}]_{[\pm 45°]}}{[S_{us}]_{[0,90°]}}\right)_{[M_2]}\right]^2$$

P_r: Pressure ratio.

θ: Fiber orientation angle in rad.

n: Number of layers.

$[S_{us}]_{[\theta,M]}$: Ultimate global shear strengths corresponding to fiber orientation and manufacturing method.

$[S_u]_{[\theta,M]}$: Ultimate global bending strengths corresponding to fiber orientation and manufacturing method.

$[S_H]_{[\theta,M]}$: The maximum hoop strength corresponding to its fiber orientations and manufacturing method.

$[S_L]_{[\theta,M]}$: The maximum longitudinal strength corresponding to its fiber orientations and manufacturing method.

The values of R.D. after modification, according to the new failure criteria, were plotted against the number of cycles to failure under both manufacturing method M_1 and M_2 for both fiber orientations as shown in Figure 6.72.

Figures 6.72 show that the modifying criterion gives excellent results for both manufacturing method M_1 and M_2 for all fiber orientations and for all pressure ratios, where, the values of R.D. are around the theoretical value of unity. For both manufacturing method M_1 and M_2 for all fiber orientations. The R.D. are ranging from 0.9166 as a minimum value to 1.1966 as a maximum value with an average value of 1.0445 and standard deviation of 0.0612 which are very near to unity, and the difference may be referred to scatter in experimental data.

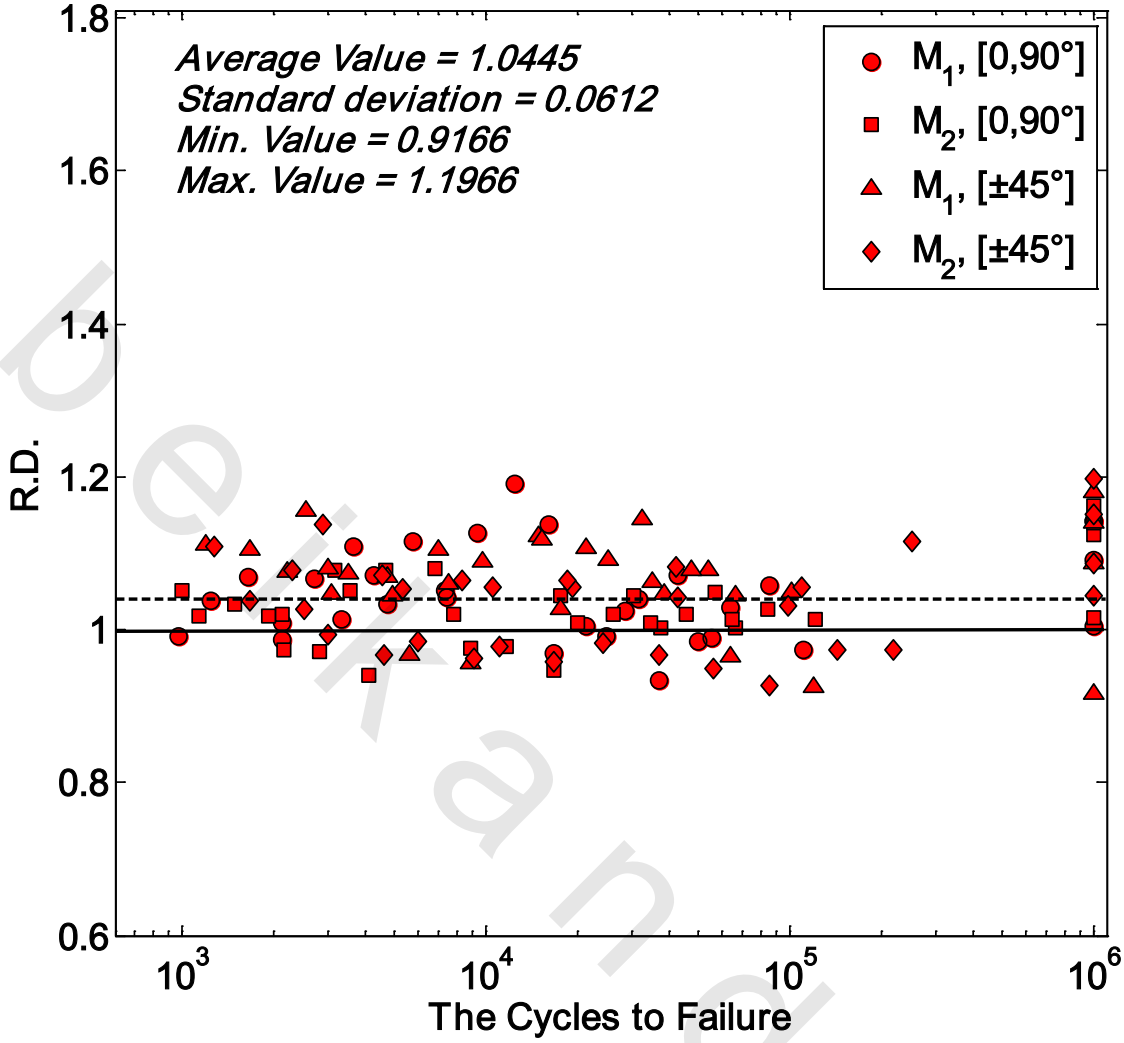

Figure 6.72.Relative damage (R.D.) applying present failure criterion for both manufacturing method M_1 and M_2 for all fiber orientations and all pressure ratios.

6.6.6 Confirmation of Modified Failure Criteria

Checking the applicability of the modified failure criterion for using in wide range of different materials, fiber orientations under different types of testing conditions, the data adapted from different works will be used to substitute in the failure criterion before and after modification, then the comparison between them to insure that the modified Tsai-Hahn equation is applicable to use or not.

In order to check the validity of modified Tsai-Hahn equation for using in wide range of different materials under different types of testing conditions, data was obtained from El-midany **[83]**, El-hadary **[86-87]** and Mohamed **[88]** they specimens had nearly the same specifications as those used in this work, being woven-roving glass fiber reinforced polyester (GFRP) tubular specimens with (V_f) ranging from 50% to 64% and two fiber

orientations $[0,90°]_{2s}$, $[\pm45°]_{2s}$ under completely reversed pure bending, Tables A3.59 to A3.72. They found when substituting by these data in Tsai-Hahn equation before modification, as shown in Figures 6.73 , 6.75 and 6.77 for the $[0,90°]_{2s}$ and $[\pm45°]_{2s}$ specimens for El-midany **[83]**, El-hadary **[86-87]** and Mohamed **[88]** respectively with average value of R.D equal to 0.944467, 0.932971 and 0.888441 respectively and standard deviation 13.05%, 11.63 and 13.1% respectively.

Figures 6.74, 6.76 and 6.78 represents the R.D. for the same set of data adapted from El-midany **[83]**, El-hadary **[86-87]** and Mohamed **[88]** respectively for the $[0,90°]_{2s}$ and $[\pm45°]_{2s}$ specimens after using the present criterion. This figures show an improving in the values of R.D. and standard deviation when using the modified equation. The average value has been improved from 0. 944467 to 0.99564 and standard deviation from 13.05% to 9.98% for data adapted from El-midany **[83]**, the average value has been improved from 0.932971 to 0.974918 and standard deviation from 11.63% to 9.47% for data adapted from El-hadary **[86-87]** and the average value has been improved from 0. 888441 to 0.929712 and standard deviation from 13.1% to 9.06% for data adapted from Mohamed **[88]**.

In order to check the validity of modified Tsai-Hahn equation for using in wide range of different fiber orientations data was obtained Mohamed **[88]**. He used specimens had nearly the same specifications as those used in this work, being woven-roving GFRP tubular specimens with (V_f) ranging from 50% to 64% and another two fiber orientations $[30°,-60°]_{2s}$, $[60°,-30°]_{2s}$ under completely reversed pure bending, Tables A3.73 to A3.76. Figures 6.79 and 6.80 show the change of average value of the R.D. from 0.8565 to 1.048556 and standard deviation from 17.44% to 7.09%.

Using the same procedure to check the applicability of the modified failure criterion for using in the other works, Amijima et al. **[72]**, used the same material as that used in this work, being a unidirectional glass/epoxy composite material with fiber volume fraction (V_f) of 64%. They tested their specimens under completely reversed bending and torsional stresses. Using this data, Table A3.77, to confirm the present criterion Figure 6.81 represents the R.D using the present failure criterion equation. This Figure shows the good average value of R.D and standard deviation when using the modified Tsai-Hahn equation. The average value of R.D. and standard deviation are 0.999529 and 8.827% respectively.

Figure 6.82 shows a good average value of R.D. and standard deviation are 0.99666 and 6.348% respectively after using the suggested failure criterion for the data adapted from

Atcholi et al. **[151]**, Table A3.80. For the data adapted from Kawakami et al. **[152]**, Table A3.79, Figure 6.83 shows the average value of R.D. and standard deviation are 0.9383 and 15.866% respectively, using the suggested failure criterion.

Ahmed M.E. et al. **[75]**, used the different material as that used in this work, being a unidirectional glass/polyester composite material with fiber volume fraction (V_f) of 44.7%, Table A3.78. They tested their specimens under completely reversed combined bending and torsional stresses in-phase. Figure 6.84 represents the R.D using the present failure criterion equation. This Figure shows also good average value of R.D and standard deviation when using the modified Tsai-Hahn equation. The average value of R.D. and standard deviation are 1.011022 and 1.396% respectively.

Finally, a new form of failure criteria was introduced to govern the fatigue behavior of woven-roving GFRE under combined completely reversed bending moment and internal pressure for both fiber orientations $[0,90°]_{3s}$ and $[\pm45°]_{3s}$ and both method of manufacturing M_1 and M_2 can be used in wide range of different materials, fiber orientations under different types of testing conditions with good results of the average value of R.D. and standard deviation.

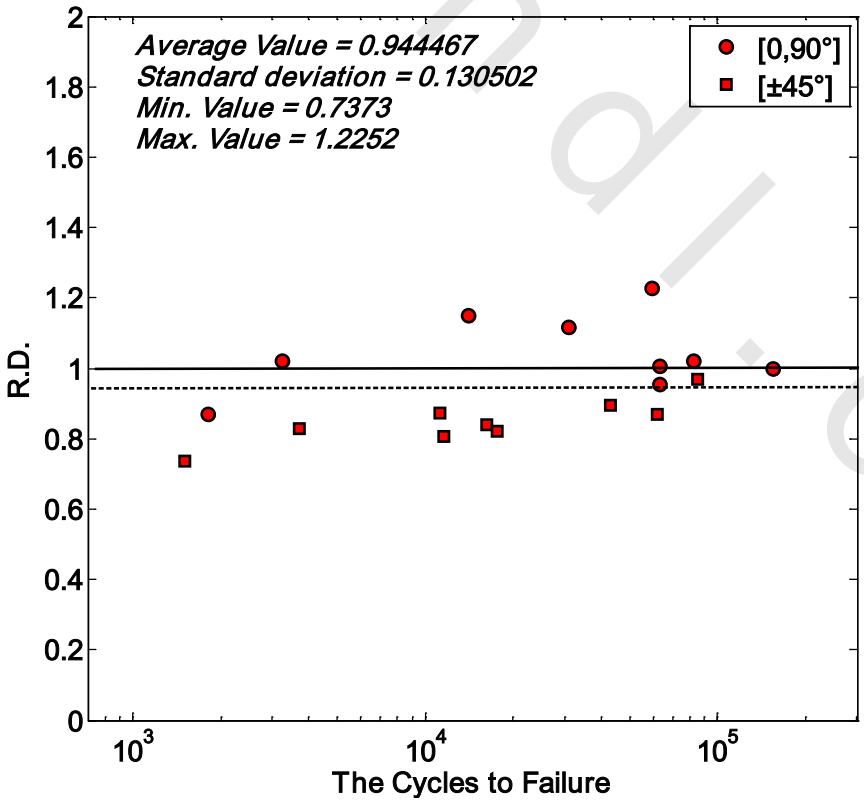

Figure 6.73.Relative damage (R.D.) applying the old failure criterion for data adapted from El-midany **[83]** Under R = -1 and Pr = 0.

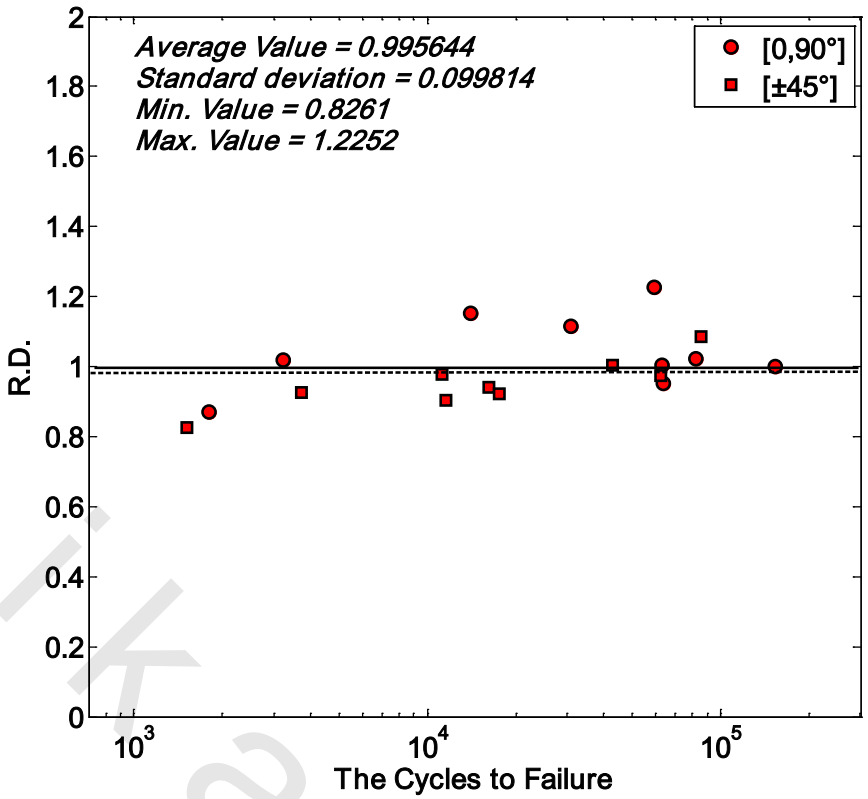

Figure 6.74.Relative damage (R.D.) applying the new failure criterion for data adapted from El-midany **[83]** Under R = -1 and Pr = 0.

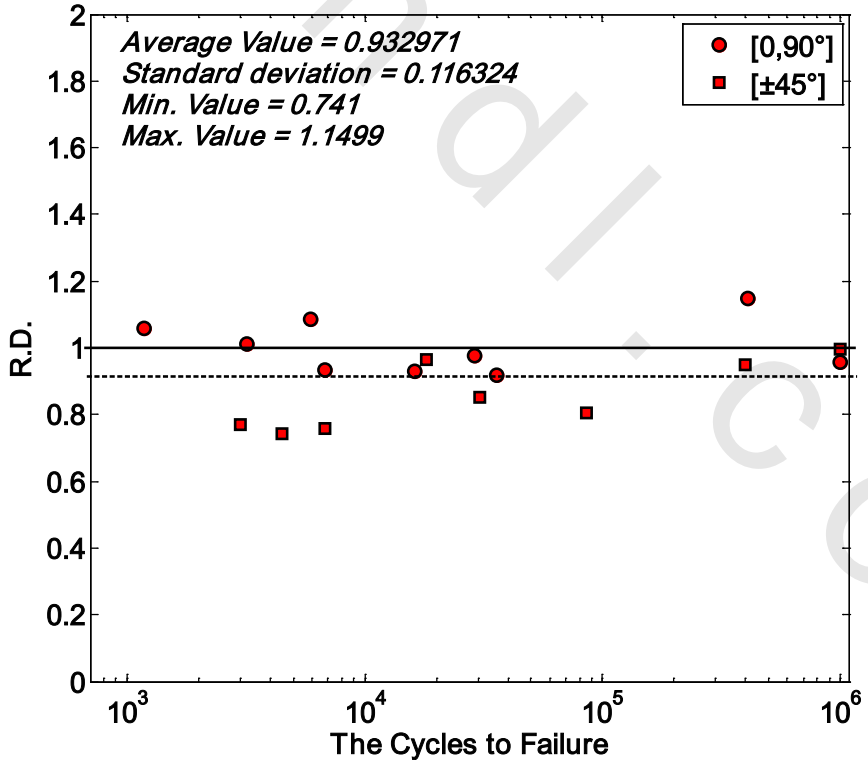

Figure 6.75.Relative damage (R.D.) applying the old failure criterion for data adapted from El-hadary **[86-87]** Under R = -1 and Pr = 0.

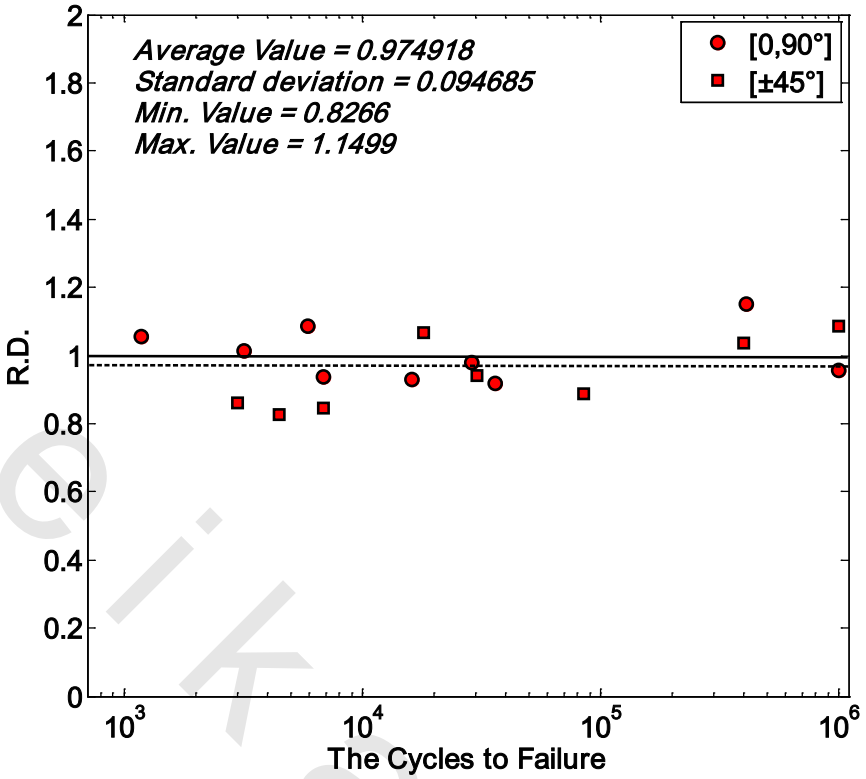

Figure 6.76.Relative damage (R.D.) applying the new failure criterion for data adapted from El-hadary **[86-87]** Under R = -1 and Pr = 0.

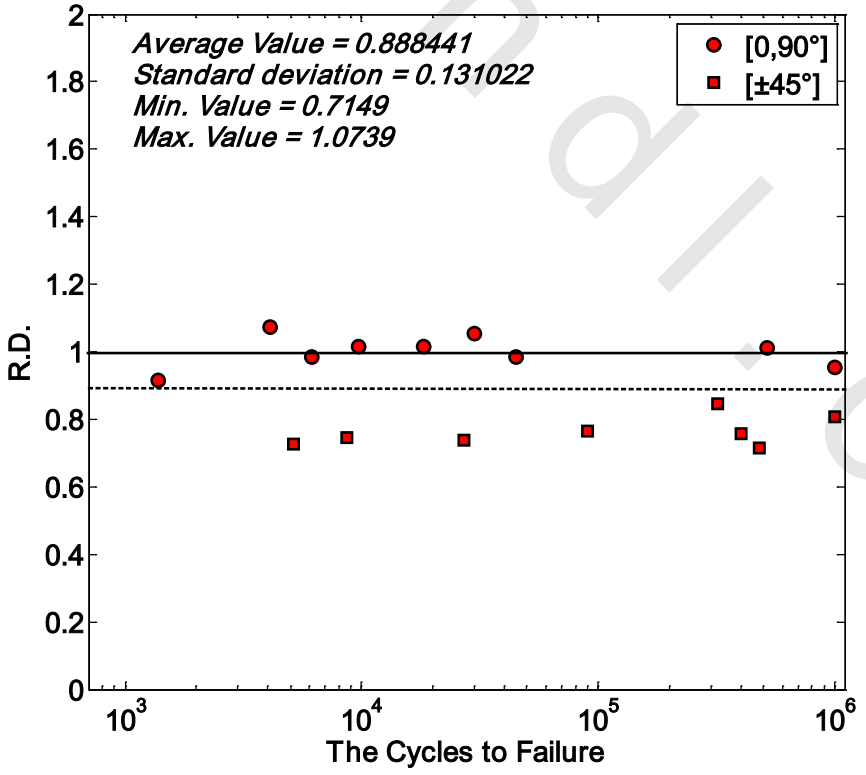

Figure 6.77.Relative damage (R.D.) applying the old failure criterion for fiber orientations $[0,90°]_{2s}$ and $[\pm45°]_{2s}$ of data adapted from Mohamed **[88]** Under R = -1 and Pr = 0.

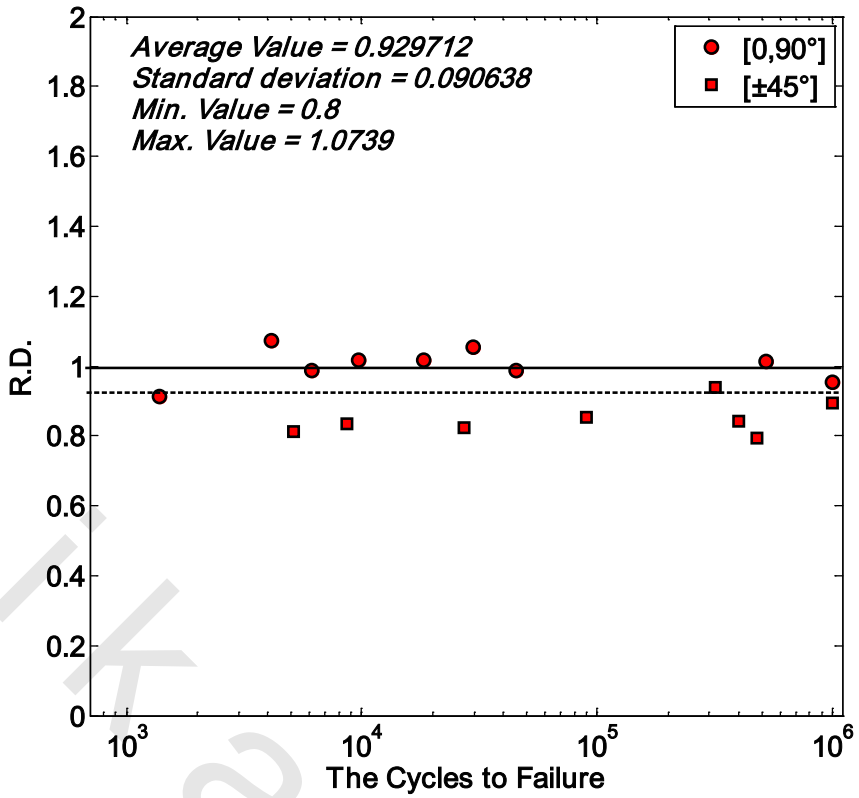

Figure 6.78.Relative damage (R.D.) applying the new failure criterion for fiber orientations $[0,90°]_{2s}$ and $[\pm45°]_{2s}$ of data adapted from Mohamed **[88]** Under R = -1 and Pr = 0.

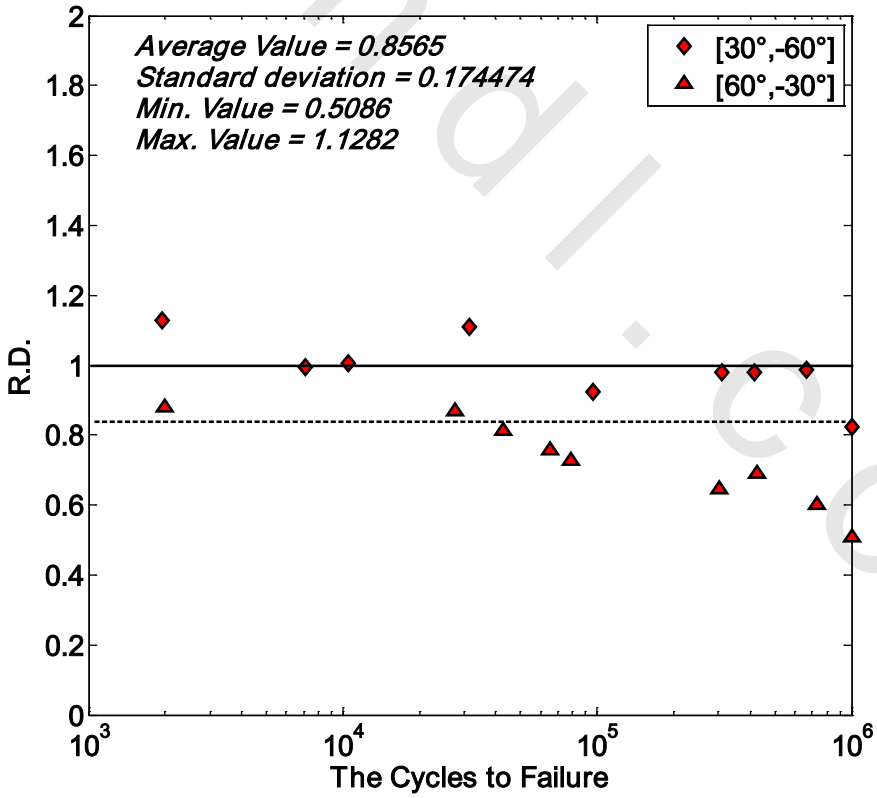

Figure 6.79.Relative damage (R.D.) applying the old failure criterion for fiber orientations $[30°,-60°]_{2s}$, $[60°,-30°]_{2s}$ of data adapted from Mohamed **[88]** Under R = -1 and Pr = 0.

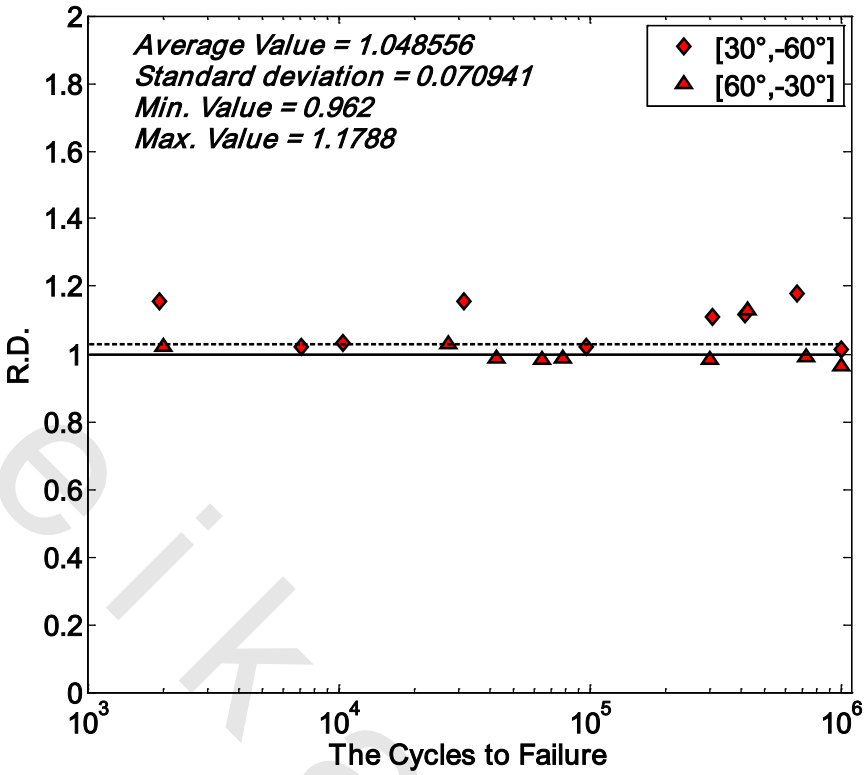

Figure 6.80.Relative damage (R.D.) applying the new failure criterion for fiber orientations $[30°,-60°]_{2s}$, $[60°,-30°]_{2s}$ of data adapted from Mohamed **[88]** Under R = -1 and Pr = 0.

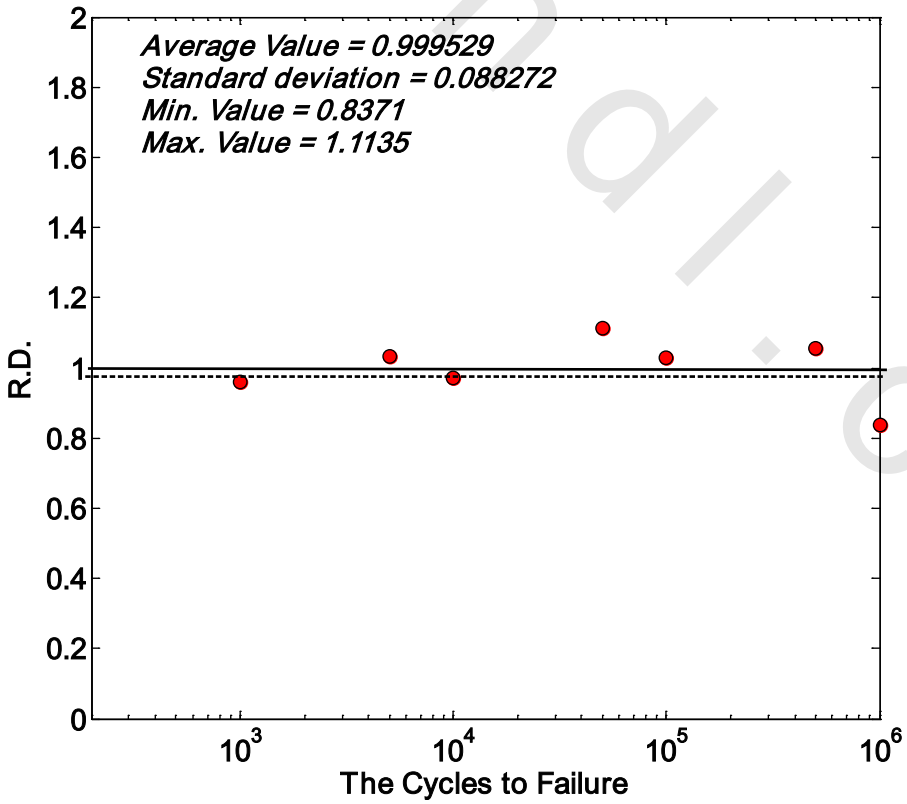

Figure 6.81.Relative damage (R.D.) applying the new failure criterion for data adapted from Amijima et al. **[72]** Under R = -1 and Pr = 0.

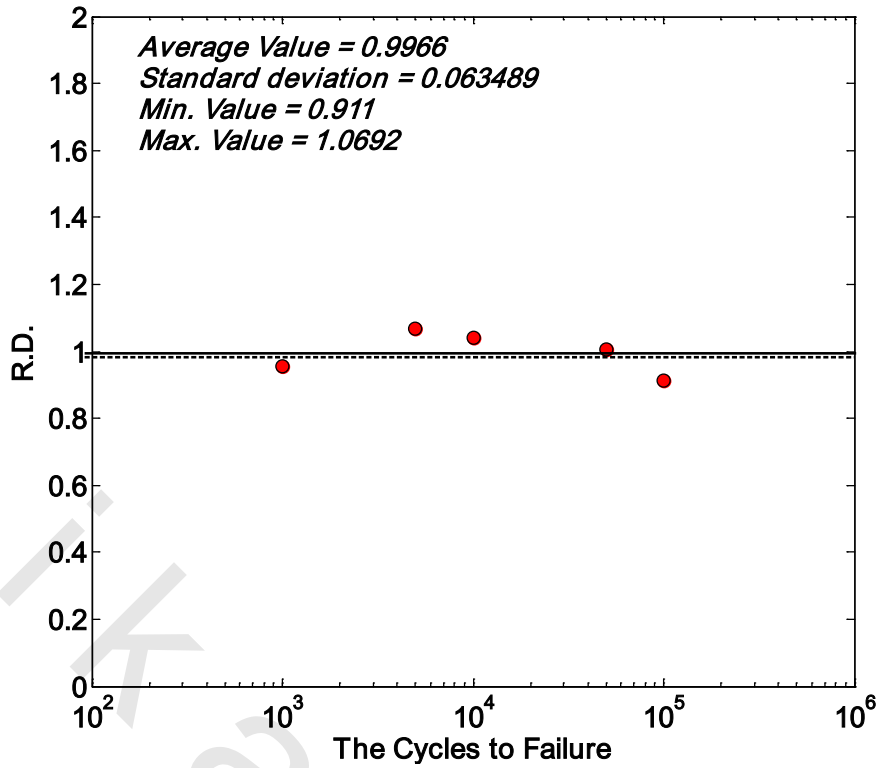

Figure 6.82.Relative damage (R.D.) applying the new failure criterion for data adapted from Atcholi et al. **[151]** Under R = -1 and Pr = 0.

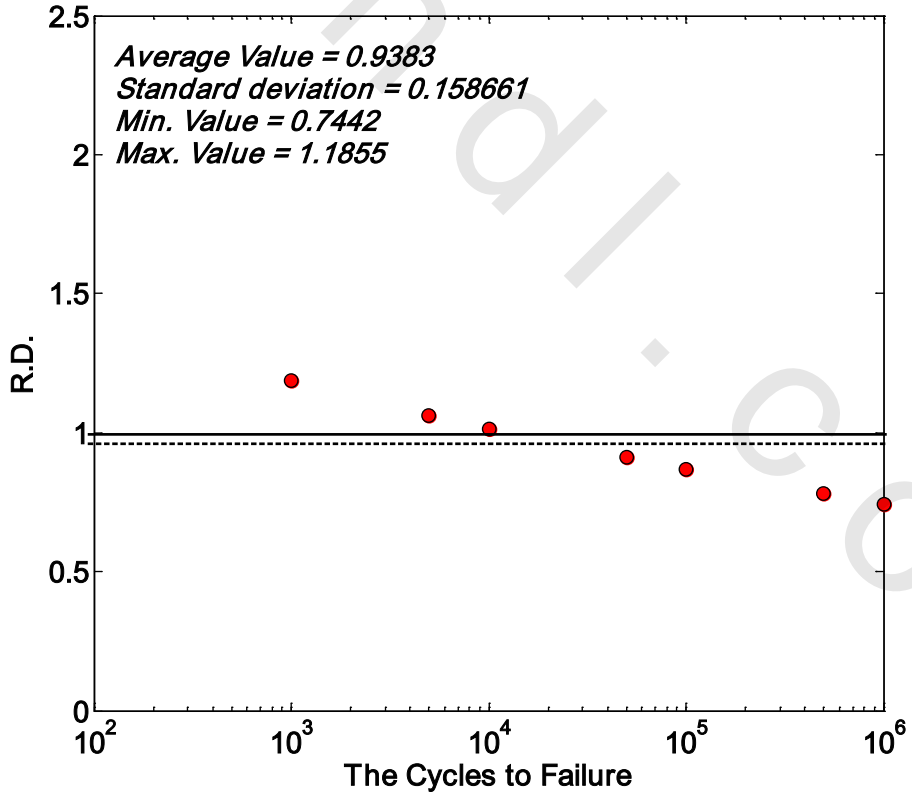

Figure 6.83.Relative damage (R.D.) applying the new failure criterion for data adapted from Kawakami et al. **[152]** Under R = -1 and Pr = 0.

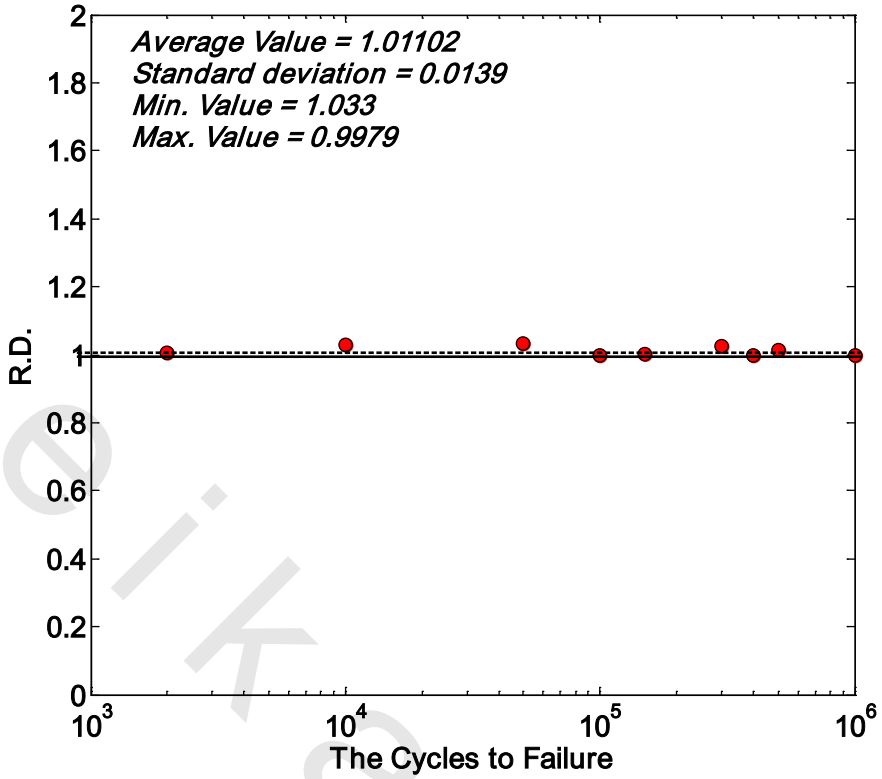

Figure 6.84.Relative damage (R.D.) applying the new failure criterion for data adapted from Ahmed M.E. et al. **[75]** Under R = -1 and Pr = 0.